UTRECHT UNIVERSITY

MASTER THESIS

Towards biomass derived phthalic anhydride via a Diels-Alder route

Author:
Bart FÖLKER

Supervisor:
Prof. Dr. P.C.A. BRUIJNINCX

Student Number:
5946824

Daily Supervisor:
Dr. C.S. LANCEFIELD

A thesis submitted in fulfillment of the requirements for the degree of Master of Science

in the

Group of Inorganic Chemistry and Catalysis
Debye Institute for Nanomaterials Science

June 21, 2018

UTRECHT UNIVERSITY

Abstract

Faculty of Science
Debye Institute for Nanomaterials Science

Master of Science

Towards biomass derived phthalic anhydride via a Diels-Alder route

by Bart FÖLKER

The global environmental impact of fossil fuels consumption has led to a growing interest in developing renewable chemicals from sustainable biomass sources. A common approach for the renewable production of aromatics is the Diels-Alder approach in which a furanic diene reacts with a dienophile to form an oxa-norbornene cycloadduct which can then be dehydrated to form the desired aromatic product. Based on this approach, this thesis sets out a new route for the direct production of phthalide from renewable furfuryl alcohol and 1,1,1,3,3,3-hexafluoroisopropyl acrylate, with the intention of eventually producing phthalic anhydride. Furthermore, due to the unstability of the Diels-Alder cycloadducts, the usual approach was adapted and an extra step involving the selective base catalysed *in-situ* lactonisation of only one of the isomeric Diels-Alder cycloadducts of furfuryl alcohol and 1,1,1,3,3,3-hexafluoroisopropyl acrylate was implemented. This lactonised product was experimentally shown to be much more thermally stable than any other investigated Diels-Alder product, allowing for the implementation of a dynamic kinetic trapping strategy in which on going equilibration of the Diels-Alder substrates/products at elevated temperatures led to an accumulation of the lactonised product in a yield of 68 %. This product was found to be very amenable to aromatisation with phthalide yields of up to 98% obtained in mixtures of MSA and Ac_2O at RT and up to 66 % using only catalytic amounts of acid and no Ac_2O. Overall, using this approach, we were able to produce phthalide (**31**) in a 66 % yield from furfuryl alcohol and 1,1,1,3,3,3-hexafluoroisopropyl acrylate.

Acknowledgements

First of all I want to thank my daily supervisor Chris Lancefield for helping me in the lab and guiding me through this thesis. Without his fruitful input this thesis wouldn't be what it is now. I want to thank my supervisor Pieter Bruijnincx for giving me the opportunity to do this project, guiding me through the process and giving feedback where necessary. Furthermore I want to thank Katarina Stanciokova and Rosa Bulo for helping me on the computational bit. Lastly, I want to thank Marc Crockatt for his input on the project and Martin Lutz for helping me with the X-Ray crystallography experiments.

Contents

List of Figures

List of Schemes

List of Tables

List of Abbreviations

ADF	**A**msterdam **D**ensity **F**unctional
ATR/FT-IR	**A**ttenuated **T**otal **R**eflectance / **F**ourier **T**ransform - **I**nfra**R**ed spectroscopy
BTX	**B**enzene, **T**oluene, **X**ylene
COSY	**CO**rrelation **S**pectroscop**Y**
DA	**D**iels-**A**lder
DCM	**D**i**C**hloro **M**ethane
DFT	**D**ensity **F**unctional **T**heory
DMAP	4-**D**i**M**ethyl**A**mino**P**yridine
ESI TOF-MS	**E**lectro**S**pray **I**onisation **T**ime **O**f **F**light - **M**ass **S**pectrometry
FA	**F**urfur**A**l
FMO	**F**rontier **M**olecular **O**rbitol
FuAce	**Fu**rfuryl **Ace**tate
FuAcr	**Fu**rfuryl **Acr**ylate
FuAl	**Fu**rfuryl **Al**cohol
GC-MS	**G**as **C**hromatography - **M**ass **S**pectrometry
GPC	**G**el **P**ermeation **C**hromatography
GUI	**G**raphical **U**ser **I**nterface
HFIP	1,1,1,3,3,3-**H**exa**F**luoro**I**so**P**ropanol
HFIPAcr	1,1,1,3,3,3-**H**exa**F**luoro**I**so**P**ropyl**Acr**ylate
HMBC	**H**eteronuclear **M**ultiple **B**ond **C**orrelation spectroscopy
HMF	**H**ydroxy**M**ethyl**F**urfural
HOMO	**H**ighest **O**ccupied **M**olecular **O**rbital
HSQC	**H**eteronuclear **S**ingle **Q**uantum **C**oherence spectroscopy
IED	**I**nverse **E**lectron **D**emand
LUMO	**L**owest **U**noccupied **M**olecular **O**rbital
MeAc	**Me**thyl **Ac**rylate
MeFuAcr	5-**Me**thyl**Fu**rfuryl **Ac**rylate
MMF	2-**M**ethoxy**M**ethyl **F**uran
MSA	**M**ethane**S**ulfonic**A**cid
NED	**N**ormal **E**lectron **D**emand
NMR	**N**uclear **M**agnetic **R**esonance
RT	**R**oom **T**emperature
SCM	**S**oftware for **C**hemistry and **M**aterials
TBAB	**T**etra-n-**B**utyl**A**mmonium **B**romide
TFE	2,2,2-**T**ri**F**luoro**E**thanol
TFEAcr	2,2,2-**T**ri**F**luoro**E**thyl**Acr**ylate
TfOH	**T**ri**F**luoromethanesulfonic acid
THF	**T**etra **H**ydro **F**uran
UFF	**U**niversal **F**orce **F**ields

Chapter 1

Introduction and Theory

1.1 How can we produce renewable aromatics?

The global environmental impact of fossil fuels consumption has led to a growing interest in developing renewable fuels and chemicals, for example from renewable biomass sources.[1] Moreover, a recent shift of naphta feedstocks towards shale gas may lead to a global tightening in the supply of commodity chemicals, further bolstering the interest in biomass derived chemicals.[2] The obvious first targets when producing biomass derived chemicals are drop in replacements for the current building blocks that are produced from naphtha. These include olefins such as ethylene, propylene and butadiene, as well as aromatics such as benzene (**1**), toluene (**2**) and xylene (BTX). It is the production of BTX chemicals that rely most heavily on naphtha feedstocks[2] and therefore alternative sustainable production routes should be investigated. BTX chemicals, and their oxygenated derivatives, are used in a wide range of applications such as in the production of polymers (PET, polystyrene etc.), solvents, additives (plasticizers) and fine chemicals. Their annual global consumption (BTX and oxygenated derivatives) therefore surpasses 140 million metric tons annually.[3]

When choosing a renewable feedstock for the production of bio-based aromatics it should ideally be low-cost, so as to be economically competitive, and highly abundant in order to be able to meet demand. Some commonly used biomass resources such as starches and vegetable oils compete directly with food production and therefore are unable to serve as reliable and low cost feedstocks in the long run.[4] Lignocellulosic biomass, on the other hand, is highly abundant, relatively low cost and does not need to compete with food production. It is therefore widely regarded as a good candidate for the production of renewable fuels and commodity chemicals.[5] Any material rich in cellulose, hemicelluloses and lignin such as wood, bamboo, cornstover and sugarcane bagasse is referred to as lignocellulosic biomass. Cellulose constitutes about 35-50 % of its dry weight, followed by hemicellulose (20–35 %) and lignin (10-25 %).[5] In terms of utilization, the cellulose component is currently the most important, followed by the hemicelluloses and lignin. In particular, lignin, as an aromatic biopolymer, is a potentially interesting feedstock for the production of aromatic chemicals, however is it highly recalcitrant and therefore challenging to upgrade to value-added chemicals.[6] This has meant that the cellulose and hemicellulose fractions are now being investigated for the production of aromatics.

To produce aromatics from (hemi)cellulose first they must be hydrolitically depolymerised to C5 (pentoses, **3**) and C6 (hexoses, **4**) monosaccharides.[7] Subsequently biological (fermentation) or chemocatalytic processes can be used to produce the building blocks required to make the desired aromatic chemicals. Fermentation processes typically convert the C6 sugars into non-aromatic platform molecules such as

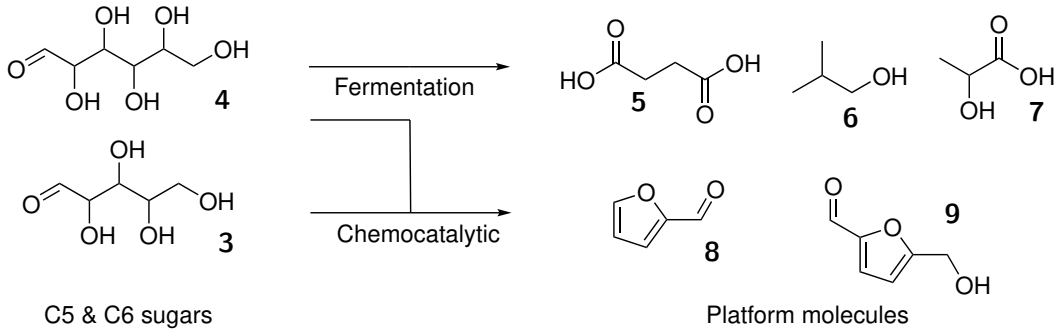

SCHEME 1.1: The production of platform molecules from lignocellulosic derived C5 and C6 sugars through chemocatalytic and fermentation processes

succinic acid (**5**), itaconic acid, bio-isobutanol (**6**) and lactic acid (**7**) (Scheme 1.1).[8,9] Alternatively, chemocatalytic processing routes for the C5 and C6 sugars commonly include their acid catalysed dehydration into furfural (FA, **8**) and hydroxymethylfurfural (HMF, **9**), respectively (Scheme 1.1).[7] These platform molecules[10] then serve as the starting point for the production of higher value chemicals. An example of this is the production of *p*-xylene (**10**) via the dimerization and dehydrocyclization of the platform molecule bio-isobutanol (**6**).[11] A common processing route for FA (**8**) and HMF (**9**) involves their conversion into a whole class of furanic diene molecules such as furfuryl alcohol (**11**), furan (**12**), methylfuran (**13**) and dimethylfuran (**14**) (Figure 1.1).[8] These molecules all contain two conjugated (electron rich) carbon-carbon double bonds, which is important for their reactivity. For example, these compounds can participate in Diels-Alder (DA) reactions with a variety of dienophiles such as ethylene (**15**), propylene (**16**), maleic anhydride (**17**) and acrylic acid (**18**), to give cycloadducts which can undergo dehydration reactions to produce aromatic chemicals (Figure 1.1).[3] Importantly, these dienophiles can also often be produced from renewable sugars by chemocatalytic routes.[3,12] As such, these DA approaches can serve as a way to access renewable aromatics from biomass

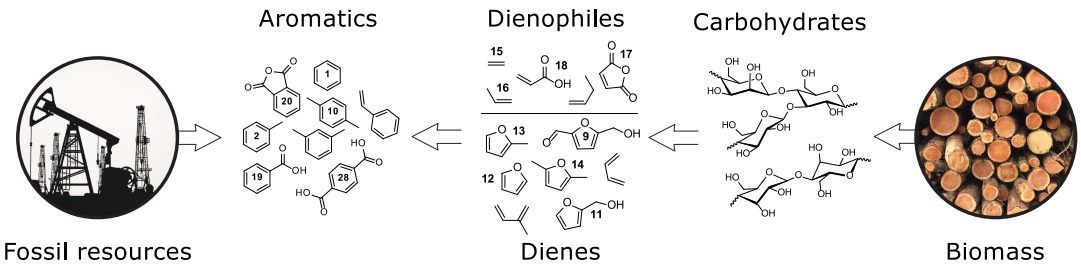

FIGURE 1.1: Biomass derived based productions of aromatics.

The general route of DA approaches to aromatics consists of two steps. First, the diene and dienophile react in a DA reaction to form a cycloadduct, typically with a oxa-norbornene ringstructure when furan derivatives are used as dienes. This adduct can then be dehydrated to form the desired aromatic product (Scheme 1.2). In fact, quite extensive efforts have already been dedicated towards utilising this process scheme for the industrial production of aromatic chemicals. For example the production and commercialization of *p*-xylene (**10**) from dimethylfuran (**14**) and ethylene (**15**) has been extensively studied using a variety of zeolite catalysts.[13–16] In the same way the production of other products such as benzoic acid (**19**) from

furan (**12**) and acrylic acid (**18**)[17]; toluene (**2**) from 2-methylfuran (**13**) and ethylene (**15**)[18]; phthalic anhydride (**20**) from furan (**12**) and maleic anhydride (**17**) (Route A, Scheme 1.2)[19] and substituted phthalic anhydrides (**21**) from methylfuran (**13**) and maleic anhydride (**17**) (Route B, Scheme 1.2)[20] have also been investigated. In order to get a better understanding of the general approach, the two reaction steps are looked at in more detail.

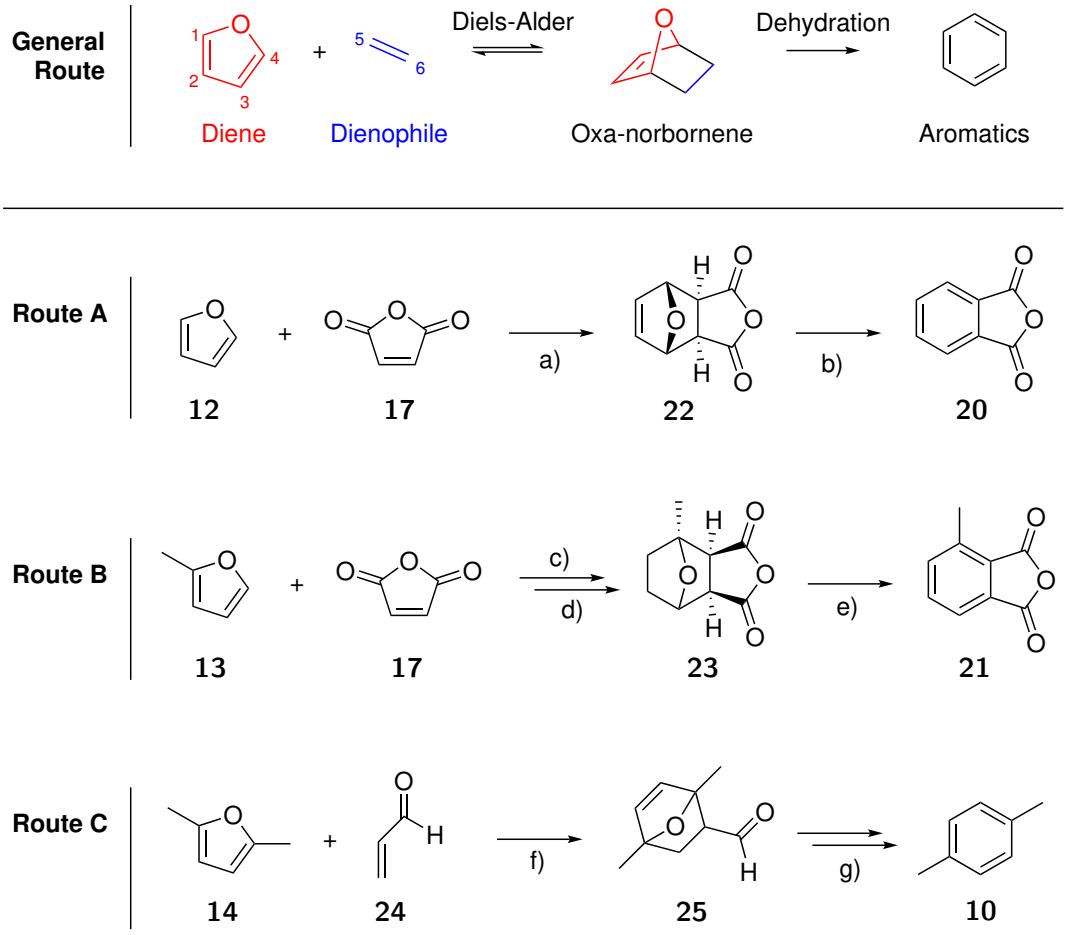

SCHEME 1.2: General route from DA addends to aromatic products and examples from literature. **Route A**: a) Neat, RT, 4 hours, yield = 96 % b) MSA, Ac_2O, RT for 2 hours and 80 °C for 1 hour, yield = 80 %.[19] **Route B**: c) Neat, RT, yield = 93 % d) H_2, THF, 3-80 bar, Pd/C, RT, yield = 95 %. e) H-VUSY, Pd/C, 200 °C, toluene, yield = 90 %.[20] **Route C**: f) $Sc(OTf)_3$, -60 °C, yield = 84 %. g) dehydration and decarbonylation of **25** to **10**, yield = 44 % yield.[15]

1.2 Theory of the Diels-Alder reaction

The Diels-Alder reaction is a pericyclic cycloaddition reaction in which a diene reacts with a dienophile to form a six membered ring ('cycloadduct'). The reaction occurs via a single step concerted mechanism in which one new π-bond and two new σ-bonds are formed at the expense of three π-bonds (Scheme 1.3)[3]. New bond formation occurs through interactions of the frontier molecular orbitals of both the diene and dienophile. Most reactions occur in a normal electron demand (NED) fashion, in which the highest occupied molecular orbital (HOMO) of the diene interacts with

the lowest unoccupied molecular orbital (LUMO) of the dienophile (Figure 1.2) to form the new molecular orbitals. An inverse electron demand (IND) reaction is also possible, in which the location of the HOMO and LUMO are reverse, but this is much less common. The energy gap between the interacting HOMO and LUMO is referred to as the frontier molecular orbital (FMO) gap. The lower this gap is, the more likely it is for DA substrate pairs to undergo reaction, though other factors such as sterics can play a significant role as well.[21]

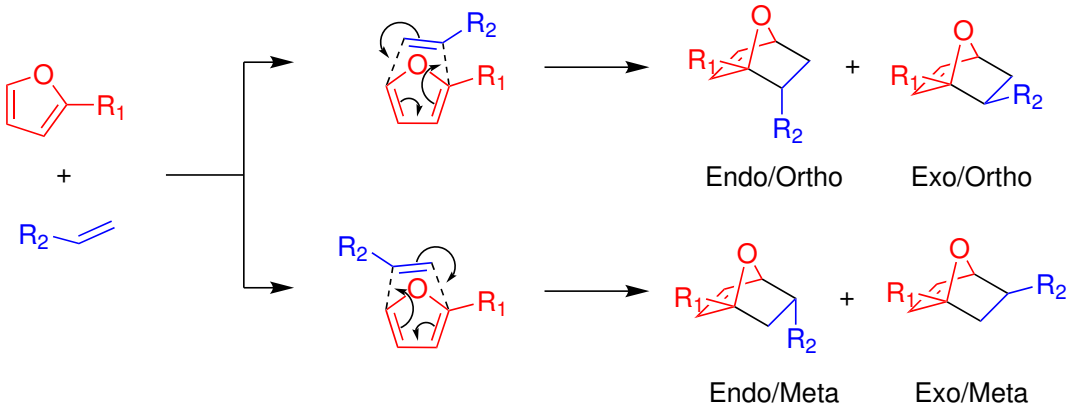

SCHEME 1.3: Mechanism and stereo/regiochemistry of the Diels-Alder reaction.

Depending on the substrates substitution pattern, the DA adducts can have different regio- and stereochemistries. When for example two asymmetric substrates react (Scheme 1.3), they can form two regioisomers, *ortho* and *meta*, as well as two sterioisomers, *endo* and *exo*, based on their orientation during reaction. This leads to a total of four different possible DA adducts (Scheme 1.3). The formation of *endo* product is usually favoured over the formation of *exo* product due to secondary orbital interactions.[22] Stereochemistry is however not of importance when targeting aromatics since all stereogenic centers are removed upon dehydration. Regiochemistry, however, is conserved during dehydration (Scheme 1.4) which can cause selectivity issues when targeting specific regioisomers such as *ortho*/*meta*-xylene. To circumvent this problem at least one of the DA substrates is often chosen to be symmetric. To our knowledge, no attempts at tuning the regioselectivity in reactions of non-symmetric DA substrate pairs for the production of aromatics have been reported so far.

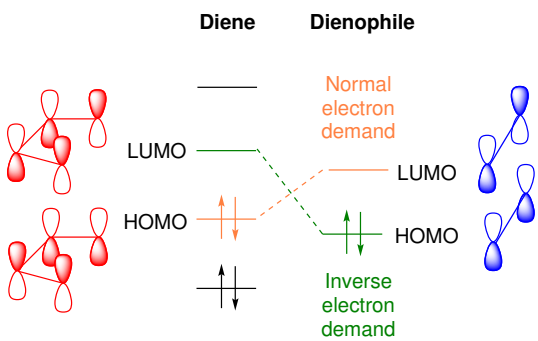

FIGURE 1.2: Frontier molecular orbital interaction of the Diels-Alder reaction.

Due to the low reactivity of some DA substrate pairs, low DA yields can be a major bottleneck in commercialisation of renewable aromatics. Tuning the reactivity of the substrates is therefore crucial and is usually done by the addition of electron withdrawing or donating groups at the 1 and 4 position of the diene,[23,24] and the 5 and 6 position of the dienophile (see Scheme 1.2 for numbering). Since most reactions occur according to a NED, the diene is often substituted with electron donating groups to increase the energy of its HOMO, while the dienophile is substituted with electron withdrawing groups to decrease the energy of its LUMO. In this way the FMO gap of the substrate pair decreases and therefore their reactivity increases.[21] Substitution can have a big effect on the DA yield. Dimethylfuran (**14**), a highly substituted electronrich diene, and ethylene can for example be converted into *p*-xylene (**10**) in a 90 % yield[13], whereas the production of benzene from the electron poorer furan (**12**) and ethylene (**15**) is not reported in literature.

One way to overcome low reactivity in DA reactions is to use lewis acid catalysts. For example, the DA reaction of furan (**12**) and acrylic acid (**18**) can be catalysed by lewis acidic zeolite catalysts yielding 51 % DA adduct, whereas no reaction is observed in the absence of zeolite.[17] The mechanism of lewis acid catalysis has been shown to involve interaction with the FMO orbitals of the reactants in a way that decreases the energy of the DA transition state.[25] Furthermore, lewis acid catalysts have been used to catalyse DA reactions at subambient temperatures. Using scandium triflate ($Sc(OTf)_3$), Shiramizu et al.[15] have shown that high yields (84 %) can be obtained for the reaction of dimethylfuran (**14**) and acrolein (**24**) at -60 °C (Route C, Scheme 1.2). Because of the negative entropy of the DA reaction, they claim that lowering the reaction temperature causes a shift in the DA equilibrium resulting in a higher DA adduct yield. At these low temperatures, catalysis is crucial.

1.3 Dehydration of Diels-Alder adducts to aromatics

The second key step in this route is aromatisation via dehydration of the DA adducts. This is often acid catalysed although base catalysis[26] is also possible. When furanic dienes are used in the DA reaction, all cycloadducts have the same basic oxanorbornene ring structure with a characteristic bridging oxygen (Scheme 1.4). Under influence of a Brønsted acidic catalyst, these adducts can eliminate one molecule of water to finally yield the aromatised product (Scheme 1.4).[3] Commonly used catalysts for the dehydration reaction include Brønsted acidic zeolites, microporous aluminosilicate crystals such as H-Y and H-BEA.[13,27]

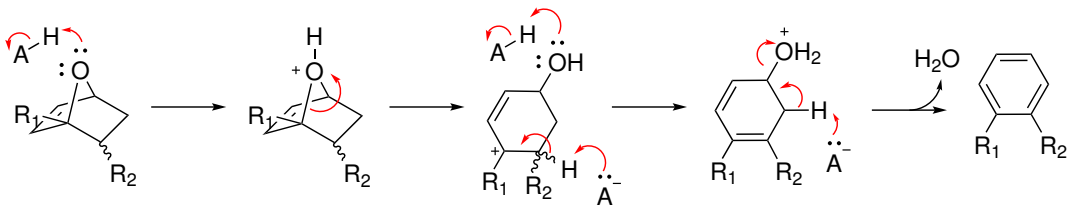

SCHEME 1.4: General aromatisation mechanism of DA adducts via ringopening and dehydration.[3]

One draw back of this approach can be rapid retro DA-reactions during the acid catalysed dehydration step, significantly eroding the yield of aromatic product. The reason for this is that the dehydration steps often need high temperatures, which can make the retro-DA very favourable. When this occurs the furan derivatives are

normally unstable in the presence of an acid and undergo non-specific condensation and decomposition reactions. Therefore, there has been a great detail of effort directed forwards decreasing the amount of DA adduct lost to retro-DA reactions. Tandem DA and dehydration reactions have for example been used to directly convert the DA substrates into aromatic products in one single step. This approach has been successful for the production of *p*-xylene (**10**)[27] and toluene.[18] Even in these optimised processes significant amounts of diene substrate is lost to side-reactions and, due to the high pressures and temperatures, it is only applicable to specific substrates. Alternatively thiyagarajan et al.[20,28,29] have demonstrated another approach to solve this problem. They show that by stabilising the DA cycloadducts by hydrogenation, the problem of retro-DA reaction during the aromatisation step can be overcome, however an additional dehydrogention catalyst is needed in this step (Route B, Scheme 1.2). As an alternative to using heterogeneous zeolite catalysts which require high temperatures for the dehydration reaction, mixtures of methanesulfonic acid (MSA) and acetic anhydride (Ac_2O, **26**) have also been shown to effectively catalyse the dehydration at room temperature. Using this method for the production of phthalic anhydride (**20**) from furan (**12**) and maleic anhydride (**17**) (Route A, Scheme 1.2), and methyl benzoate from furan (**12**) and methyl acrylate (**27**), Mahmoud et al.[17,19] have reported excellent yields of 80 % and 96 % respectively.

1.4 Goal of this thesis

Traditional routes from fossil fuel resources produce oxygen depleted aromatics (BTX) that often undergo extensive functionalisation as they are used to produce downstream products. Due to the high oxygen content of biomass, it opens up the possibility of directly targeting higher value, oxygenated aromatics.[3] There are already some studies that directly target renewable terephthalic acid (**28**) via the discussed DA approach,[30,31] as well as some studies on the direct targeting of phthalic anhydride (**20**) from maleic anhydride (**17**) and furan (**12**) (Route A, Scheme 1.2).[19,20,32] While maleic anhydride (**17**) and furan (**12**) can both be produced renawable from FA (**8**), in a 73 % yield[33] and 99.5 % yield[34] respectively, both substrates require decarbonylation leading to poor atom economies.

In this thesis a new route for the direct production of phthalide (**31**) with the intention of producing phthalic anhydride (**20**), is investigated based on the discussed DA approach (Scheme 1.5). Phthalic anhydride (**20**), with a global consumption surpassing 4.3 million tons (2012), is consumed in large amounts for the production of plasticisers, unsaturated polyester resins and alkyd resins.[35] We will attempt its synthesis from completely renewable furfuryl alcohol (FuAl, **11**) and acrylic acid (**18**). FuAl is chosen since approximately 60 % of lignocellulosic derived FA (**8**) is converted into FuAl (**11**) making it a highly abundant molecule.[36] Acrylic acid (**18**) can also be synthesised from the dehydration of renewable lactic acid[37] (**7**) or in a two-step catalytic process from glycerol.[38] The renewable production of these substrates do not require decarbonylation, making them more interesting from an atom economical point of view then the previously used substrates, furan and maleic anhydride.[19] Both FuAl (**11**) and acrylic acid are however non-symmetric and will therefore produce a mixture of *ortho* and *meta* aromatisation products in this approach (Scheme 1.3). To overcome anticipated selectivity issues it was planned to make use of a previously reported intramolecular DA reaction of furfuryl acrylate (FuAcr, **29**), i.e. the ester of FuAl (**11**) and acrylic acid (**18**) (Scheme 1.5).[39] It was then

planned that dehydration of the cycloadduct would give phthalide (**31**) which could then be selectivity oxidised to phthalic anhydride, as reported for similar systems in literature.[40,41]

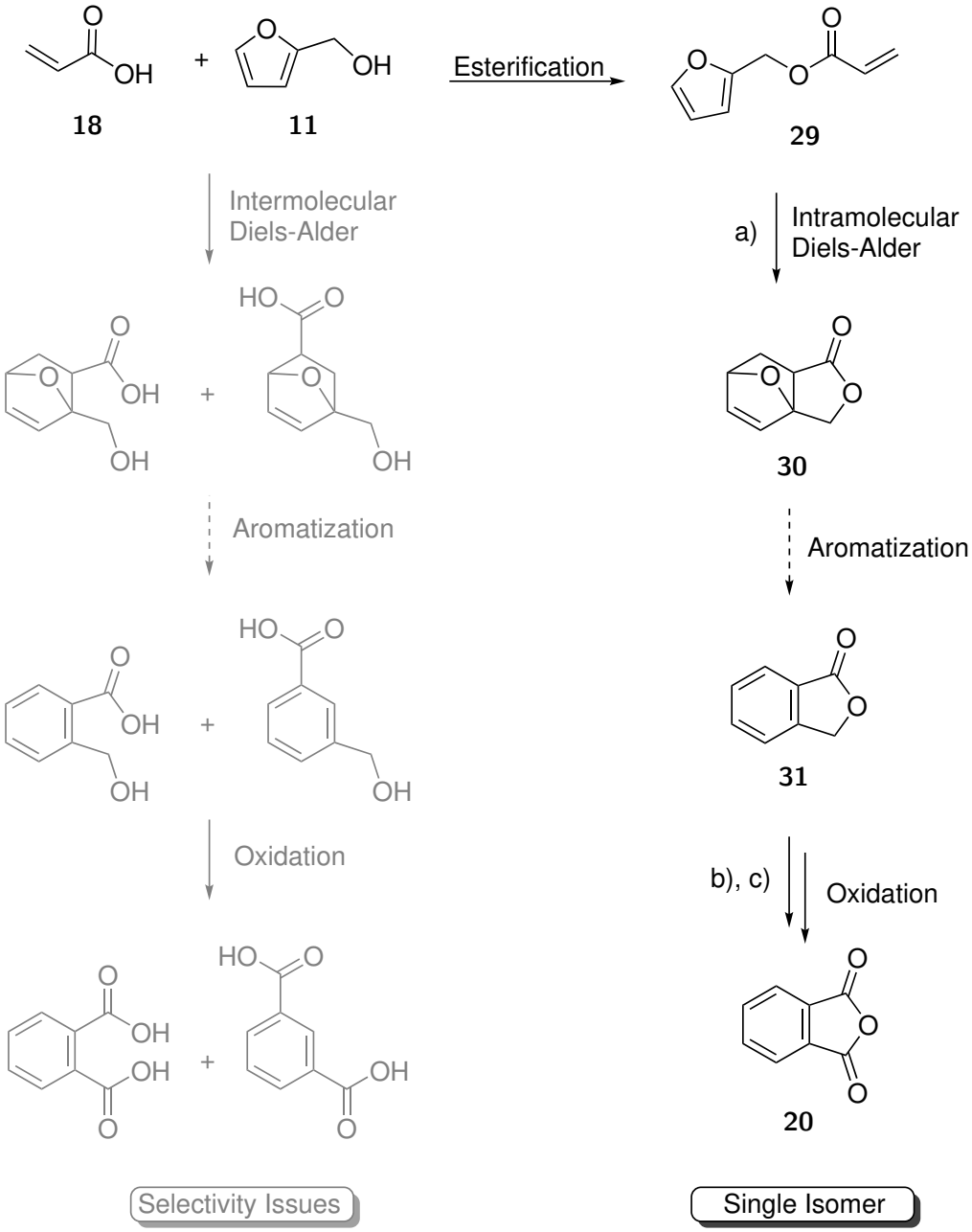

SCHEME 1.5: Proposed route to phthalic anhydride investigated in this thesis. a) Neat, diatomacious earth, 80 °C, 60 hours.[39] b) $KMnO_4$, NaOH, RT, 4 days. c) Ac_2O, 2 hours.[40,41]

Chapter 2

Results and Discussion

2.1 Intramolecular DA reaction of FuAcr

2.1.1 Attempts at the intramolecular DA reaction of FuAcr

In order to revisit the intramolecular DA reaction of FuAcr (**29**), this compound first had to be synthesised. Most simple acrylate esters such as MeAc (**27**) are synthesised by direct Fischer (acid catalysed) esterification of the parent alcohol and acrylic acid.[42] In contrast, higher alcohols (C_5+) or more complex esters are often synthesised by transesterification of lower (e.g. methyl) acrylates,[43] also in the presence of an acid catalyst. Unfortunately, FuAl (**11**) is acid sensitive[44] precluding the use of such methods. Thus, FuAcr (**29**) has previously been prepared by the reaction of furfuryl chloride with sodium acrylate[39] or acrolyl chloride (**32**) with FuAl (**11**) in the presence of a base.[45] Based on the availability of starting materials, the latter method was used here to prepare FuAcr (**29**) in a 95 % yield (Scheme 2.1).

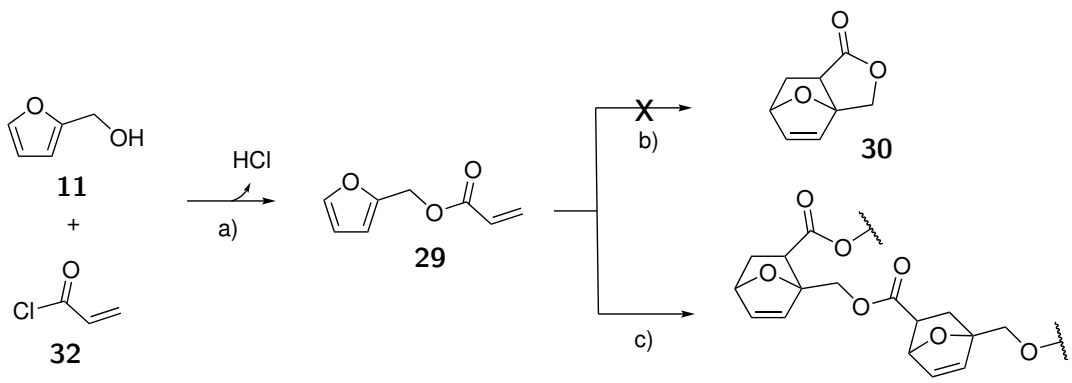

SCHEME 2.1: Synthesis of FuAcr (**29**) with subsequent attempts on DA reaction. **a)** 1.25 eq NEt_3, DCM, 20 °C, 2 hours, 94 %. **b)** Celite, $M(OTf)_x$, $ZnCl_2$, Heating. **c)** Standing, RT.

With FuAcr (**29**) in hand, the intramolecular DA reaction first reported by Babayan et al.[39] could be attempted. Originally, a rather unusual procedure was reported which involved supporting the compound on diatomaceous earth and then heating this material at 80 °C for 60 hours.[39] Diatomaceous earth is normally considered to be a quite inert material and its role in the reaction was not discussed, however an attempt was made to replicate the original synthetic procedure. Therefore FuAcr (**29**) was supported on 'Celite® Hyflo Supercel', a commercially available diatomaceous earth, and heated at 80 °C for 56 hours. Unfortunately, subsequent extraction of the supported material with $CDCl_3$ and NMR analysis indicated that the starting material was recovered unchanged. With no clear explanation for why the reaction

failed in our hands, it was decided to study the reaction in the solution phase, as is more typical for DA reactions.

Although most DA reactions exhibit only small solvent effects owing to their concerted and nearly synchronous nature,[46] some particular systems can show significant solvent effects. For example, the intra-molecular DA reaction of 2-furfuryl methyl fumarates, which are very similar in structure to FuAcr (**29**), can show rate enhancements of up to about 3200 in moving from non-polar (toluene) to highly polar (DMSO) solvents.[47] An NMR solvent screen was therefore carried out for our reaction using DMSO-d_6, acetone-d_6, chloroform-d_1, benzene-d_6, methanol-d_4, D_2O) at 80 °C. The reaction was followed by ^{1}H NMR which indicated that none of the intended product was formed in any of the solvents. In general, FuAcr (**29**) appeared stable in all solvents except D_2O, which led to hydrolysis of the ester.

Given the apparent low reactivity of FuAcr (**29**) towards DA reactions, a range of metal triflate lewis acids (Ga^{3+}, Hf^{4+}, In^{3+}, Sc^{3+}, Y^{3+}) and $ZnCl_2$ were investigated as catalysts.[15,17] For convenience of analysis these reactions were run in $CDCl_3$. In all cases a colour change (to black) was immediately observed at RT but no obvious reaction was detectable by NMR. Heating at 60 °C led to some hydrolysis of the ester but still no DA products, or the subsequent aromatised products, could be detected.

Interestingly, after prolonged standing at RT it was noted that a number of impurities were forming in the FuAcr (**29**). Based on NMR analysis these impurities were assigned to DA adducts, however the characteristic peaks observed in the NMR spectra did not match those reported for compound **30**. This lead us to propose that these impurities could be the result of intermolecular DA reactions (Scheme 2.1). This proposal was supported by the appearance of higher molecular weight material as judged by GPC analysis (Figure 2.1), suggesting that in this system and in our hands, intermolecular DA reactions are more favourable than the intramolecular one. This finding combined with other reports on the difficulty of performing intramolecular DA reactions in related systems due to the energetically challenging conformational preorganisation required,[48] led us to study both the intra- and intermolecular DA reactions (Scheme 2.2) using computational methods in order to learn more about the feasiblity of the intended reaction.

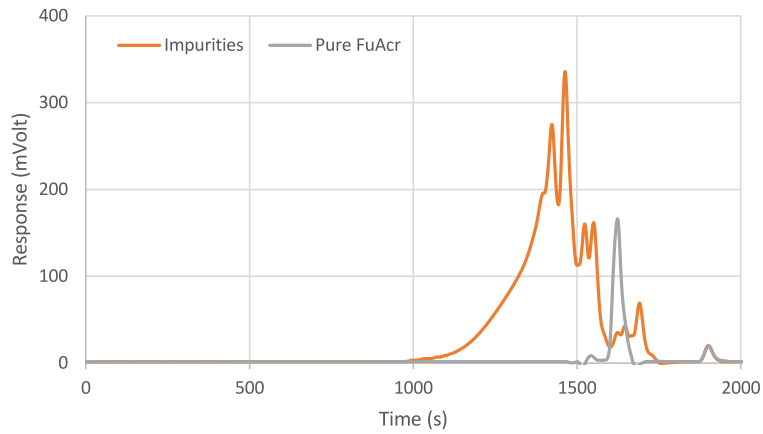

FIGURE 2.1: GPC data on DA polymerisation of FuAcr (**29**). GPC data was obtained after seperation of the impurities from FuAcr (**29**) using column chromatography.

2.1.2 Calculations on intra- and intermolecular DA reactions

For the intramolecular DA reaction of FuAcr (**29**), two possible stereoisomeric products, *endo* (**30**A) and *exo* (**30**B) are expected. In our calculation both reaction pathways were therefore considered. These were then compared to the same reaction pathways of structurally similar intramolecular as well as some intermolecular reactions (Scheme 2.2). In the intermolecular reaction both the *endo* and *exo meta* DA adducts can be formed (Scheme 1.3), therefore these pathways were considered as well.

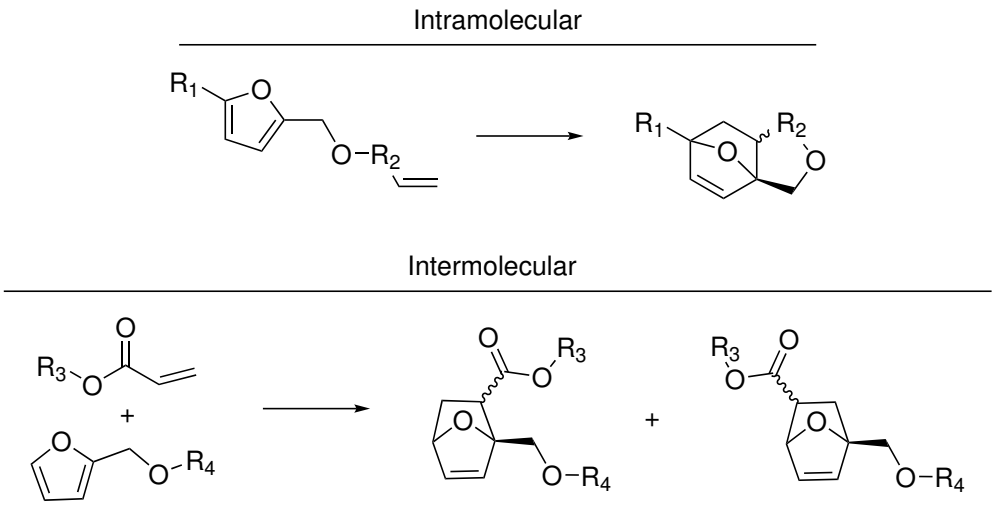

SCHEME 2.2: Different intra- and intermolecular DA reactions investigated by DFT computational methods. In our calculations R_1 is either H or CH_3, R_2 is either CO or CH_2, R_3 is either CH_3 or $(CF_3)_2CH$ and R_4 is either H or $COCH_3$.

Since the uncatalysed DA reaction is known to proceed via a single transition state, it was only necessary to calculate the Gibbs free energies of the substrates (G_{GS}, 1 in Figure 2.2), transition states ($G^{\ddagger}$, 3 in Figure 2.2) and products (G_{Pr}, 4 in Figure 2.2) for each of the possible reaction pathways. Unlike in the intermolecular reaction, all intramolecular DA substrates first need to undergo a large conformational preorganisation before being able to proceed to the DA reaction. Therefore, the energy of this preorganised confirmer was calculated for all intramolecular reactions as well (G_{Conf}, 2 in Figure 2.2). All Gibbs free energies were calculated using the ADF modeling suite[49–51] at the DFT level using the hybrid B3-LYP-D3 XC functional together with the TZ2P basis set, which is known to work well for organic molecules.[52,53]

From this data, we were able to calculate the Gibbs free energy change of reaction ($\Delta_r G$) as a measure of the thermodynamic feasibility, and the Gibbs free energy of activation or transition state energy ($\Delta G^{\ddagger}$) as a measure of the kinetic feasibility for all of the possible reaction pathways. For the intramolecular reaction the energy required to go from the global minimum conformer (G_{GS}) to the preorganised reactive confirmation was calculated as well (ΔG_{Conf}). The main results are summarized in Figure 2.3 and numerical results can be found in appendix A. Next to this, the NED FMO gap was calculated for all intramolecular substrates and intermolecular substrate pairs, to get a simple measure for their reactivity (Table 2.1).

Starting with the intramolecular reaction of FuAcr (**29**), both the transition and final state of the *endo* product (**30**A) are much higher in energy than the *exo* product

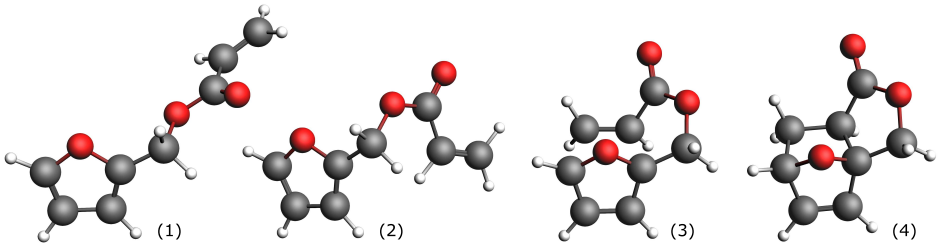

(A) Intramolecular DA reaction to *exo* product of FuAcr (**29**).

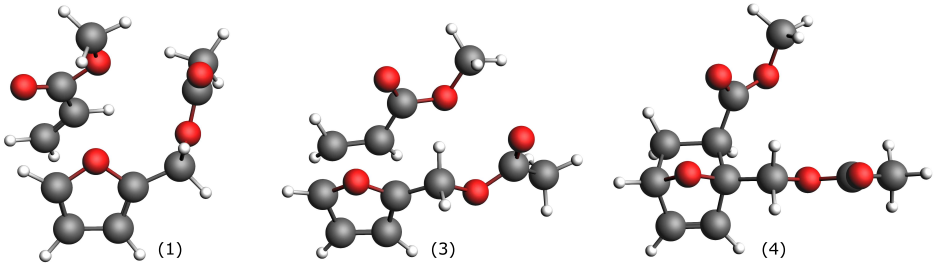

(B) Intermolecular DA reaction to *exo/ortho* product of FuAce and MeAc.

FIGURE 2.2: **A**: *Exo* intramolecular DA reaction pathway of FuAcr (**29**) as an example for the intramolecular DA reaction. (1) Global minimum conformer of substrate (2) Substrate conformer needed for DA reaction (3) Transition state (4) Product. **B**: *Exo/ortho* intermolecular DA reaction pathway of FuAce and MeAc as an example for intermolecular DA reactions. (1) Global minimum of interacting substrates (3) Transition state (4) Product. Note that (2) is left out since no conformational change is necessary for intermolecular DA reaction.

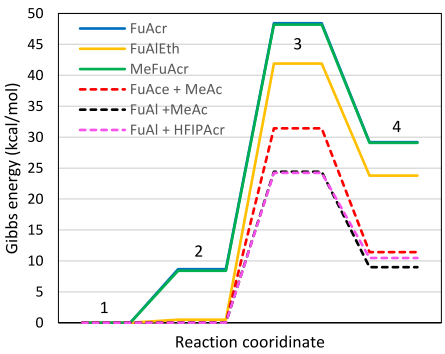

(A) *Endo/Ortho* products

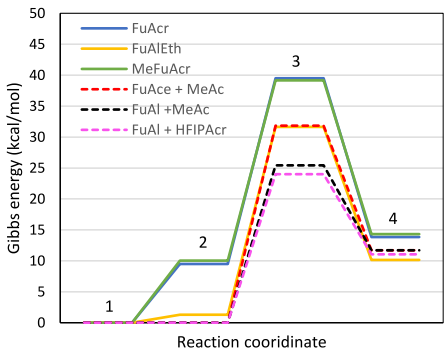

(B) *Exo/Ortho* products

FIGURE 2.3: Gibbs free energy profiles of intra and intermolecular DA reactions calculated in gas phase at 323K using B3-LYP-D3 XC functional together with the TZ2P basis set. For all intramolecular DA reactions, the global minimum substrate conformer was set to zero and for all intermolecular reactions the global minimum of the two interacting substrates was set to zero. All other energies were calculated with respect to these zero points. The numbers 1,2,3 and 4 correspond to the different stages in the reaction pathway and can be seen in Figure 2.2. Note that the colours used for the substrates/substrate pairs in Table 2.1 are the same here.

(**30**B) (8 and 15 kcal/mol respectively). Looking at the optimised geometries of the products, the C_1-C_2-C_3 bond angle in Scheme 2.3 is significantly further from the optimal tetrahedral angle (109.5 °) in the *endo* product (**30**A) (133°) than it is for the *exo* product (**30**B) (118°). The increase in strain associated with this distortion likely results in the higher transition state and final product energies for the *endo* product (**30**A).

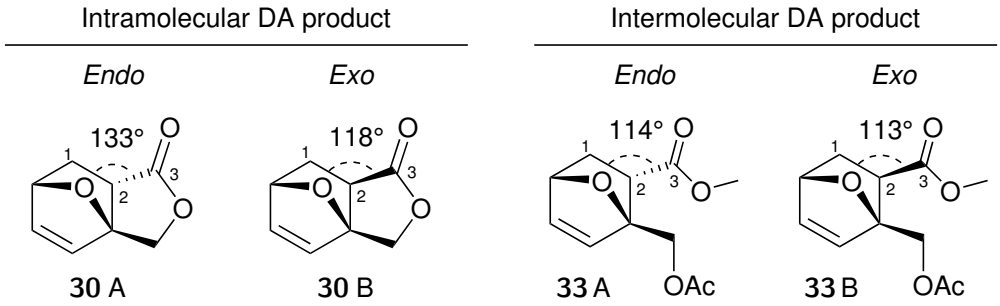

SCHEME 2.3: Comparison of angles in different DA products

Moreover, FuAcr (**29**) first has to undergo a conformational preorganisation, associated with an increase in Gibbs free energy of about 8-10 kcal/mol (ΔG_{Conf}) for both *endo* and *exo* DA routes (Figure 2.3). This therefore drives up the total activation energy of the intramolecular reaction compared to the intermolecular one. Based on experimental observations, this preorganization and large energy pentalty was also proposed by Jung et al.[48] for a series of intramolecular DA reactions of substituted 2-furfuryl methyl fumarates. They suggest that the required rotation around the ester bond (S-cis ester conformation) results in a significant increase in the dipole moment of the molecule, thus increasing its energy. Judging from the optimised structures, this same rotation around the ester bond is also required for FuAcr (**29**) (Figure 2.2 a).

Unfortunately attempts to compute the energy levels for the intermolecular DA reaction of FuAcr (**29**) failed therefore the DA reaction with substrates furfuryl acetate (FuAce, **36**) and MeAc (**27**) was used as a model system to compare inter- and intramolecular reaction pathways. For this substrate combination, all possible products and transition states (**33**) are very similar in energy (Appendix A, Table A.2). Comparing the energies of the intramolecular FuAcr DA products (**30**) with the *ortho* products of the intermolecular reaction (**33**A,B), a higher product energy is observed for both products from the intramolecular reaction. Interestingly, whilst the *endo* product from the intramolecular reaction (**30**A) suffers from high internal strain, there is no such issue in the intermolecular reaction product (**33**A, Scheme 2.3). This is explained by the fact that the absence of the 5-membered lactone ring allows for a different conformation to be adopted, minimising the internal strain/energy of the product.

Additionally, comparison of the transition state energies between the two reaction modes shows that in all cases the intermolecular pathway is predicted to be much more favourable, presumably because no large conformational preorganisation penalty is required (Figure 2.2 b). In fact, the differences in activation (*endo*: 15 kcal/mol and *exo*: 8 kcal/mol) and final product energies are so high that the intramolecular reaction of FuAcr should dominate leading to polymerisation. This then explains what we observe experimentally when the FuAcr (**29**) is left at RT for a few weeks, as previously noted (Figure 2.1).

Since the FMO gap for the combination of FuAce (**36**) and MeAc (**27**) is slightly lower then the gap for FuAcr (**29**) (Table 2.1), there is a possibility that the product and transition state energies of FuAce and MeAc (**33**) are lower because of favoured electronics. It was therefore decided to calculate the product and transition state energies of the substrate 5-methylfurfuryl acrylate (MeFuAcr, **35**), which is similar to FuAcr (**29**) but has a lower FMO gap then FuAce (**36**) and MeAc (**27**) (Table 2.1). According to our calculations, small changes in the FMO gap do not significantly change the energy of the product and transition state (Figure 2.3). This means that the preorganisation energy probably does indeed play a determining role in the feasibility of the intramolecular reaction.

TABLE 2.1: All FMO gaps are normal electron demand. Colours of molecules are the same as colours used in Figure 2.3

Substrate(s)		FMO gap (kcal/mol)
29	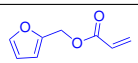	116.5
34		136.8
35	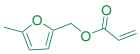	107.5
36 & 27	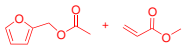	110.7
11 & 27	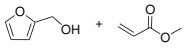	104.8
11 & 37		87.1

Furfuryl allyl ether (**34**), another compound reported to undergo intramolecular DA reaction,[39] is electronically less activated towards DA reaction then FuAcr (**29**) (Table 2.1), but due to the absence of the ester functional group, the energy penalty for preorganisation should be much lower. This is reflected in the lower energy of the products and transition states which are about 7 kcal/mol lower in energy than both *endo* and *exo* products of FuAcr (**30**). However, the *endo* product, as well as its transition state, are still relatively strained, being about 10 kcal/mol higher in energy compared to the energies for the DA adducts of FuAce and MeAc (**33**A,B). For the *exo* product and transition state of **34** this is not the case. The energies are very similar to those found for the adducts of FuAce and MeAc (**33**B), suggesting that based on these calculations this reaction might have a potential to succeed (assuming the reaction of FuAce (**36**) and MeAc (**27**) happens). Attempts were therefore made to repeat the reported method for carrying out this DA reaction ,[39] however this was again not successful. Based on the large difference of 26 kcal/mol in the FMO gaps of the intramolecular substrate **34** and the intermolecular substrates FuAce (**36**)and MeAc (**27**), we would suggest that **34** is simply not activated enough for DA addition. Reasons as to why our calculations nonetheless suggest that the *exo* transition state and product energies of **34** are similar to those of FuAce and MeAc (**33**B) remain unclear to us.

Finally, the energies of the products and transition states of the intermolecular DA reaction of FuAl (**11**) and MeAc (**27**), a reaction described in patented literature,[54] were calculated as a comparison to FuAce (**36**) and MeAc (**27**) (not found in literature). The energies of the *ortho* DA products of FuAl and MeAc (**38**) are very similar to those of FuAce and MeAc (**33**), differing only by 1 - 2 kcal/mol. This reaction should therefore, based on the literature and these results, be thermodynamically possible. The transition states for forming the FuAce and MeAc DA adducts (**33**) are

however about 6 kcal/mol higher than those for FuAl and MeAc (**38**), suggesting this reaction should be kinetically slow in comparison. This may be caused in part by the lower FMO gap for FuAl (**11**) and MeAc (**27**) (Table 2.1). Alternatively, coordination of the free alcohol group of the diene to the ester group of the dienophile may play a role in stabilizing the *ortho* FuAl and MeAc transition states (**38**). We found that the *meta* transition states of FuAl and MeAc (**38**), in which this coordination is not possible, were typically 3.5 - 4.5 kcal/mol higher in energy and closer to the *meta* transition states of FuAce and MeAc (**33**) (Appendix A), further suggesting that hydrogen bonding of the free hydroxyl group to the incoming acrylate may play a role in promoting this reaction. This led us to look at the structures of the optimised *ortho* transition states of FuAl and MeAc (**38**). From these structures the proposed coordination was visible, therefore confirming our hypothesis (Figure 2.4).

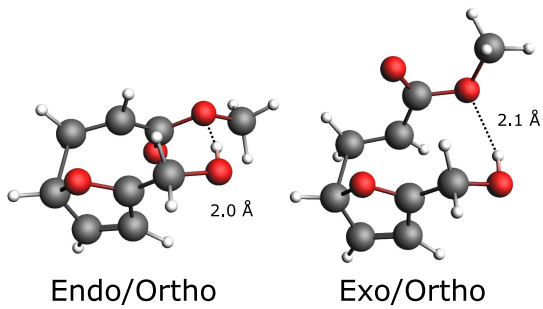

FIGURE 2.4: Evidence for the stabilization of the *ortho* transition states of FuAl and MeAc through internal hydrogen bonding. Displayed structures are those of the DFT optimised transition states.

Overall we have seen that the intramolecular DA reaction of FuAcr (**29**) is both thermodynamically and kinetically very unlikely due to the large transition state and product energies caused by the energy penalty associated with the required conformational preorganisation. Since the intermolecular model reaction of FuAce (**36**) and MeAc (**27**) was found to be thermodynamically and kinetically favoured over the intramolecular reaction of FuAcr (**29**), we predicted that intermolecular DA addition would dominate. Further theoretical attempts at decreasing the product and transition state energies by using the activated, methyl substituted, MeFuAcr (**35**) resulted in little change, whereas substituting the ester for an ether group (**34**) in order to decrease the energy penalty for preorganisation, led to significant deactivation towards DA addition.

These results suggest that if the intramolecular DA reaction is to be used successfully, then a large structural change in the substrates would be required, necessitating additional processing steps if phthalide (**31**) is still targeted. Together with the failed experimental attempts discussed in section 2.1.1, this then led us to abandon the intramolecular DA route. Since our calculations did not exclude the intermolecular DA reaction of FuAce (**36**) or FuAl (**11**) with MeAc (**27**), and in the literature the DA reaction of FuAl (**11**) and MeAc (**27**) is reported[54], we decided to focus on attempting the intermolecular DA reaction of FuAl (**11**) and acrylic acid (**18**) derivatives instead (Scheme 2.4).

2.2 Intermolecular DA reactions and aromatisation

2.2.1 Intermolecular DA reactions

FuAl and MeAc DA reaction

The first section of this thesis concluded that FuAcr (**29**) (and furfuryl allyl ether, **34**) were unreactive toward the intended intramolecular DA reactions and that routes using FuAl (**11**) and acrylic acid (**18**) derivatives appear to be most promising next based on calculations and literature.[54] This intermolecular DA approach, would however naturally produce a mixture of *ortho* and *meta* aromatisation products (Scheme 1.3), whereas the goal of this thesis was to selectively target phthalic anhydride (**20**), a single aromatic product. Therefore, the design of this route would have to include a way of steering the DA selectively towards *ortho* product in order to keep phthalic anhydride (**20**) as the main target. Alternatively a method in seperating the regio isomers after aromatisation would have to be developed, meaning that *meta* aromatisation product i.e. iso-phthalic acid would be a co-product of this route. Since, this compound is also widely used in the chemical industry it is still a good aromatic target as well.[55] For now, we will focus on attempting the intermolecular DA reaction and aromatisation of its products as a proof of concept before dealing with the selectivity issues.

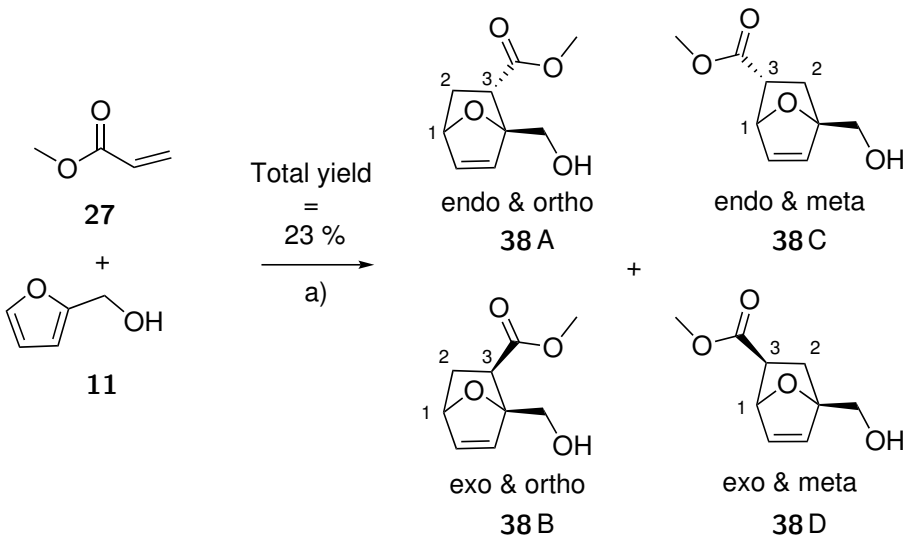

SCHEME 2.4: DA reaction of FuAl (**11**) with MeAc (**27**) into the four expected isomers. **a)** Neat, molar ratio of 1:1, 70 °C, 23 %.

Following patent literature,[54] FuAl (**11**) and MeAc (**27**) were reacted (1:1) neat at 70 °C. NMR analysis of the crude reaction mixture indicated that DA products were forming. In order to fully characterise each of the DA products their purification was attempted. Starting from the crude reaction mixture obtained by reacting FuAl (**11**) and MeAc (**27**) for 6 h at 70 °C, excess FuAl (**11**) and MeAc (**27**) were removed by vacuum distillation giving a crude mixture (24.15 g crude product from 50 g FuAl (**11**) and excess MeAc (**27**)) containing mostly the 4 expected DA products (**38**A-D, Scheme 2.4). Initial, attempts to separate the crude isomers, as well as their benzoylated derivatives, by silica gel column chromatography failed and therefore further investigations focused on the characterisation and use of the product mixture.

To further support the assignment of the products, 2D NMR experiments (COSY, HSQC) were used. As anticipated, four different DA products could be tentatively

assigned and quantified based on the characteristic NMR shifts (Figure 2.5 a) of the proton at position 1 (See Scheme 2.4). The *ortho* (**38**A,B) and *meta* (**38**C,D) DA products could be distinguished based on their different characteristic COSY coupling of the proton at position 1 to either the protons at position 2 for the *ortho* products (**38**A,B), or the proton at position 3 for the *meta* products (**38**C,D) (Appendix B.9). However, only one of the possible stereoisomers (*endo* or *exo*) of the *meta* DA products (**38**C,D) shows this characteristic coupling, suggesting that either the *endo* or *exo* product should have a dihedral angle of $\sim 90°$ between the hydrogens at position 1 and 3 resulting in the absence of this coupling.[56] Looking at our optimised DFT structures, we indeed see a dihedral angle of 84° for the *exo*/*meta* product (**38**D), whereas the *endo*/*meta* (**38**D) has an angle of 46°, allowing for the distinction of these products. Furthermore, the NMR signal of the proton at the 3 position is significantly shifted downfield (**38**A,C) in both *endo* products (**38**A,C) with respect to the *exo* products (**38**B,D), making it easy to distinguish between *endo* and *exo* for this proton. By correlating the proton at the 3 position to the 1 position via the protons at the 2 position in the COSY, we were able to also distinguish between *endo* (**38**A) and *exo* (**38**B) *ortho* product.

Further support for the assigned DA products came from GC-MS analysis of the crude products following hydrogenation (Pd/C, H_2).[20] This showed the presence of four peaks with similar retention times and the same molecular ion peak (m/z=186), as expected for the hydrogenated DA products (Figure 2.5 b). It should be noted that hydrogenation was required prior to GC-MS analysis due to the facile retro-DA reaction at elevated temperatures (as required for GC-MS).

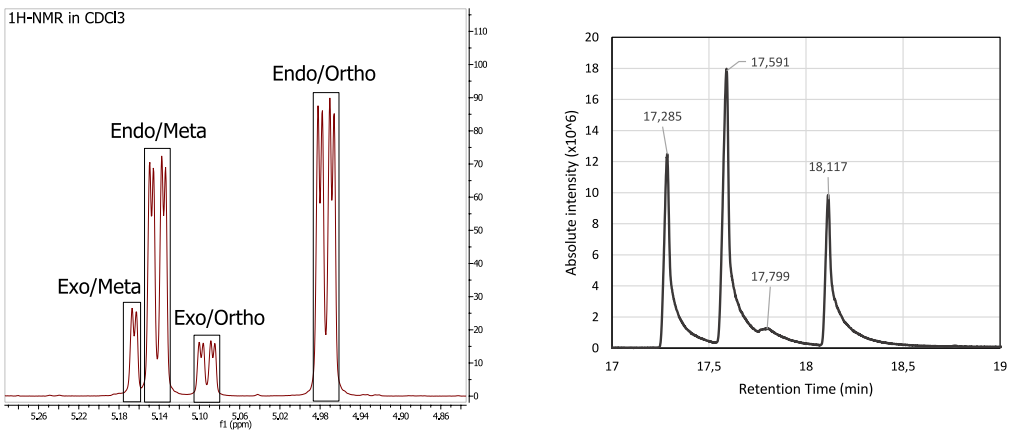

(A) Characteristic NMR peaks

(B) GC-MS signals of hyd. DA products

FIGURE 2.5: NMR and GC-MS data on DA products of FuAl and MeAc (**38**A-D). **A**: NMR results were obtained after 4 hours of reaction at 70 °C. **B**: GC-MS TIC chromatogram of hydrogenated DA products.

Time experiments of FuAl and MeAc DA reaction

To get a better understanding of the DA equilibrium and the selectivity for the different DA products, especially the different regioisomeric products (*ortho* and *meta*), the reaction of FuAl (**11**) and MeAc (**27**) was followed in time by quantitative ^{1}H-NMR (Figure 2.6 a) using nitrobenzene as an internal standard (IS). The total DA product yield at equilibrium was calculated to be 23 % after 71 h at 60 °C, with 94

% selectivity with respect to FuAl (**11**). The selectivity based on MeAc (**27**) conversion was however lower (31 %). This might either be explained by polymerisation of the dienophile or evaporation due to improper sealing of reaction vessels (boiling point MeAc (**27**) ≈ 80 °C). Since no side products could be detected by NMR analysis and the reaction mixture was homogeneous throughout the reaction, it was assumed that evaporation was the cause. However this was not confirmed by any additional experiments.

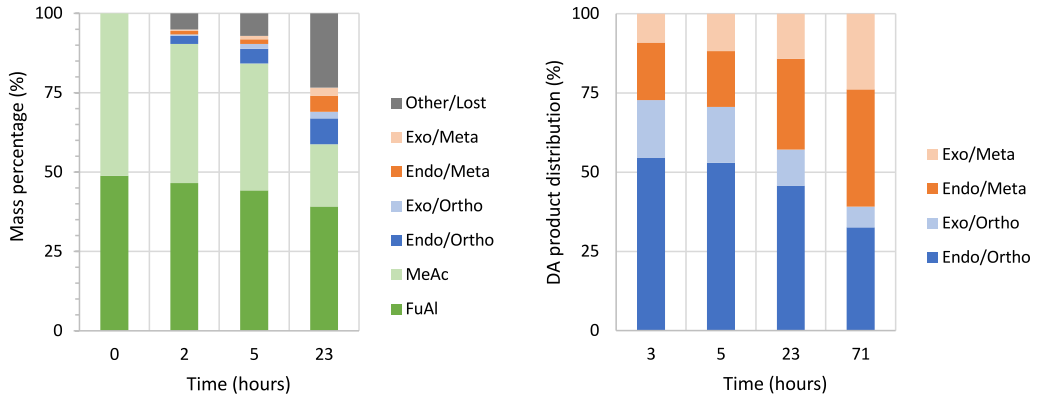

(A) Molar distribution (B) DA product distribution

FIGURE 2.6: Time course experiment of DA reaction of FuAl (**11**) and MeAc (**11**) at 60 °C with nitrobenzene as IS. **A**: Mass of FuAl and MeAc were normalised to 1 and mass of all DA products to 2. Mass percentage is calculated with respect to the total normalised mass (FuAl and MeAc combined) at 0 hours. Note that the mass percentages for the DA products represent their yield. **B**: DA product distribution followed in time. For a specific DA product its percentage is calculated with respect to total DA product at the specific point in time.

Interestingly, the ratio of *ortho*:*meta* DA product (**38**) changed from 70:30 after 3 h to 40:60 after 72 h (Figure 2.6 b). Both *endo* (**38**A) and *exo* (**38**B) *ortho* DA product show a decrease with respect to the total DA product overtime, while both *endo* (**38**C) and *exo* (**38**D) *meta* product increase. One explanation for this is that the *ortho* product is kinetically favoured over the *meta* product, but not thermodynamically. This is supported by our calculations in which we found that the activation energy for forming the *ortho* DA products (**38**A,B) was typically about 3.5 - 4.5 kcal/mol lower than for the *meta* products (**38**C,D) (Appendix A, Table A.2). As explained before, this kinetic preference could be explained by stabilisation of the *ortho* transition states through hydrogen bonding effects (Figure 2.4). Furthermore, the product energies were calculated to be very similar except for the *exo*/*ortho* product (**38**B), which was 2-3 kcal/mol higher in energy than both *meta* products (**38**C,D). This result is consistent with the experimental observations of product ratios at longer reaction times (71h), with the *exo*/*ortho* (**38**B) product being the minor product of the four and the others being more or less equally distributed (Figure 2.6 b). Alternatively, preferential degradation of the *ortho* products (**38**A,B) could result in the same change in *ortho*:*meta* ratio.

Additionally, the *endo* products (**38**A,C) are favoured over the *exo* products (**38**B,D) under these conditions. This effect is very pronounced for the *ortho* products (**38**A,B) but less so for the *meta* products (**38**C,D). The preferential formation of *endo* product

(**38**A,C) is also supported by our calculations, in which the activation energy associated with the formation of the *exo* product (**38**B,D) is 1 kcal/mol higher than for the *endo* one, for both *ortho* and *meta* product (Table A.2). The extra preference for *endo* in the *ortho* products (**38**A,B) can be explained by the fact that the *exo* product (**38**B) was calculated to be 2-3 kcal/mol higher in energy than the *endo* product (**38**A), whereas both *meta* products (**38**C,D) are similar in energy (and similar to *endo*/*ortho*).

To see the effect of temperature on the yield and distribution of the products, the same reaction was conducted at RT. The total DA yield was however only 6 % after 72 hours compared to 23 % at 60 °C. For extended reaction times (168 h) at RT the yield increases to about 10 %. No further time points were taken because the reaction was deemed impracticable due to its slow rate. However, it has to be noted that the equilibrium yield might not have been obtained yet and the yield is therefore potentially higher. Interestingly, at this lower temperature, the *ortho* products (**38**A,B) are even more favoured, with an *ortho*:*meta* ratio of 73:27 after 168 h, consistent with our hypotheses of this being the kinetic product.

Due to the difficulty in purifying these compounds (**38**) and their potential to undergo retro-DA reactions upon storing, we decided to focus on trying to increase the yields of these products with the intention to then use them immediately as an inconsequential mixture of isomers in the aromatisation reaction.

$Sc(OTf)_3$ catalysis at lower temperatures

Shiramizu et al.[15] have shown for acrolein (**24**) and dimethylfuran (**14**) that high yields (84 %) of cycloadducts can be obtained at sub ambient temperatures (−60 °C) and long reaction times (68.5 h), using lewis acidic scandium triflate ($Sc(OTf)_3$) as a catalyst (Route C, Scheme 1.2). As explained before, they state that due to the negative entropy of the DA reaction, the reaction should be more efficient at these lower temperatures. This, of course, tends to lead to very slow reaction rates and so the use of a catalyst is crucial to lower the activation energy.

In a first attempt to increase the yield of the DA reaction of FuAl (**11**) and MeAc (**27**), the conditions used by Shiramizu et al. were tested. First, FuAl (**11**) and MeAc (**27**) were reacted neat at RT, instead of - 60 °C, in the presence of 8 mol % of $Sc(OTf)_3$, to test whether the reactants were stable under these conditions. Upon adding $Sc(OTf)_3$ to the mixture of substrates, the reaction mixture turned black within seconds. NMR analysis indicated no DA products but instead more than 50 % of FuAl (**11**) was consumed after 1-2 h. FuAl (**11**) is known to polymerise into a black cross-linked material, under acidic reaction condition and the free alcohol group is thought to play a key role in the mechanism of polymerisation.[44] Therefore FuAce (**36**) and 2-methoxymethylfuran (MMF, **39**) were used in an attempt to increase the stability of the diene.

The DA reaction of FuAce (**36**) and MeAc (**27**) without $Sc(OTf)_3$ (neat, molar ratio 1:1) yielded some DA product (< 3 %) at both 70 and 20 °C. Unfortunately, when 8 mol % ScTr was added at 20 °C the reaction mixture also immediately turned black and no DA Product was detected.

With MMF (**39**) and MeAc (**27**) the neat reaction at 20 °C with 8 mol % $Sc(OTf)_3$ yielded 14 % DA product (**40**) after only 3 hours compared to only 1-2 % yield without 8 mol % $Sc(OTf)_3$ (Scheme 2.5). There was however a fast conversion (60 %) of MMF (**39**) after 3 hours together with a fast formation of black insoluble material, indicating a poor selectivity of 23 % towards the DA products (**40**). For longer reaction times there was no significant increase in yield. When the catalyst loading was decreased, both the yield and selectivity decreased. Moreover, testing different

lewis acids such as zinc chloride and other triflate acids such as $Hf(OTf)_4$, $Yt(OTf)_3$, $In(OTf)_3$ and $Ga(OTf)_3$, gave no increase in selectivity or yield. Upon decreasing the reaction temperature to 0 °C, we saw a slight increase in yield to 19 % after 19h of reaction with similar selectivity. Additionally, increasing the amount of MeAc (**27**) to 500 mol % (at 20°C) increased selectivity to 36 % with a yield of 23 %.

Altough lower temperatures such as those employed by Shiramizu et al.[15] could have been tested for their increase in selectivity towards DA adduct, the sensitivity of FuAl (**11**), FuAce (**36**) and MMF (**39**) to lewis acids is still a major problem for these kinds of reactions. It was therefore decided to leave further investigation of these lewis acid catalysed DA reactions and focus on different ways of improving the yield.

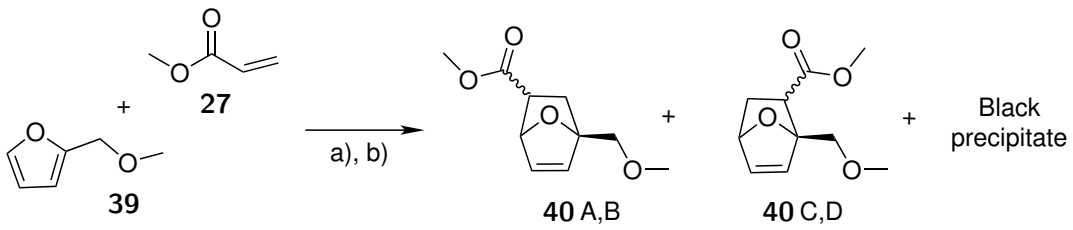

SCHEME 2.5: Catalysed DA reaction of MMF (**39**) and MeAc (**27**). **a)** $Sc(OTf)_3$ (8 mol %), **39**:**27** = 1:1, 0 °C, 19 hrs, neat, 19 %. **b)** $Sc(OTf)_3$ (8 mol %), **39**:**27** = 1:5, RT, 19 hrs, neat, 23 %

Activation of the dienophile

Since FuAl (**11**) (and derivatives) were shown to be unstable under the acidic conditions needed for catalysis, a different approach for increasing the DA yield was necessary. Tuning the reactivity of the diene and dienophile by means of substitution with electronrich and -deficient groups respectively, was thought to be a good method for this. Activation of the furanic diene by means of methyl substitution is however not possible, since this would result in producing different aromatic products then the aromatic diacids targeted in this thesis. For similar reasons the C3 acrylate group of the dienophile must be left unchanged as well. It was therefore decided to activate the ester group of the dienophile.

2,2,2-trifluorethyl acrylate (TFEAcr), the ester of acrylic acid (**18**) and 2,2,2-trifluoroethanol, is already used in literature as a highly electrondeficient dienophile for DA addition.[57,58] Using this activated dienophile instead of MeAc (**27**) would result in the same aromatic products after hydrolysis of the ester, making it a good candidate. Calculating the FMO gap for the DA reaction of this substrate with FuAl (**11**), as a measure of its reactivity, showed that it was a stunning 10 kcal/mol lower compared to FuAl (**11**) and MeAc (**27**). Moreover, the more electron deficient dienophile 1,1,1,3,3,3-hexafluoroisopropyl acrylate (**37**), showed an even greater decrease of 17 kcal/mol compared to MeAc (**27**) (Table 2.1). This dienophile, which is commercially available, was therefore chosen for further investigation and the DA reaction of FuAl (**11**) and HFIPAcr (**37**) was first trialled under similar conditions to those used for FuAl (**11**) and MeAc (**27**) (Scheme 2.6).

The DA reaction of FuAl (**11**) and HFIPAcr (**37**) (neat, molar ratio 1:1) was therefore followed in time at 20 and 70 °C (Figure 2.8). At 70 °C, NMR analysis showed that the equilibrium mixture of DA products (**41**) is already formed in about 4 hours (Figure 2.7 a). For longer reaction times both the yield and DA product distribution do not change significantly. Again, four isomers could be distinguished based on the

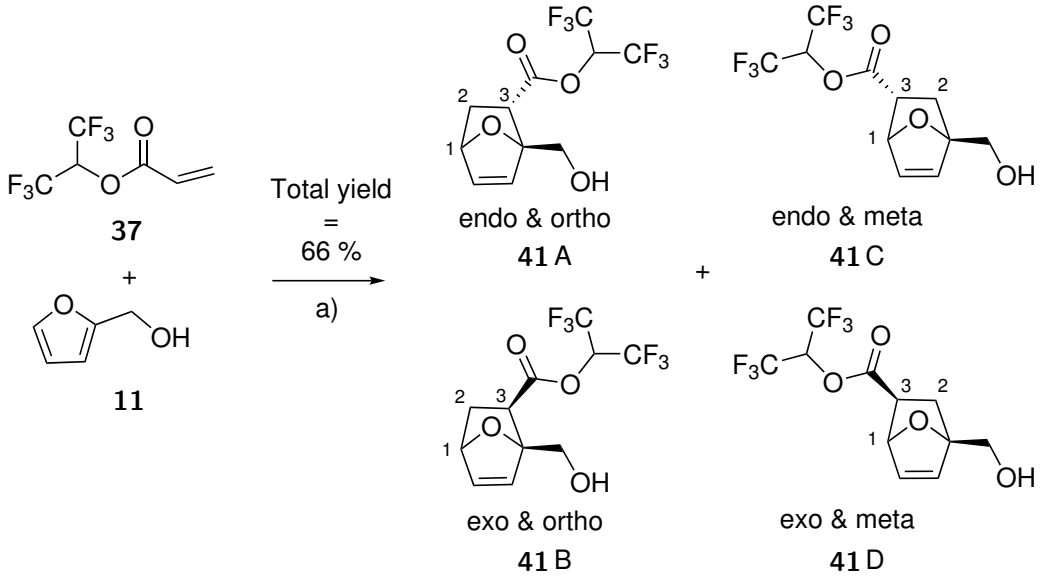

SCHEME 2.6: DA reaction of FuAl (**11**) with HFIPAcr (**37**). **a) 11**:**37** = 1:1, RT, neat, 22 hrs, 66 %.

characteristic NMR peaks (Figure 2.8 a) of the protons at position 3 (See Scheme 2.6 for numbering). Based on the integration of these peaks, the total equilibrium yield of DA products (**41**) was calculated to be 25 % (at 4 hours) with 100 % selectivity based on FuAl (**11**) conversion. The selectivity with respect to the dienophile HFIPAcr (**37**) was again lower (70 %). This difference can be explained by the same effects as discussed for the reaction of FuAl (**11**) and MeAc (**27**).

Interestingly, the DA equilibrium of this reaction was reached much faster than for the reaction of FuAl (**11**) and MeAc (**27**) at 70 °C (71 hours), as expected based on the increased reactivity of HFIPAcr (**37**). This is however only reflected partially by our calculations, which show a lower activation energy of about 1-3 kcal/mol for all isomers except for the *endo/ortho* product (**41**A) (Appendix A, Table A.2). This activation energy is only a minor 0.2 kcal/mol lower compared to the *endo/ortho* DA adduct of FuAl and MeAc (**38**A). Comparing the geometries of the DFT optimised transition states, it was clear that for the *endo/ortho* DA product of FuAl and HFIPAcr (**41**A), no internal hydrogen bond was present whereas for the similar FuAl and MeAc DA transition state (**38**A) it was present, as discussed before (Figure 2.4). It is expected that hydrogen bonding will stabilise the *endo/ortho* transition state of FuAl and MeAc and so the similar transition state of FuAl and HFIPAcr will not be stabilised in the same way, thus decreasing the energy difference of the two activation energies.

After 4 hours at 70 °C, the DA products distribution does not change over time and so it is believed that all the DA products (**41**) are in thermodynamic equilibrium. As seen for the reaction with FuAl (**11**) and MeAc (**27**), the *exo/ortho* product (**41**B) is again the minor product whereas the other products are approximately equally distributed. This is partially reflected by our calculations, which show the *exo/ortho* DA product of FuAl and HFIPAcr **41**B) to have the highest product energy (Table A.2). Additionally, the *endo/ortho* product (**41**A) is also calculated to be about 2 kcal/mol higher in energy than both *meta* products (**41**C,D), however this is not reflected in the product distributions. The reasons for this discrepancy are not clear at this time.

When conducting the DA addition at RT, the reaction is significantly slower, but

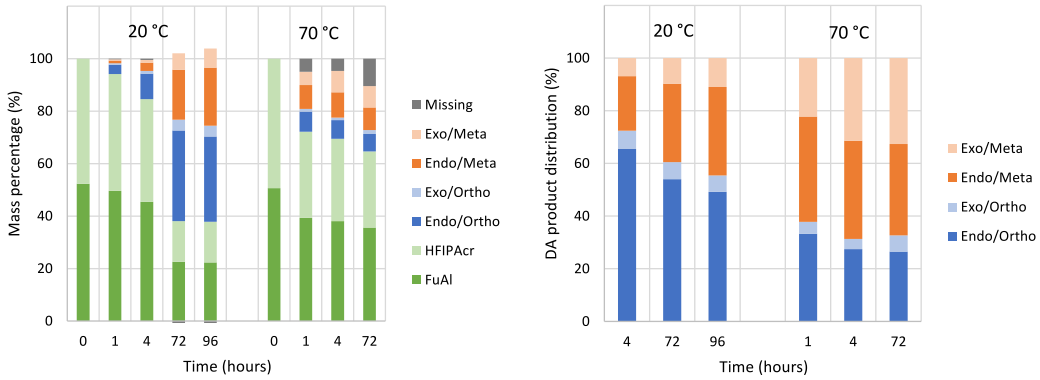

(A) NMR (B) GPC

FIGURE 2.7: Time course of DA reaction of FuAl (**11**) and HFIPAcr (**37**) at 20 and 70 °C. **A**: Mass of FuAl and HFIPAcr were normalised to 1 and mass of DA product to 2. Mass percentage is calculated with respect to the total normalised mass (FuAl and HFIPAcr combined) at 0 hours. Note that mass percentages for DA products are equal to yield. **B**: DA product distribution at different time point. For a specific DA product its percentage is calculated with respect to total DA product.

the total yield of products (**41**A) after 96 hours (at equilibrium) is 66 % (100 % selectivity with respect to both FuAl (**11**) and HFIPAcr (**37**)) which is significantly higher than the equilibrium yield at 70 °C (Figure 2.7 a). In general, the reaction entropy of the DA reaction is negative and therefore higher equilibirum yields at lower temperatures are expected, as was discussed before (2.2.1). This effect was not seen for the reaction of FuAl (**11**) and MeAc (**27**) at 20 °C, presumably because of the slow reaction rate.

At RT, the *ortho* products (**41**A,B) are kinetically favoured, as illustrated by the decrease in ratio of *ortho*:*meta* products from 73:27 after 1 hour to about 55:45 after 96 h (Figure 2.7 b). The computed activation energies support this result by showing barriers that are 1 kcal/mol or higher for both *meta* products (**41**C,D) (Table A.2). This result is also consistent with what was found in the reaction of FuAl (**11**) and MeAc (**27**) (Figure 2.6 b).

In order to characterise all the products, purification was attempted in the same manner as for the DA products of FuAl and MeAc (**38**). Starting from the crude reaction mixture obtained by reacting FuAl (**11**) and HFIPAcr (**37**) overnight at 20 °C, excess HFIPAcr (**37**) was removed by means of rotary evaporation. Attempts to separate the isomers by means of silica gel column chromatography only partially succeeded as only one out of four DA products was seperated into a pure fraction (Figure 2.8 a). NMR analysis indicated that this fraction consisted of only *endo*/*ortho* DA product (**41**A) with a small amount of FuAl (**11**) (Appendix B.10). High resolution mass spectrometry was performed on this fraction to confirm the mass and molecular formula of the product, however unfortunately this was not succesful. The rest of the isomers could be distinguished based on similar 2D NMR COSY analysis as was done for FuAl (**11**) and MeAc (**27**) (Appendix B.11).

Furthermore, as for FuAl (**11**)and MeAc (**27**), the crude DA mixture was hydrogenated (**42**) in order to confirm the mass of the DA adducts by GC-MS. Only three peaks with similar retention times were observed, all having the same molecular ion peak (m/z=322) as expected for the hydrogenated DA products (Figure 2.8 b). It was

unclear what happened to the other DA adduct but judging from another peak with m/z=154 at a retention time of 17.72 minutes, it was suggested that one of the DA adducts lost a $(CF_3)_2CHOH$ group (HFIP, m/z=168) upon internal transesterification during hydrogenation.

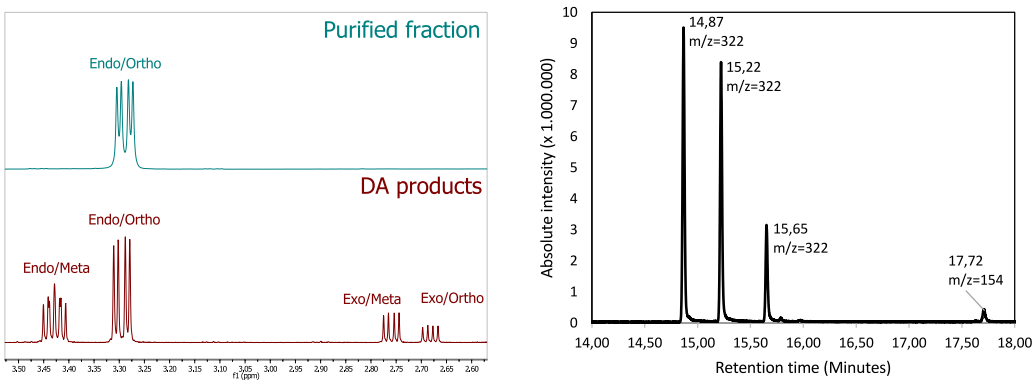

(A) NMR

(B) GC-MS

FIGURE 2.8: **A**: Characteristic NMR peaks of FuAl and HFIPAcr DA products (**41**A-D). DA products: all DA products present in reaction mixture (20 °C and 96h) before column chromatography. Purified fraction: Pure *endo/ortho* product after purification of reaction mixture using column chromatography. **B**: GC-MS results of hydrogenated DA products of HFIPAcr and FuAl.

Now that we were able to perform the DA reaction of FuAl (**11**) and HFIPAcr (**37**) with a reasonable yield of 66 %, it was decided to shift focus to the dehydration of these DA adducts (**41**) to give aromatised products. Since separation of the different DA products only partially succeeded, the DA adducts of FuAl and HFIPAcr (**41**) were directly aromatised as an inconsequential mixture of isomers.

2.2.2 Aromatisation of the DA products

Stability of the DA products

With DA products now in hand, investigation into the aromatisation reaction could commence. As detailed in chapter 1, such reactions can generally be grouped into two categories: low temperature methods using strong Brønsted acids[17,19] and higher temperature methods using zeolites.[13,27] Clearly the thermal stability of the DA adducts will play a large role in determining the most appropriate method for aromatisation. Therefore, the thermal stability of both MeAc and HFIPAcr product sets (**38**, **41**) was investigated.

For each DA combination, the mixture of partially purified DA isomers (mixture of the four isomers, no *exo/ortho* product (**41**B) for FuAl and HFIPAcr mixture) were dissolved in benzene-d_6 and heated at 60 and 80 °C in an NMR tube (Figure 2.9). Following the conversion of DA product over time it is apparent that for the FuAl and HFIPAcr adducts (**41**), temperatures of 60 °C already cause 40 % of total product to undergo retro-DA reaction within an hour, and at 80 °C this is already 75 %. This poses a big problem for aromatisation at elevated temperatures. For the DA products of FuAl and MeAc (**38**), temperature induced retro-DA reactions seems to be less of a problem. Still at 80 °C about 25 % and at 60 °C about 10 % of DA product is converted via retro-DA reactions within 4 hours. These results clearly indicate

that high temperature conversion routes should be avoided unless the aromatisation reaction is sufficiently fast so as to negate the impact of retro-DA reactions.

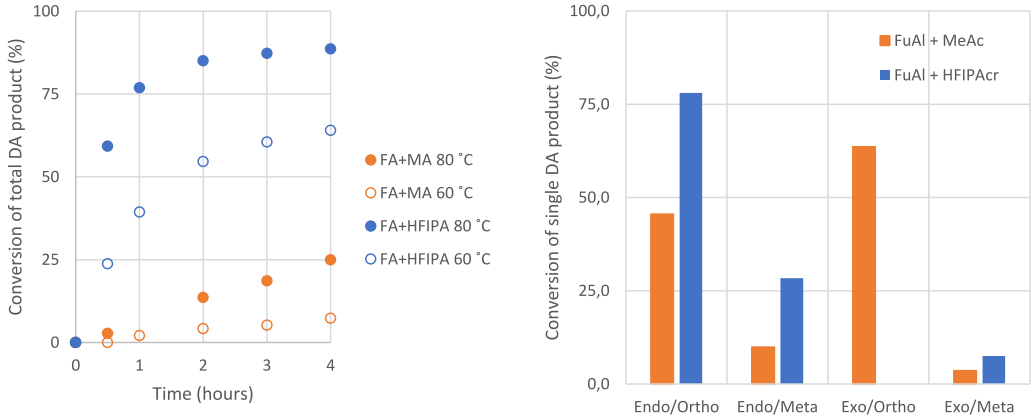

(A) Total degradation (B) Selective degradation

FIGURE 2.9: Stability time course of isolated DA products of FuAl and MeAc/HFIPAcr at 60 and 80 °C in benzene-d_6. **A**: Conversion of all DA products over time. **B**: Conversion for each of the DA products with respect to the initial amount of product for that isomers. Conversions are calculated after heating the FuAl/HFIPAcr and FuAl/MeAc DA products at 60 °C for 1 and 22 hours respectively.

Looking more closely at the degradation of each of the individual DA adducts, it can be seen that the *ortho* products are preferentially degraded over the *meta* products (Figure 2.9 b) and the *endo/meta* product is preferentially degraded over the *exo/meta* product, for both DA combinations (**38**, **41**). For the *ortho* DA adducts of FuAl and MeAc (**38**A,B), we observe the opposite with the *exo* being preferentially degraded over the *endo* product. The *exo/ortho* DA adduct of FuAl and HFIPAcr (**41**B) could not be purified and therefore no degradation data on this compound could be obtained.

In order to compare these experimental results to our computational results, the activation energies for all of the retro-DA reactions were calculated ($\Delta G_r^{\ddagger}$, Appendix A). It was expected that the isomers that preferentially degrade over others should also have a lower retro-DA activation energy. Since both the forward and retro-DA reaction take the same path and go through the same intermediate, the activation energy of the retro-DA reaction could easily be calculated by substracting $\Delta_r G$ from $\Delta G^{\ddagger}$ of the forward reactions. Comparing the results, it was found that isomers that showed lower activation energies, also showed a slower degradation (Table A.2). Moreover, the activation energies for retro-DA were typically lower for the FuAl and HFIPAcr DA adducts (**41**) compared to those of FuAl and MeAc (**38**), which also nicely fits the degradation profiles.

Aromatisation of the hydrogenated DA products

Given the relatively poor thermal stability of the cyclo adducts, initial aromatisation attempts followed the example of Thiyagarajan et al.[20] For the DA reaction of methylfuran (**13**) and maleic anhydride (**17**), they showed a significant increase in the stability of the DA products by irreversibly hydrogenating its double bonds. They were then able to aromatise these hydrogenated adducts in the presence of Brønsted acidic zeolite and Pd/C at 200 °C. Because HFIPAcr (**37**) is highly activated

and expected to be very reactive, it was decided to trial this aromatisation method on the DA adducts of FuAl and MeAc (**38**) first. Thus, the mixture of isolated DA products were first hydrogenated as described earlier (Pd/C, THF, H_2, 1 atm) to increase their thermal stability and subsequently their aromatisation in the presence of Pd/C and a zeolite catalyst was attempted.[20]

First, the aromatisation of the hydrogenated adducts (**43**) was trialled in toluene at 100 °C (compared to 200 °C in literature) with 10 wt % HVUSY (Si:Al = 30, calcined) and 6 wt % Pd/C (5 wt % metal on carbon)[20] yielding a complex mixture of products after 24 hours. Only 3-formyl benzoic acid (**44**) could be clearly assigned as a product by NMR and GC-MS analysis (Appendix B.12). The majority of the other products were unidentifiable by either NMR or GC-MS. Other experiments at 150 °C in toluene and neat at 150 °C and 200 °C did not yield any more promising results. Given the poor performance of this methodology in this particularly system, alternative aromatisation methods were investigated.

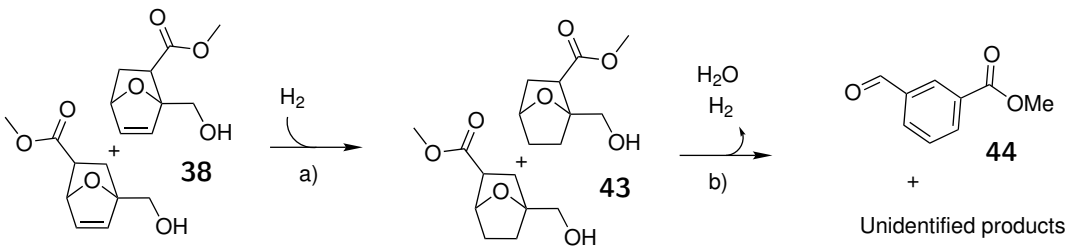

SCHEME 2.7: Aromatisation of hydrogenated DA product of FuAl and MeAc. **a)** Hydrogenation of **38** in THF with 1 wt % Pd/C in 1 atm of H_2 at RT.**b)** Hydrogenated products in toluene with 10 wt % HVUSY (Si:Al = 30) and 6 wt % Pd/C (5 wt % metal on carbon) at 100 °C for 24 hours.

Ac_2O assisted acid catalysed aromatisation of the DA products

Mahmoud et al.[19] have reported highly efficient aromatisation conditions for the DA adduct of furan (**12**) and maleic anhydride (**17**) (Route A, Scheme 1.2). In their work, mixtures of MSA and Ac_2O (**45**) (5,63 : 1 molar ratio) were shown to convert the furan/maleic anhydride DA adduct to an acetylated intermediate at RT. This intermediate is then converted slowly to phthalic anhydride at 80 °C, giving a final aromatisation yield of 80 %.

When these conditions were tranferred to the aromatisation of the crude mixtures of FuAl and MeAc DA adducts (**38**) (distilled only), the reaction mixture immediately turned black. Upon stirring at RT for 2h it was clear that all DA products were converted. Subsequent heating at 80 °C for another hour yielded only one product. After work up it was clear from NMR analysis this product was phthalide (**31**). Surprisingly, no products originating from the *meta* DA adducts (**38**C,D) were detected. *In-situ* quantification of phthalide (**31**) showed a yield of only 18% with respect to the total amount of precursor DA adduct (**38**) and 33 % with respect to the total amount of *ortho* product (**38**A,B) - the only one which can give phthalide (**31**).

Using the same conditions for the crude mixture of FuAl and HFIPAcr DA adducts (**41**), again phthalide (**31**) was observed as the only aromatisation product (Scheme 2.8). The yield was calculated to be 40 % relative to the total precursor DA product (**41**) and 67 %, relative to the total amount of *ortho* DA products (**41**A,B). Just as for the FuAl and MeAc adducts (**38**), the reaction mixture turned black immediately after

addition of the DA products. When the DA adducts (**41**) were aromatized in pure MSA, the yield of phthalide (**31**) was significantly lower, namely 10 % with respect to total (**41**) and 16 % with respect to *ortho* DA adduct (**41**A,B), showing that the addition of Ac_2O (**45**) has a significant positive effect on the total yield, as was also observed by Mahmoud et al.[19]. Since NMR analysis did not show any other products or remaining DA substrates, it was assumed that the other isomers were lost to non-specific degradation reactions.

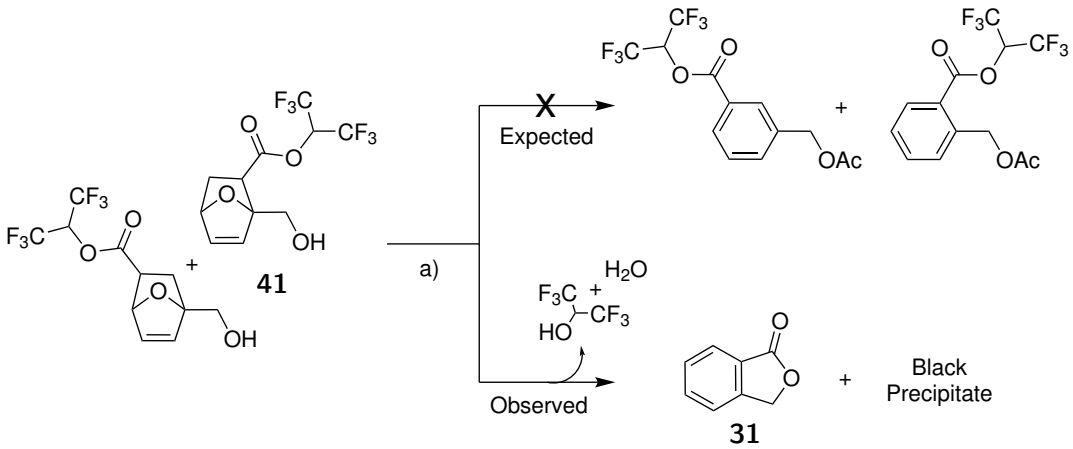

SCHEME 2.8: Aromatisation of DA product of FuAl and HFIPAcr (**41**) using mixtures of MSA and Ac_2O a) MSA:Ac_2O = 5.63:1 (1.2 M), RT for 2 hours then 80 °C for 1 hour.

Overall, this 2-step approach served as a useful proof of concept, allowing us to access the targeted product, phthalide (**31**), from FuAl (**11**) and a simple acrylate. Unfortunately, based on the maximum yields obtained for each step the yield of phthalide (**31**) is just 27 %, based on initial FuAl intake. Clearly this route was not fit for purpose and so a modified route needed to be developed.

Interestingly, the results from the MSA/Ac_2O aromatisation reactions helped to guide the rational design of a new approach. In particular, the lack of (acetylated) non-lactonised products suggested that lactonisation might play a key role in the success of the reaction, and if this pathway can be promoted then improved yields should be obtainable. This was already illustrated by the higher yields observed for the aromatisation of the adducts of FuAl and the activated ester HFIPAcr (**41**) as compared to MeAc (**38**), a dienophile which is less activated towards lactonisation. With the DA reaction being in dynamic equilibrium we did not believe there was significant scope to optimise the reaction towards the formation of exclusively the *ortho* products, as required for lactone (**30**) formation. It was therefore postulated that if a selective lactonisation step could be coupled to the DA reaction, rather than the aromatisation reaction, then the required selectivity and improved yields might be obtainable. The key to this is that *in-situ* lactonisation of the *ortho* product(s) effectively traps *ortho* product bringing it out of the equilibrium process. According to Le Chatelier's principle, on going equilibration of the DA substrates/products should eventually lead to an accumulation of the lactone (**30**) product. Attempts to put this proposal Scheme 2.9 into practice are discussed in the following section.

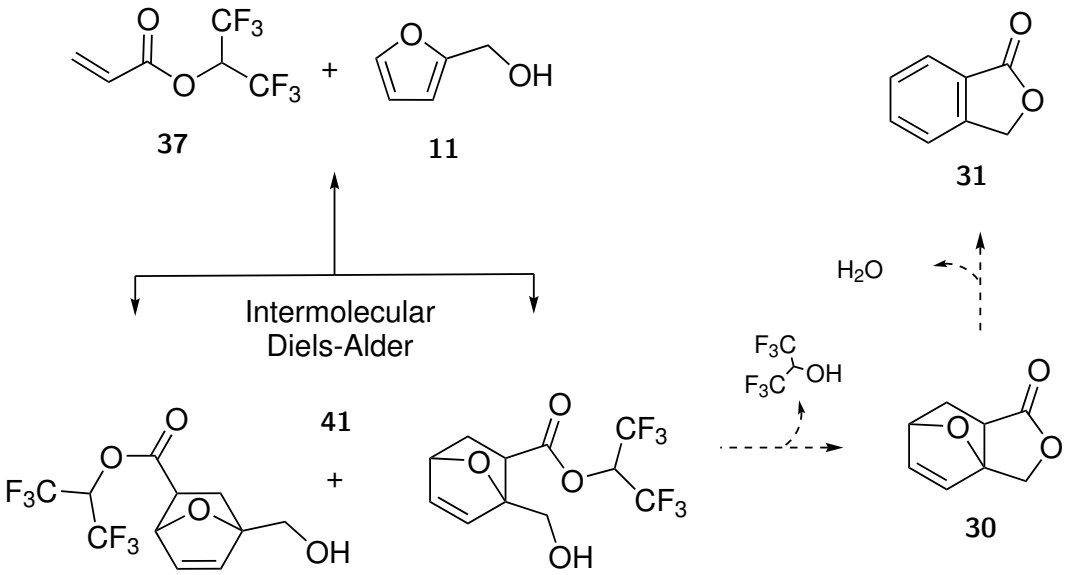

SCHEME 2.9: Proposed new route for synthesis of phthalide (**31**)

2.3 Synthesis and aromatisation of lactonised DA product

2.3.1 Synthesis and characterisation of lactonised DA product

Section 2.2 of this thesis ended by proposing that several of the major limitations of our current approach could potentially be overcome by targeting the synthesis of the lactone (**30**) by a 2-step, 1 pot approach. In particular, this approach should improve yields and selectivities in the DA reaction towards *ortho* products, thus negating the apparent inability to aromatise the *meta* products under the aromatisation conditions explored to date. However, in order to achieve this, modified reaction conditions would have to be developed which could fulfill a number of important criteria such as 1) promoting selective intramolecular lactonisation over intermolecular esterification, 2) allow fast and selective retro-DA reaction of non-lactonised DA products and 3) ensure the stability of starting materials and products.

Based on the results presented in 2.2, HFIPAcr (**37**) was again identified as the most promising dienophile for several reasons. By using an activated dienophile, the rate of forward and retro-DA reactions should both be increased compared to MeAc (**27**), as needed for successful implementation of a dynamic kinetic trapping approach. Additionally, HFIP esters are known to be activated towards nucleophilic displacement by e.g. amines,[59] which should facilitate lactonisation. It was envisage that either acid or base catalysis could be used to further promote the lactonisation, however as FuAl (**11**) is highly susceptible to acid catalysed polymerisation reactions, we decided to focus on base catalysis.

In order to establish a proof-of-concept for the lactonisation reaction, the crude mixture of FuAl/HFIPAcr DA adducts (**41**) was treated with 20 mol% $NaHCO_3$, at RT in $CDCl_3$ (Scheme 2.10). $NaHCO_3$ was chosen as a starting point as it is a weak base which we thought should not catalyse the intermolecular transesterification reaction, but may be sufficiently basic to catalyse the intramolecular reaction which we believed would be significantly facilitated by proximity effects. Gratifyingly, this reaction proved successful with one isomer being converted to a product which was assigned as the intended lactone (**30**B) based on detailed NMR analysis, together with the release of the expected HFIP. Based on our earlier calculations we would

have predicted that only the *exo/ortho* isomer (**41**B) of the DA products should be able to lactonise, based on the high product energy of the FuAcr *endo/ortho* DA adduct (**30**A) (Figure 2.3). Indeed, only one isomer is observed to react under these conditions (Figure 2.10 a). This clearly indicated that our new approach should be feasible, however due to to the relatively slow rate of the DA reaction at RT (96h to reach equilibrium), optimisation of the reaction conditions was needed to improve yields and productivity.

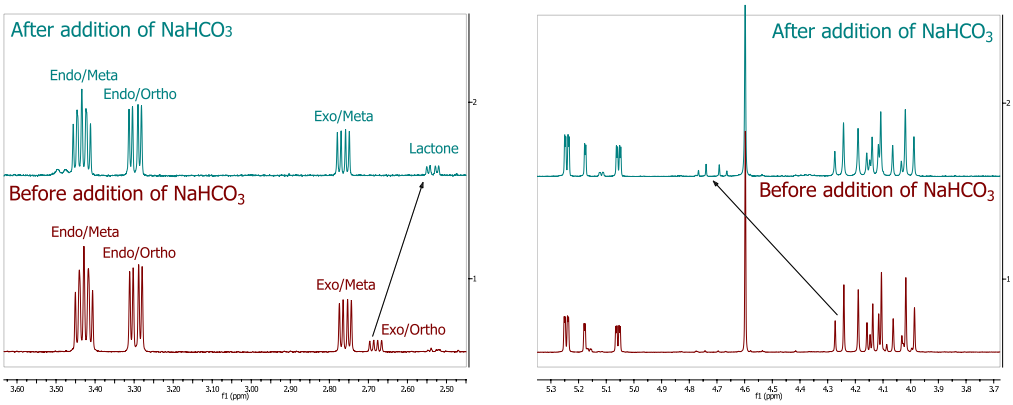

(A) (B)

FIGURE 2.10: Conversion of FuAl HFIPAcr exo/ortho DA product to lactone (**30**B): **A**: NMR zoom of the characteristic isomer NMR peaks. **B**: Deshielding of protons at position 1 (see Figure 2.11 for numbering).

Previously, it had been discussed how DFT calculations had shown that the transition state for the intramolecular DA reaction of FuAcr (**29**) had a prohibitively high energy, so as to make the reaction unfeasible (2.1.2). By considering the reverse reaction, i.e. the retro-DA reaction of lactone (**30**), it is possible to see that a similarly high activation energy is observed, suggesting that the lactone (**30**) should be much more thermally stable than the parent DA product(s). Indeed, looking at the activation energies of intramolecular retro-DA reaction, we see that for **30**B it is at least 3 kcal/mol higher than for any of the other intermolecular retro activation energies calculated (Appendix A). Therefore, a one-pot synthesis protocol was developed whereby a neat mixture of FuAl (**11**) and HFIPAcr (**37**) was heated at 80 °C in the presence of 2 mol% $NaHCO_3$ overnight. Gratifyingly, the crude reaction mixture from this experiment was found to contain predominantly the intended lactone (**30**) product, together with smaller amounts of FuAcr (**29**) as a side product. The crude products could be purified by column chromatography yielding a pure sample of lactone (**30**B) suitable for more detailed structural characterisation.

2D COSY and HSQC experiments allowed us to assign all peaks in the ^{1}H and ^{13}C spectra to the specific hydrogens and carbons of the lactone (**30**) (Figure 2.11 a). Interestingly, the protons at the 1 positions were shifted downfield significantly with respect to those of the *exo/ortho* DA adduct of FuAl and HFIPAcr (**41**B), consistent with a deshielding effect due to lactonisation (Figure 2.10b). From HMBC NMR experiments it was also clear that the hydrogens at position 1, coupled to the carbon at position 8. This coupling is only possible in the presence of an internal ester, confirming our hypothesis. From ESI-MS experiments we were then also able to confirm the mass (m/z = 327.0845) and molecular formula ($C_8H_8O_3$) of the lactone (**30**).

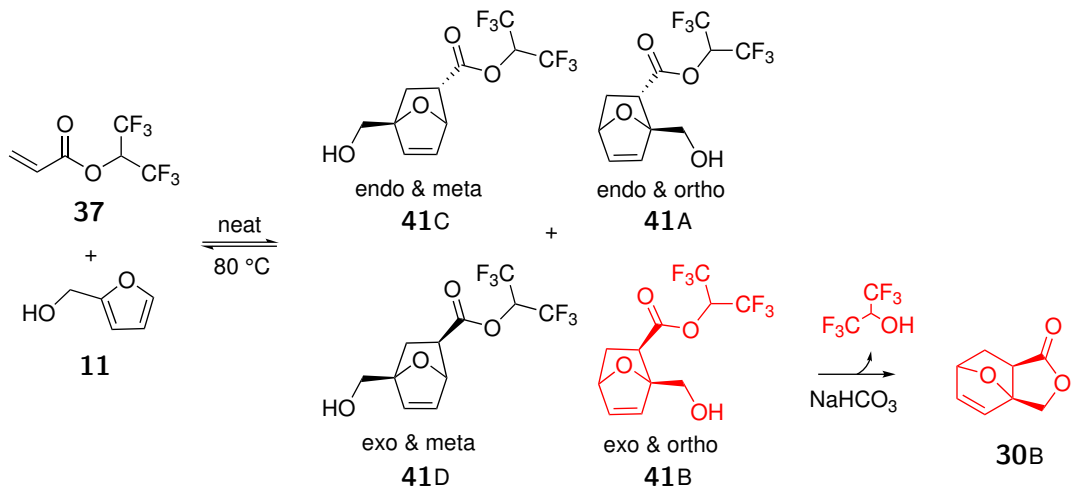

SCHEME 2.10: Selective production of lactone (**30**) from HFIPAcr and FuAl DA products mixture (**41**A-D) in the presence of $NaHCO_3$.

Finally, a crystal of lactone (**30**) suitable for single crystal x-ray diffraction analysis was obtained by slow evaporation from methanol. This analysis finally confirmed the assignment and relative stereochemistry of the product (Figure 2.11 b). This prompted us to look again at the analytical data reported by Babayan et al. for this compound[39]. Interestingly, the multiplets they reported at 3.82 ppm and 1.10-1.45 ppm in the ^{1}H-NMR, did not match with the chemical shifts we found for the same hydrogens (Figure 2.11 c) Furthermore, the melting point we found for the lactone (**30**) ($\sim$ 80 °C) is significantly different to that previously reported (119-121 °C). This, combined with the computational results demonstrating that the alternative *endo/ortho* lactone (**30**A) product is too high in energy to form (Figure 2.3 a), suggests that the previous assignment of lactone (**30**) product(s) is very unlikely to be correct.

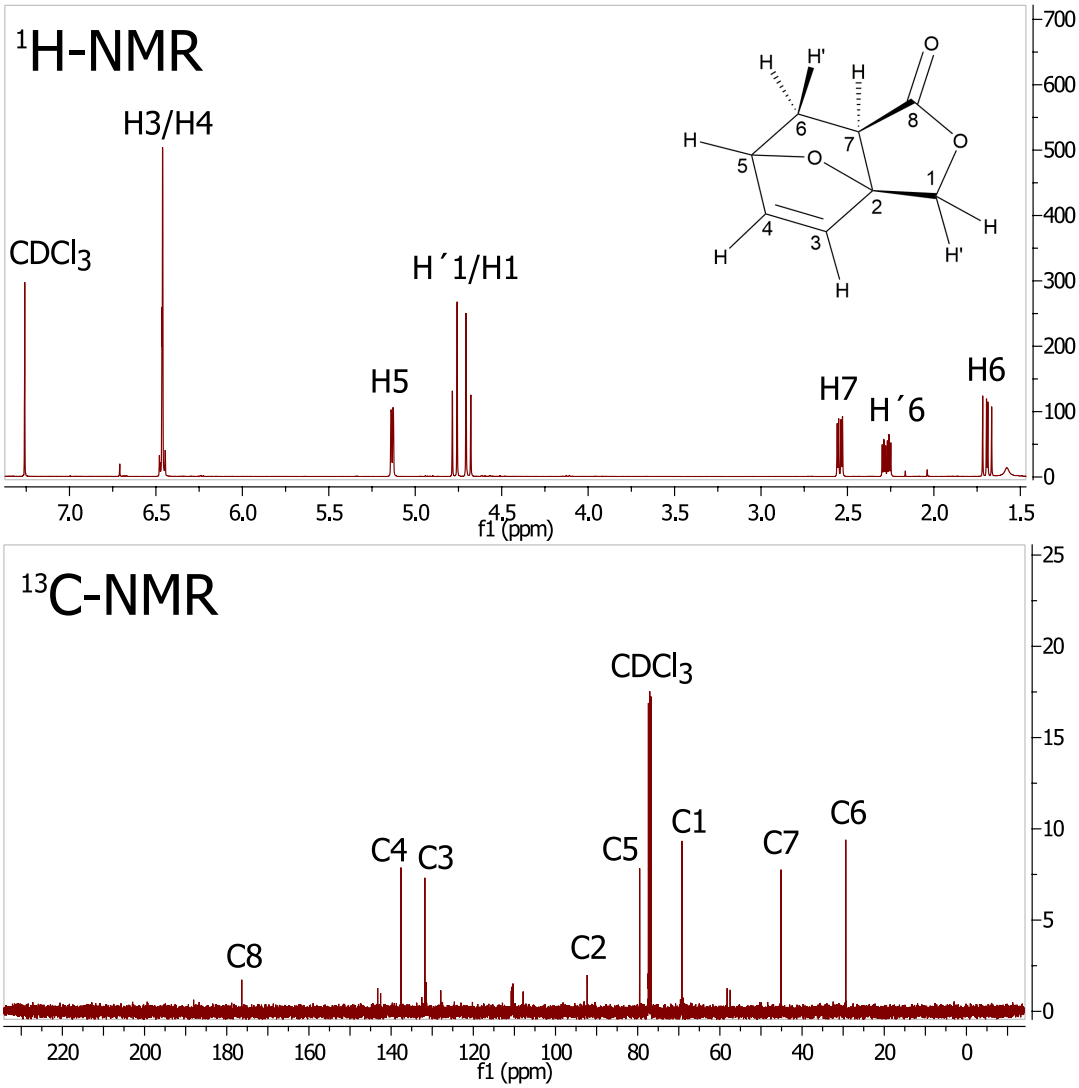

(A) NMR analysis of lactone (**30**)

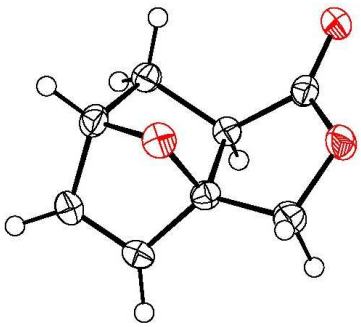

(B) Crystal structure

^{1}H-NMR Shift	Literature	Observed
H6 and H′6	1.10-1.45	2.28 and 1.70
H7	1.10-1.45	2.54
H1 and H′1	3.82	4.68-4.79
H5	5.12	5.13
H3 and H4	6.50	6.46

(C) ^{1}H-NMR Shift comparison

FIGURE 2.11: Characterisation of lactone (**30**): **A**: ^{1}H and ^{13}C NMR assignment. **B**: Single crystal XRC structure of lactone (**30**). Thermal elipsoid plot at 40 % probability. **C**: Comparison of ^{1}H-NMR chemical shifts reported in literature[39] and observed. Both ^{1}H-NMR spectra were measured in $CDCl_3$.

2.3.2 Stability of lactonised DA product

With some lactone (**30**) now in hand, its thermal stablity could now be investigated prior to aromatisation attempts. Heating the lactone (**30**) in DMSO-d_6 or toluene-d_8 allowed for its thermal stability to be assessed by ^{1}H-NMR based on its conversion, via retro-DA reaction, to FuAcr (**29**) (Figure 2.12). Comparing these results to those obtained for the DA products of FuAl and MeAc/HFIPAcr (**38**, **41** in 2.2.2) it becomes clear that the lactone (**30**) is much more thermally stable than any other DA product, as predicted based on our calculations (Appendix A). While the DA products (mixture of 4 isomers) of FuAl and MeAc (**38**) already show a conversion of about 25 % after 4 hours at 80 °C, the lactone (**30**) only shows a conversion of 9 % after 24 hours at 100 °C in DMSO, and 5 % conversion in toluene. Even the *exo/meta* DA product of FuAl and MeAc (**38**D), which was shown to be the most stable DA product (Figure 2.9 b), already has a conversion of 23 % after 22 hours at 80 °C and was therefore found to be much more unstable than the lactone (**30**). Interestingly, the rate of conversion of the lactone (**30**) was found to be faster in DMSO than in toluene. It is not understood what causes this solvent effect.

Increasing the temperature further, naturally leads to faster retro-DA reaction, however even at 120 °C, only 57 % conversion is observed after 24 hours. These results suggest that thermal instability is much less of a problem with the lactone (**30**) than it is with the other DA products (**38**, **41**), although certainly not absent and as such aromatisation conditions still need to be carefully considered going forward.

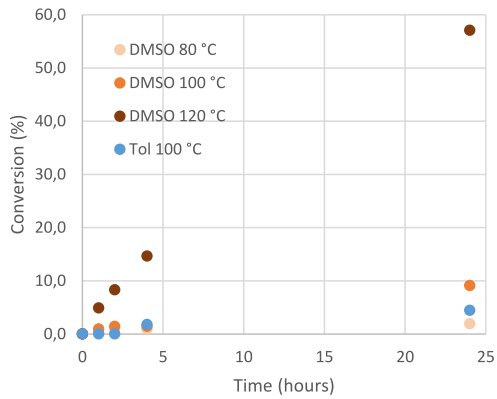

FIGURE 2.12: Conversion of lactone (**30**) into FuAcr (**29**) as measured from quantative ^{1}H-NMR analysis using nitrobenzene as internal standard. Reactions were done inside NMR tube in either DMSO-d_6 or toluene-d_8.

2.3.3 Optimisation of lactone synthesis

Lactone synthesis time series

In order to understand the reaction in more detail and to inform further optimisation attempts a NMR timecourse experiment was performed (Figure 2.13). This time course confirmed what was postulated before, showing that the lactone (**30**) gradually builds up during the reaction with a maximum yield of 56 % after 26 hours. In the beginning of the reaction (after 1.5 hours) the DA products of FuAl and HFIPAcr (**41**A,C,D) are also present. The *exo/ortho* product (**41**B) is however not observed,

showing that the rate of conversion into lactone (**30**) is faster than the rate of formation for this product. For longer reaction times the yield of the other DA products drop, since they are in dynamic equilibrium with the substrates which are consumed as the formation of the lactone (**30**) progresses.

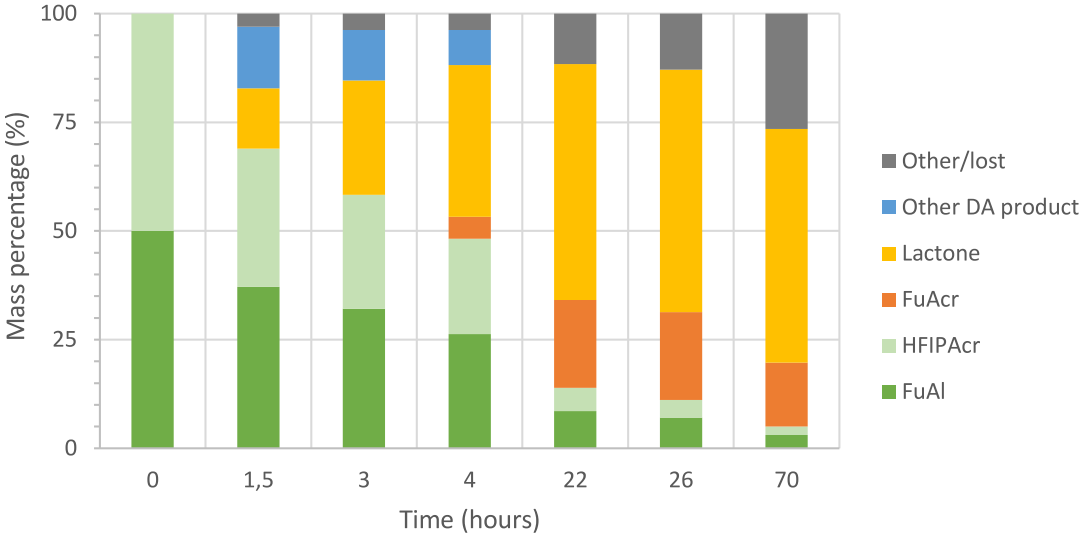

FIGURE 2.13: Timeseries of neat DA reaction of FuAl and HFIPAcr (1:1) in the presence of 2 mol % $NaHCO_3$ at 80 °C. Mass of FuAl and that of HFIPAcr were normalised to 1 and mass of lactone (**30**), DA products and FuAcr (**29**) to 2. Mass percentages are calculated with respect to the total amount of normalised mass (FuAl and HFIPAcr combined) at 0 hours. HFIPropanol was also formed in this reaction but is accounted for in the lactone (**30**) and FuAcr (**29**) mass. Note that mass percentages of lactone and FuAcr (**30**) are the same as yields.

NMR analysis also indicated that FuAcr (**29**) was the most prominent side product of this reaction. Some other minor side products were also noted in the NMR spectra and are thought to consist of acrylate conjugate addition products. This assignment is based on the appearance of pairs of characteristic aliphatic triplets in the ^{1}H-NMR. This is presumably due to one or a combination of FuAl (**11**), H_2O and DA products (**41**) adding to the HFIPAcr (**37**), possibly promoted by the presence of a base. Unfortunately, these products could not be isolated and characterised succesfully, and are therefore not displayed individually in Figure 2.13 but are thought to account for most of the other mass in this figure.

Another thing that became apparent was that the yield of lactone (**30**) plateaus after 22 hours, even though there is still DA substrate left in the reaction mixture (Figure 2.13). Extending the reaction time beyond 22 hours led to a lowering of the selectivity due to side product formation. The fact that no DA products (**41**) are visible in the NMR spectra after 22 hours may indicate that the equilibrium for the DA reaction had significantly shifted towards the starting materials, suggesting product inhibition in the reaction, possibly due to dilution effects.

Since FuAcr (**29**) was identified as the most prominent side product, the following section will focus on its formation. Furthermore a detailed screening of the reaction conditions will be conducted in an attempt to minimise its formation, increasing the selectivity towards the lactone (**30**).

FuAcr formation and the effect of base concentration on selectivity

FuAcr (**29**) can either be formed directly by transesterification of HFIPAcr (**37**) with FuAl (**11**) (route 1, Scheme 2.11) or by retro-DA reaction of the lactone (**30**) (route 2, Scheme 2.11). The possible contribution of route 2 was ruled out by stirring the purified lactone (**30**) in the presence of 20 mol % $NaHCO_3$ overnight at 80 °C (0.33M in $CDCl_3$), which yielded no FuAcr (**29**). Thus route 1 was thought to be responsible for the formation of this side product.

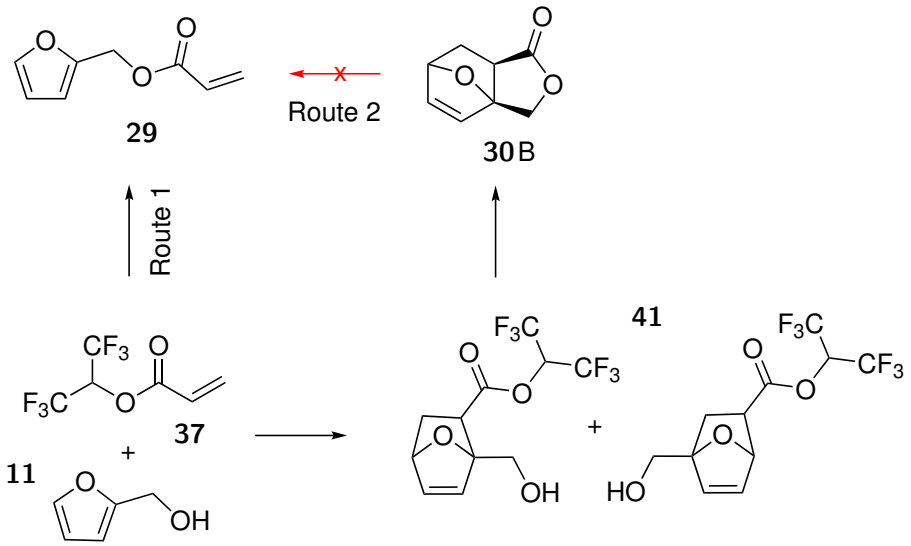

SCHEME 2.11: Routes to FuAcr (**29**) from FuAl (**11**) and HFIPAcr (**37**).

Since FuAl (**11**) and HFIPAcr (**37**) when reacted neat at 70 °C (Figure 2.7) did not produce any FuAcr (**29**), the transesterification reaction must be catalysed by $NaHCO_3$. The obvious place to start with regard to reaction optimisation was therefore the base. Firstly, as the earlier discussed time course experiment (Figure 2.13) showed that no detectable amounts of *exo/ortho* product (**41**B) are ever present in the reaction mixture, the $NaHCO_3$ loading should be able to be lowered without affecting the rate of the reaction for lactone (**30**) formation, but should slow the rate of formation of FuAcr (**29**) thereby increasing the selectivity of the reaction. Indeed, when the $NaHCO_3$ loading is lowered from 20 to 2 and to 1 mol %, we see an increase in the lactone (**30**) yield after 22 hours from 26 % to 64 %, whereas the yield of FuAcr (**29**) decreases from 52 to only 9 % (Table 2.2, entry 3 to 6). When the loading is lowered to 0.5 mol %, the FuAcr (**29**) yield decreases even further, yet the yield of lactone (**30**) does not increase but instead decreases to about 34 %. At this base loading, the catalysed intramolecular esterification of the *exo/ortho* product (**41**B) seems to become the rate limiting step in the formation of the lactone (**30**). This is confirmed by the fact that trace amounts of the *exo/ortho* DA product are again visible from NMR analysis at the low base loadings of 0.5 and 1 mol %, whereas at 2 and 20 mol % base they are not seen from NMR analysis.

Effect of base strength on selectivity

Due to the absence of proximity effects, it was hypothesized that the intermolecular esterification of FuAl (**11**) and HFIPAcr (**37**) would need a relatively stronger base catalyst than the intramolecular lactonisation of the *exo/ortho* product (**41**B). In this way tuning the strength of the base might increase the selectivity towards

TABLE 2.2: Yields and selectivities for the one-pot two-step production of lactone from FuAl (**11**) and HFIPAcr (**37**) as calculated from *in-situ* quantitative NMR analysis at 22 hours with respect to FuAl (**11**). The ratio of reactants was always 1:1 unless stated otherwise. [1]Dienophile was TFEAcr instead of HFIPAcr. [2] Dienophile was MeAc instead of HFIPAcr. [3] 50 mol % excess of HFIPAcr. [4]Concentration of substrates was 1.1 M. [4]Yield of lactone (**30**) and FuAcr (**29**) after 216 hours.

#	Solvent	Catalyst	mol %	T (°C)	Yield (%)	Selectivity (%)	FuAcr Yield (%)
1	Neat	$NaHCO_3$	2	60	34	43	26
2			20	60	17	20	50
3			0.5	80	38	70	3
4			1	80	64	82	9
5			2	80	54	66	20
6			20	80	26	28	52
7			20[1]	80	33	39	22
8			20[2]	80	2	8	6
9			1[3]	80	68	88	2
10		$NaCH_3COO$	2	80	44	55	26
11			20	80	23	27	50
12		$NaCHCl_2COO$	2	80	31	50	5
13			20	80	45	58	4
14		NEt_3	2	80	30	34	45
15	Ethylacetate[4]	$NaHCO_3$	2	80	43 (68[5])	83 (74[5])	7 (17[5])

only lactonisation. Since bases significantly stronger than $NaHCO_3$ are known to readily catalyse transesterification reactions (e.g. Na_2CO_3), the range of possible bases is relatively small. When CH_3COONa as well as its weaker chlorinated relative $CHCl_2COONa$ were tested, it was found that CH_3COONa performed slightly worse than $NaHCO_3$ with a 44 % yield and 55 % selectivity towards lactone (**30**), at 2 mol % (Table 2.2, entry 10). Moving to the even weaker base $CHCl_2COONa$ gave lower yields of FuAcr (**29**) at both 2 and 20 mol % of base, however the selectivity for the lactone (**30**) did not improve (Table 2.2, entry 12 and 13). Unlike for $NaHCO_3$, there were still some DA products visible from NMR analysis after 20 hours of reaction when using $CHCl_2COONa$, allowing for the possibility that the *exo/ortho* DA product is still formed in sufficient amounts and thus the yield may still increase for longer reaction times. However, no increase in yield was observed when this reaction was followed for longer times.

When triethylamine (NEt_3), a stronger base than $NaHCO_3$ was tested, it was found that the selectivity for the lactone (**30**) dropped and the selectivity for FuAcr (**29**) increased (Table 2.2, entry 14).

Although it appears that stronger bases certainly favour FuAcr (**29**) formation, it should be noted that the difference in solubility across these different bases makes it difficult to draw direct comparisons (i.e. on a mol% basis). For example $NaHCO_3$ appears to be essentially heterogeneous while NEt_3 is completely soluble in the reaction medium. Taking into account surface area for heterogeneous bases, may therefore be important for improving reproducibility.

Temperature effect of lactone selectivity

The reaction temperature affects many aspects of this reaction; increasing the temperature should increase the rate of all reactions (DA, lactonisation, transesterification, side reactions) and also shift the position of the DA equilibrium.

By decreasing the reaction temperature, it was envisaged that the rate of FuAcr (**29**) formation may be reduced relatively more than the rate of *exo/ortho* DA adduct (**41**B) production, which is the rate limiting step in the formation of the lactone (**30**) at [$NaHCO_3$] > 0.5 mol %. In this way, despite having to increase the reaction time, it was hoped that the selectivity towards the production of lactone (**30**) would increase. Unfortunately, when the reaction was performed at 60 °C with 2 mol % $NaHCO_3$, a decrease in the yield of the lactone (**30**) from 54 % to 34 % as well as a decrease in selectivity from 66 % to 43 % was however observed (Table 2.2, entry 1 and 5). Surprisingly, the formation of FuAcr (**29**) seems to be less temperature sensitive and, in fact, actually shows a slightly higher yield of 26 % at 60 °C compared to 20 % at 80 °C. The selectivity towards the lactone (**30**) therefore decreases at lower temperatures.

Higher temperatures (>80 °C) were avoided, since it was already shown that (irreversible) retro DA reaction of lactone (**30**) to FuAcr (**29**) starts to occur at these high temperatures (Figure 2.12). Moreover, at these temperatures $NaHCO_3$ starts to decompose to Na_2CO_3. 80 °C was therefore determined to be the optimum temperature for this tandem reaction.

Rate of lactone formation

Since the production of lactone (**30**) was found to stall around 64%, a reaction with a 50 mol % excess of HFIPAcr (**37**) was attempted in order to drive the DA reaction towards completion. Unfortunately, this gave little benefit with the yield increasing only from 64 to 68 % (Table 2.2, entry 4 and 9). On balance, a 1:1 substrate ratio was therefore found to be optimal.

Neat versus solution

The reaction was run in a solvent to see its effect on the selectivity of the formation of lactone (**30**). Ethylacetate was chosen as a solvent since it was found to dissolve all of the substrates and products of this reaction and is a relatively benign solvent. The results show that both the formation of FuAcr (**29**) and the lactone (**30**) is slower in a solvent, as one would expect for DA and trans-esterification reactions which are both second order reactions. When the reaction is followed for extended periods of time (216 h), the lactone (**30**) yield increases to about 68 %, which is higher than the comparable neat reaction yield of 54 % (Table 2.2, entry 5 and 15).

Different dienophiles

Lastly, less activated dienophiles were tested for their ability to produce the lactone (**30**) under the same conditions. These could in theory show a higher preference for lactonisation compared to intermolecular esterification because of their lowered activity. When MeAc (**27**) was tested at the same conditions (80 °C, 20 mol % $NaHCO_3$), it was found that hardly any lactone (**30**) or FuAcr (**29**) was produced and thus some activation of the ester was needed for lactonisation (Table 2.2, entry 8). Using a stronger base could potentially increase the rate of lactonisation, however it would also significantly contribute to side reactions and was therefore not tested. Using TFEAcr as a dienophile instead of HFIPAcr showed a higher yield of 33 % and selectivity of 39 % for the lactone (**30**) at 20 mol % $NaHCO_3$ after 22 hours, together with the selectivity for FuAcr (**29**) dropping significantly (Table 2.2, entry 7). Unfortunately, some *exo/ortho* product was observed during the reaction, even at a high base concentration of 20 mol %, indicating that the rate of lactonisation was rate determining and much slower than in the reaction of HFIPAcr. This would mean that a

decrease of base loading would significantly slow down the formation of the lactone (**30**). Testing this reaction at lower base loadings was therefore deemed impracticable and HFIPAcr (**37**) was found to work best for our purposes. It should also be noted that even though increasing the reactivity of the ester is thought to logically promote lactonisation and transesterification, the increased steric bulk of HFIP over TFE may also affect the relative rates of the two reactions.

To summarise, the selective one-pot two-step synthesis of the lactone (**30**) was found to work best at 80 °C with small amounts (1 mol %) of the weak base $NaHCO_3$. A maximum yield of 68 % with 88 % selectivity in 22 hours could be obtained at a substrate ratio diene:dienophile of 2:3. This proves that the lactone (**30**) can selectively be synthesised in a reasonable yield. Our focus therefore turned towards the aromatisation of this product into phthalide (**31**).

2.3.4 Aromatisation of lactone

Ac_2O assisted acid catalysed lactone aromatisation

Given the moderate thermal stability of the lactone (**30**), aromatisation was again attempted using the conditions of Mahmoud et al.[19] as used earlier for aromatisation of the DA products of FuAl and HFIPAcr (**41**) (Scheme 2.12). Addition of the MSA/Ac_2O mixture (5,63 : 1 molar ratio) to the lactone (**30**) at RT resulted in an immediate colour change to black. NMR analysis showed that the lactone (**30**) was fully converted within 10 minutes and the expected aromatisation product phthalide (**31**) was formed. Calculating the yield by *in-situ* quantitative NMR experiments, indicated a greatly improved yield of 75 % (Table 2.3, entry 1).

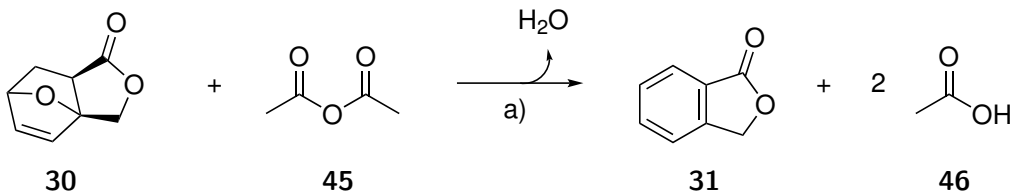

SCHEME 2.12: Aromatisation of lactone (**30**) to phthalide (**31**) a) MSA (0.5 eq.), Ac_2O (4 eq.), 80 °C, 1 hour, 97 %.

Since MSA (rather than Ac_2O) is expected to play a significant role in catalysing polymerisation side reactions, the molar ratio of MSA to Ac_2O was changed to 1:8 (0.5 eq. : 4 eq.) in order to make sure that only acetyl methanesulfonate and no free MSA was present in the reaction mixture. This reaction was followed in time and the results can be seen in Figure 2.14. When one equivalent of lactone (**30**) was added to this pre-stirred mixture at 0 °C no colour change and no lactone (**30**) conversion was observed based on quantitative NMR analysis. When the reaction mixture was warmed to RT, the lactone (**30**) was converted slowly overnight with the reaction mixture turning darker. NMR analysis after 21 hours indicated that phthalide (**31**) was formed in a 67 % yield together with two other products present in a combined 32 % yield. The temperature was then increased to 80 °C and after 1 hour, it was clear from NMR analysis that the two unidentified products had disappeared while the yield of phthalide (**31**) had increased to 97 % (Table 2.3, entry 2). This led us to propose that these two compounds were the reaction intermediates (structure discussed below). Furthermore, the almost quantitative yield of phthalide (**31**) compared to a yield of only 75 % in the case of molar ratio 5,63 : 1, suggests that free MSA is the

main cause for the formation of side products. Alternatively, doing the reaction at 0 °C instead of RT may also cause the improved yield.

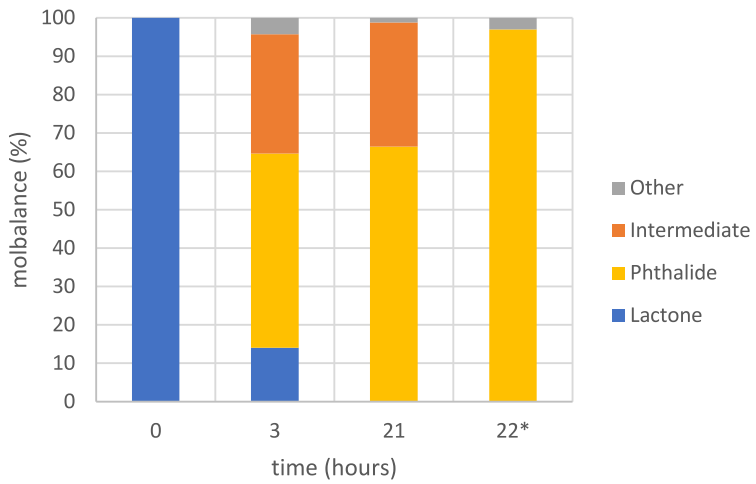

FIGURE 2.14: Timeseries of aromatisation reaction of the lactone (**30**) in 4 eq Ac_2O and 0.5 eq of MSA. Lactone (**30**) was added at 0 °C and then stirred at 20 °C. Amounts are calculated from quantitative NMR analysis. * After 21 hours the mixture was heated to 80 °C for one hour to convert all the products.

In an attempt to decrease the reaction time, the reaction was conducted by addition of the lactone (**30**) at RT and then immediate heating to 80 °C, with all other reaction conditions staying the same. When the lactone (**30**) was added to the mixture of MSA and Ac_2O at RT and stirred at 80 °C, the mixture turned black again during the course of the reaction. After 1 hour, the lactone (**30**) had been fully converted into phthalide (**31**) in a calculated yield of 98 % (Table 2.3, entry 3). Lowering the ratio of MSA:Ac_2O from 1:8 to 1:40 and even further to 1:200 (Ac_2O loading is 4 eq. for all reactions) resulted in an increase of the reaction time (2-20h), however similar yields of phthalide (**31**) could still be obtained (Table 2.3, entry 4). Leaving out MSA entirely, however resulted in no reaction.

To see if the reaction could also be performed with a solid acid catalyst, MSA was replaced with commercially available amberlyst-15 resin (hydrogen dry form). Based on information received from industrial collaborators the reaction was performed with a molar ratio of Amberlyst acid sites to Ac_2O of 20:1 in ethyl acetate (1 M) at 80 °C. Full conversion and a 89 % yield (calculated *in-situ*) of phthalide (**31**) was obtained within 2 hours (Table 2.3, entry 5). During the reaction no colour change of the reaction mixture was observed, however the amberlyst was black thus making it difficult to judge whether any black substance formed had been adsorbed. It also has to be noted that the amberlyst was not washed when calculating the yield so some phthalide (**31**) may still have been adsorbed on the catalyst. To see if the amberlyst resin could be reused it was washed with ethyl acetate and dried at 80 °C. The reaction was then run again with the same amberlyst resin yielding 80 % phthalide (**31**), indicating that recycling is indeed possible.

Characterisation of intermediates and Ac_2O assisted reaction mechanism

To better understand the underlying mechanism of the aromatisation reaction, isolation of the reaction intermediates was attempted from the MSA/Ac_2O reaction

run at RT. Unexpectedly, during workup one of the two intermediates was found to convert into a new product. Unfortunately, we were not able to seperate this new product from the other stable reaction intermediate by means of column chromatography. However, detailed NMR analysis of the semi-purified mixture together with comparison to the crude mixture, allowed us to tentatively assign both reaction intermediates. The new product formed during work-up was assigned as the monoacetate compound **48** (Appendix B.14). The other, stable, reaction intermediate was assigned as the diacetate compound **47** (Appendix B.13). Since *in-situ* ^{1}H-NMR (1D and COSY) analysis of the intermediates showed compound **47** to be very similar to the unstable intermediate, and since this intermediate seems to convert to compound **48**, the unstable intermediate was believed to be a diastereomer of compound **47**. Based on these findings the reaction was proposed to proceed following the mechanism in Scheme 2.13. Mahmoud et al.[19] proposed a similar mechanism for the aromatisation of the DA adduct of furan (**12**) and maleic anhydride (**17**) to phthalic anhydride (**20**) based on a structurally related diacetate intermediate that they found. Interestingly, they reported only one diasteriomer of the diacetate intermediate, however it should be noted that the structure of their intermediate was reported following work-up and column chromatography offering ample opportunity for decomposition of one intermediate.

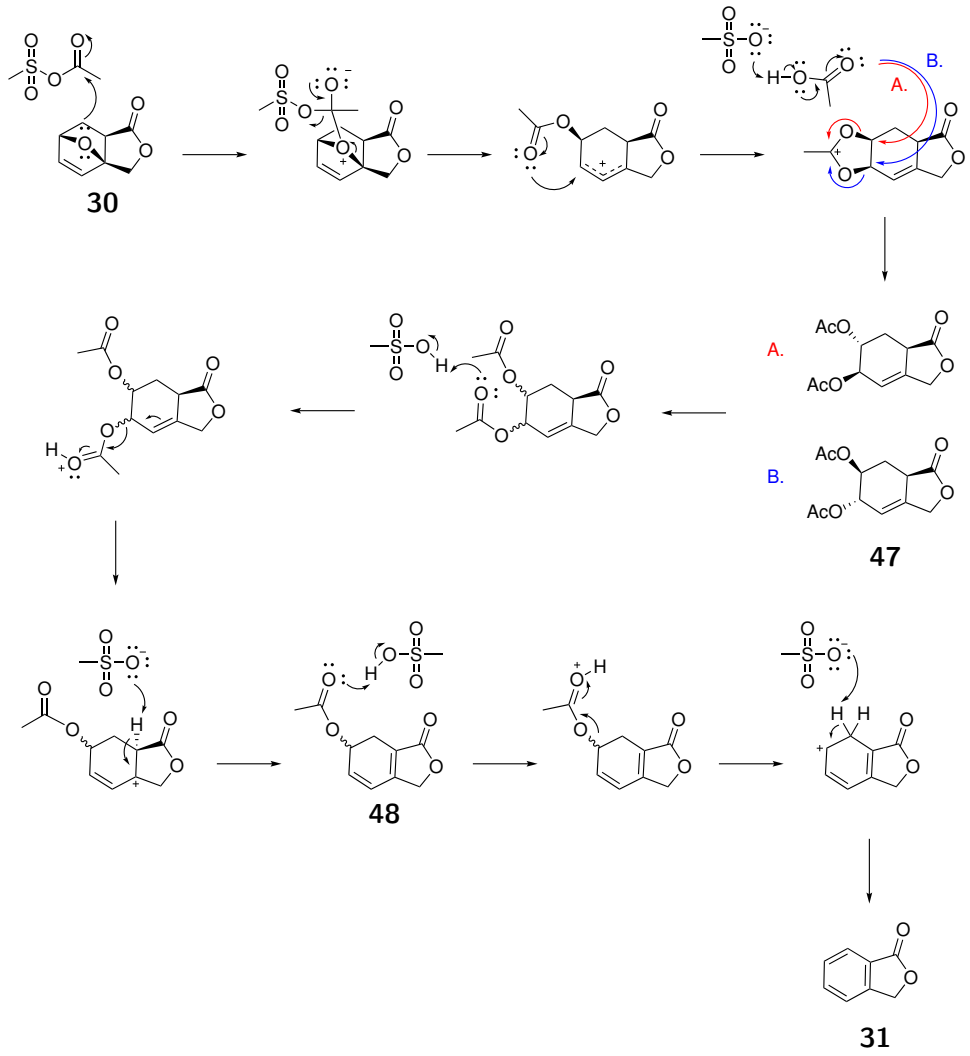

SCHEME 2.13: Proposed acid catalysed aromatisation mechanism of lactone (**30**) in the presence of Ac_2O based on mechanism reported by Mahmoud et al.[19]

Acid catalysed aromatisation

From the results above it is clear that the Ac_2O assisted acid catalysed aromatisation of the lactone (**30**) was found to produce phthalide (**31**) with almost full selectivity. This reaction however requires one equivalent of Ac_2O (**45**) which is converted to 2 eq. of acetic acid (**46**) during the reaction (Scheme 2.12). Although this can be recovered and either recycled or considered a co-product, clean aromatisation conditions without the use of Ac_2O (**45**) would, almost certainly, be economically preferred over the conditions used so far if similar yields and selectivities can be obtained.

As a starting point, the aromatisation conditions of Mahmoud et al.[19] were repeated, but leaving out Ac_2O entirely (Scheme 2.14). When the lactone (**30**) was added to the 1.2 M solution of pure MSA, substantial amounts of black insoluble precipitate were formed, indicating that polymerisation is occurring, probably either by direct polymerisation of lactone (**30**) or the intermediates formed during the aromatisation reaction. The *in-situ* NMR yield of phthalide (**31**) was calculated to be about 66 % after 10 minutes at RT compared to a 75 % yield when the conditions of Mahmoud et al. were used (Table 2.3, entry 1 and 6).[19] No other intermediates or side products could be detected. Interestingly, this difference in yield when omitting Ac_2O is far less pronounced than that observed previously for the DA adducts of FuAl and HFIPAcr (**41**), clearly indicating that the lactone (**30**) is much more amenable to aromatisation under acidic conditions. A slower rate of retro-DA and the decrease in polymerisation side reactions compared to the DA adducts of FuAl and HFIPAcr (**41**) are thought to play a crucial role here.

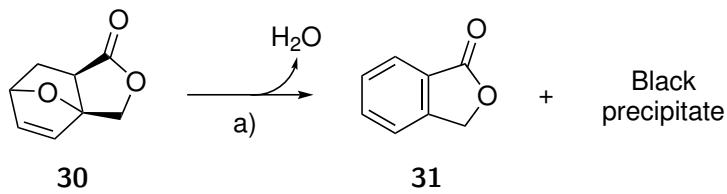

SCHEME 2.14: Aromatisation of lactone (**30**) to phthalide (**31**). a) MSA (1.2M), RT, 10 minutes, 66 %.

Since super stoichiometric amounts of MSA are thought to significantly increase the amount of polymerisation side reactions and are not applicable at a larger scale, it was decided to look at aromatisation using catalytic amounts of acid. Previously, lactone (**30**) had been dissolved in either Ac_2O or MSA but now when using catalytic amounts, a solvent was needed. Aromatisation of the lactone (**30**) in toluene-d_8 (0.33M, an inert solvent) was therefore attempted in the presence of 10 mol % MSA (Figure 2.15). When MSA was added to the lactone (**30**) solution at RT the mixture immediately turned dark and a black precipitate was formed. After stirring at 80 °C for 22 hours, the lactone (**30**) was almost fully converted (96 %) and the yield of phthalide (**31**) was calculated to be 66 % with a selectivity of only 68 % (Table 2.3, entry 7). Even though not all the lactone (**30**) was converted, the selectivity to phthalide (**31**) in this reaction was similar to the selectivity obtained neat in pure MSA (66 %). Interestingly, some trace amounts of acrylic acid (**18**) were detected as well after about 1.5 hours as judged by ^{1}H-NMR (discussed below).

Different acids were then tested in toluene to see how they compared to MSA. The stronger Brønsted acid, trifluoromethanesulfonic acid (TfOH), and the lewis acid hafnium trifluoromethanesulfonate ($Hf(OTf)_4$) both gave similar yields as MSA, yet full conversion was already reached after 1.5 hours for these acids (Table 2.3, entry 8 and 9). Lowering the concentration of TfOH to 1 mol % did not alter the results

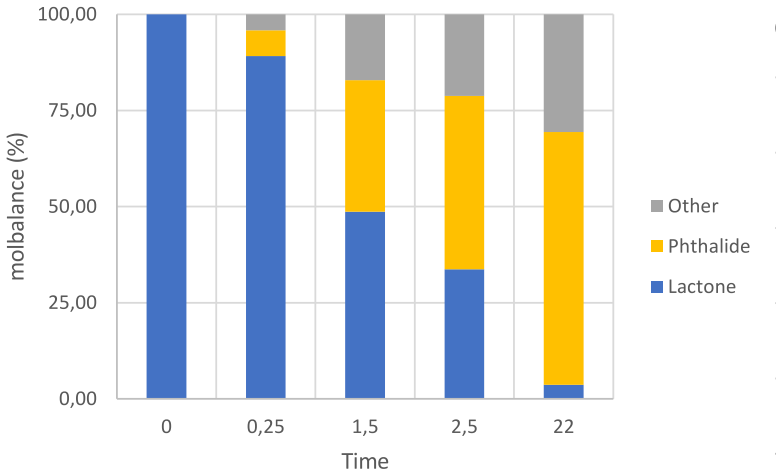

FIGURE 2.15: Timeseries of aromatisation reaction of the lactone (**30**) with 10 mol % of MSA as a catalyst in toluene-d_8 (0.33M). Lactone (**30**) was added at 20 °C and then stirred at 80 °C. Amounts are calculated from quantitative NMR analysis.

significantly and neither did a mixture of TfOH and $Hf(OTf)_4$ (Table 2.3, entry 10). Performing the reaction of 10 mol % TfOH in chloroform resulted in a surprising increase in yield to 79 % at full conversion, whereas a slight decrease in yield to 56 % was obtained when acetic acid was used as the solvent (Table 2.3, entry 12 and 13).

To compare the performance of a homogeneous catalyst with a heteregeneous catalyst, TfOH was adsorbed onto simple chromatographic silicagel according to literature procedures.[60] The obtained silica supported triflic acid (0.5 mmol/g) was then used as a heterogeneous catalyst for the aromatisation of the lactone (**30**). When 1 mol % of the silica was added to a lactone (**30**) solution (toluene), the silica turned black. After 1.5 hours at 80 °C the selectivity for phthalide (**31**) was only 58 %, while the selectivity of the unsupported TfOH was 64 % under similar reaction conditions (Table 2.3, entry 9 and 10). Other reactions with this system in which the solvent, acid loading and concentration of substrate was varied did not yield any higher selectivities towards phthalide (**31**) as compared to the non supported system. Then, in a last attempt at catalysing the aromatisation heterogeneously, the solid acid catalyst zeolite Y (ultra stable) was used. After mixing the lactone (**30**) and the zeolite (10 wt %) neat, the temperature was increased to 100 °C, thus melting the lactone (**30**). Even at this temperature NMR analysis after 3 hours indicated that the majority of the lactone (**30**) was recovered unchanged. There were however some trace amounts of phthalide (**31**) present from the NMR spectrum. It was nevertheless decided to not investigate this reaction any further due to the high temperatures needed.

Formation of black precipitate

As formation of the black insoluble material seems to be the reason for the drop in selectivity when using only acid catalysis, attempts were made to characterise this material and how it might form. Thus, the aromatisation reaction mixture of 10 mol % TfOH in $CDCl_3$ was filtered after the addition of the lactone (**30**) at RT and formation of the precipitate. The obtained transparent reaction mixture still contained some lactone (**30**) and so was heated to 80 °C, however no further conversion of lactone (**30**) was observed. This indicates that the solution phase of the reaction mixture

is no longer catalytically active in the aromatisation reaction. Surprisingly, when another equivalent of lactone (**30**) in $CDCl_3$ was added to the recovered precipitate and heated at 80 °C, full conversion was observed. Thus the black precipitate adsorbs the TfOH and serves as a supported acid catalyst during the reaction.

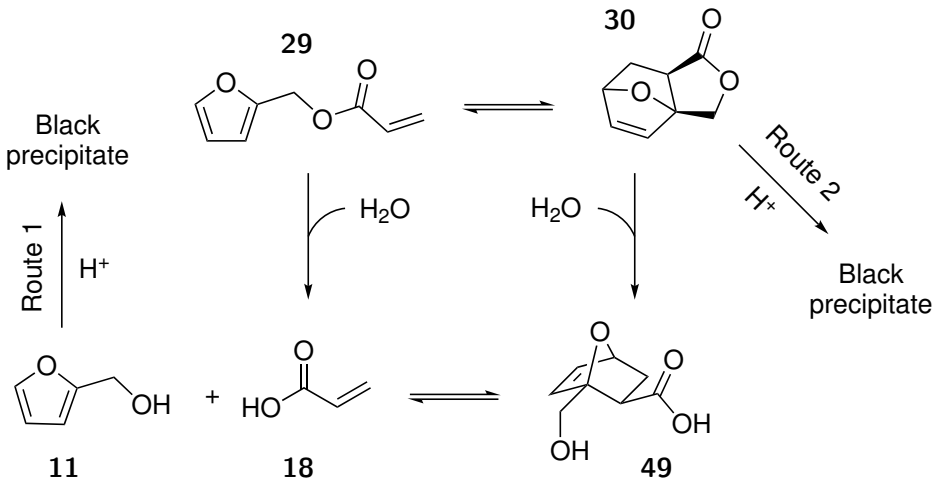

SCHEME 2.15: Routes to formation of black precipitate from the lactone (**30**)

It was then investigated by which mechanisms the black precipitate might be formed. As described before, FuAl (**11**) is known to polymerise into black cross-linked material when treated with acid.[44] Therefore, if FuAl (**11**) is formed during aromatisation through some retro DA reaction/hydrolysis mechanism it will be able to readily polymerise into black precipitate (route 1, Scheme 2.15). Formation of FuAl (**11**) should however be paired with the formation of acrylic acid (**18**). Altough this product is observed for the reaction with 10 % MSA in toluene, it is only visible by ^{1}H-NMR after 1.5 hour of heating at 80 °C whereas the reaction mixture already goes black upon addition of lactone (**30**) at RT. This then suggests a different mechanism is also at play. The lactone (**30**) might immediately polymerise to form a black precipitate on its own or via one of the aromatisation intermediates (route 2, Scheme 2.15). To test this hypothesis FuAl (**11**) was polymerised in $CDCl_3$ using 10 mol % MSA and the black precipitate formed was compared to the black precipitate formed by the lactone (**30**) under the same conditions. Since the precipitates did not dissolve in any commercially available NMR solvents ($CDCl_3$, DMSO-d_6 and toluene-d_8), the solids were compared by ATR/FT-IR (Figure 2.16). Qualitative comparison of the two IR spectrum showed the two precipitates to be slightly different. Although this data is not conclusive, it at least suggests that the lactone (**30**) is able to polymerise on its own when subjected to acid. More extensive investigation is however necessary to get a better understanding of this complex process.

Base catalysed aromatisation

In an attempt to move away from acid catalysis, the aromatisation reaction was attempted under base catalysis. Based on patent literature,[26] aromatisation was attempted with 25 wt % NaOMe in MeOH. Upon addition of the base solution to the lactone (**30**) (0.33M), the reaction mixture turned amber but no precipitate was present. After 2 hours at RT the mixture was put at 80 °C for 1 hour but NMR analysis indicated that no phthalide (**31**) had been formed. Doing the reaction with 10

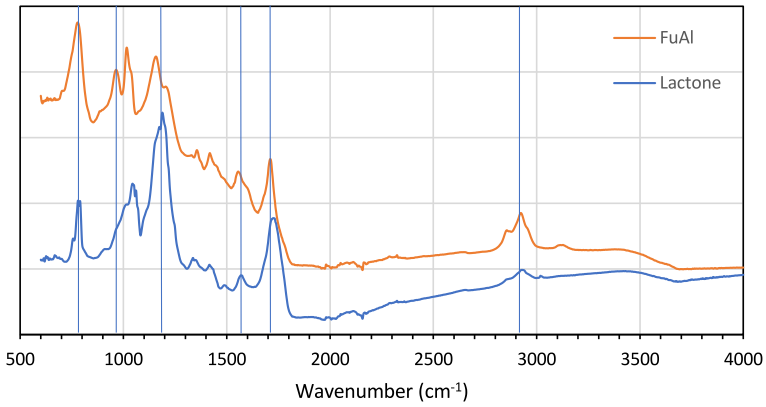

FIGURE 2.16: ATR-IR spectra of acid catalysed polymerised samples of FuAl (**11**) and lactone (**30**).

mol % KtBuOH in ethanol and $CDCl_3$ (0.33M) overnight at 80 °C also did not result in any formation of phthalide (**31**).

Initially, it was thought that the proton at the 7 position of the lactone (**30**) (See Figure 2.11 for numbering) would be easily deprotonated and the negative charge created would be resonance stabilised by the carbonyl group. These results however suggest that this negative charge may not be delocalised so easily and thus this proton might not be so acidic after all. The base catalysed aromatisation was therefore not investigated further.

Overall we have seen that the lactone (**30**) can be very selectively converted to phthalide (**31**) in a 98 % yield using mixtures of MSA (0.5 eq) and Ac_2O (4 eq) at RT. Attempts at acid catalysed aromatisation without the use of Ac_2O resulted in lower yields, typically 60-70 %, which are still significantly better than those reported in the literature to date for similar systems[17,19]. The acid catalysed formation of large black polymeric structures was found to be the main reason for the decrease in phthalide (**31**) yield. Attempts at circumventing this problem by performing base catalysed aromatisation failed.

TABLE 2.3: All phthalide (**31**) yields for the aromatisation of lactone (**30**), calculated at full conversion from *in-situ* quantitative NMR analysis. Acid catalyst is added to lactone (**30**) at 20 °C before heating to 80 °C. When TfOH is used, it is added to the lactone (**30**) in half an amount of solvent. Concentration of lactone (**30**) in case of solvent is 0.33 M. [1]MSA/Ac_2O is added at 0 °C and brought to RT. [2]lactone (**30**) concentration is 1 M. [3]Yield after reusing Amberlist catalyst with extra equivalent of lactone (**30**).[4]Yield is calculated at 96 % conversion of lactone (**30**). [5]Reaction of TfOH supported on silica.

	Solvent	**Catalyst**	**Ac_2O**	**T (°C)**	**Yield (%)**
		Ac_2O assisted			
1	Neat	MSA (1.2 M)	20 vol %	20	75
2		MSA (0.5 eq)	4 eq.	20[1]	97
3		MSA (0.5 eq)	4 eq.	80	98
4		MSA (0.02 eq)	4 eq.	80	94
5	AcOEt [2]	Amberlist (0.1 eq)	2 eq.	80	89 79[3]
		Non Ac_2O assisted			
6	Neat	MSA (1.2 M)	No	20	66
7	Toluene-d_8	MSA (0.1 eq)	No	80	66[4]
8		$Hf(OTf)_4$ (0.1 eq)	No	80	60
9		TfOH (0.1 eq)	No	80	63
10		TfOH (0.01 eq)	No	80	63
11		TfOH[5] (0.01 eq)	No	80	58
12	$CDCl_3$	TfOH (0.1 eq)	No	80	79
13	CH_3COOH	TfOH (0.1 eq)	No	80	56

Chapter 3

Conclusions and Outlook

3.1 Conclusions

In this thesis, a new route for the selective production of biomass derived phthalide (**31**) from FuAl (**11**) and acrylic acid (**18**) derivatives, via a two-step DA approach was investigated. Based on literature precedent a route involving the preparation of FuAcr, subsequent intramolecular Diels-Alder cycloaddition and then a dehydration-aromatisation reaction was designed to overcome the *ortho/meta* selectivity problems when using non-symmetric substrates. Unfortunately, we were not able to reproduce from literature the key Diels-Alder reaction[39] which led us to study the reaction in more detail using DFT calculations. This revealed that the intramolecular reaction is both thermodynamically and kinetically very unlikely due to the large transition state and product energies. The main reason for this was the need for extensive pre-organisation of the substrate prior to DA reaction leading to the need to access a high energy conformer. We did however find that the intermolecular reaction is feasible and does indeed occur for furfuryl acrylate upon standing at room temperature, as judged by NMR and GPC analsysis.

Since FuAcr (**29**) proved unreactive toward the intended intramolecular DA reaction, it was decided, based on our calculations together with patented literature,[54] to study the intermolecular DA reaction of FuAl (**11**) and MeAc (**27**) instead. Reacting these substrates at 60 °C, resulted in a 23 % yield of DA adducts, with the four expected *ortho/meta* and *endo/exo* DA products (**38**) being identified. Attempts at increasing the yield of this reaction by means of lewis acid catalysis proved ineffective due to the instability of FuAl (**11**) under these conditions. Activation of the DA reaction was therefore achieved by using more activated dienophiles, namely HFIPAcr. This change resulted in a significant increase in yield of DA adducts to 66 % (**41**) after 22 hours at 20 °C.

The synthesised DA products (**38**, **41**) were found to readily undergo retro-DA reaction at elevated temperatures. Based on previous work with the group[20] the DA adducts were therefore hydrogenated before aromatisation was attempted in the presence of a zeolite and Pd/C catalyst. Unfortunately, with this system this methodology did not yield satisfactory results, and so direct aromatisation of the DA adducts of FuAl and HFIPAcr (**41**) in mixtures of MSA and Ac_2O at RT was investigated.[19] This method yielded the intended product phthalide (**31**) in a 40 % yield, however no *meta* aromatisation product was detected and thus this two-step approach was only able to produce aromatics (phthalide, **31**) in a 27 % yield based on the initial FuAl (**11**) intake.

Interestingly, the lack of (acetylated) non-lactonised product and absence of *meta* products suggested that intramolecular lactonisation might play a key role in aromatisation. This helped to guide the rational design of an improved approach involving the *in-situ* lactonisation of the DA adduct, formally, giving the intramolecular

DA adducts initially targeted, allowing for the implementation of a dynamic kinetic trapping strategy. This approach gave a significantly improved selectivity and yield of (lactonised) Diels-Alder product (68%), compared to the standard reaction. The lactone product was experimentally shown to be much more thermally stable than any other investigated DA product and this was supported by the results of DFT calculations. This product was found to be very amenable to aromatisation with phthalide (**31**) yields of up to 98% obtained in mixtures of MSA and Ac_2O at RT and up to 66% using only catalytic amounts of acid and no Ac_2O. Overall, using this approach, we were able to produce phthalide (**31**) in a 66 % yield from FuAl (**11**) and HFIPAcr (**37**) by a two-step DA approach (Scheme 3.1).

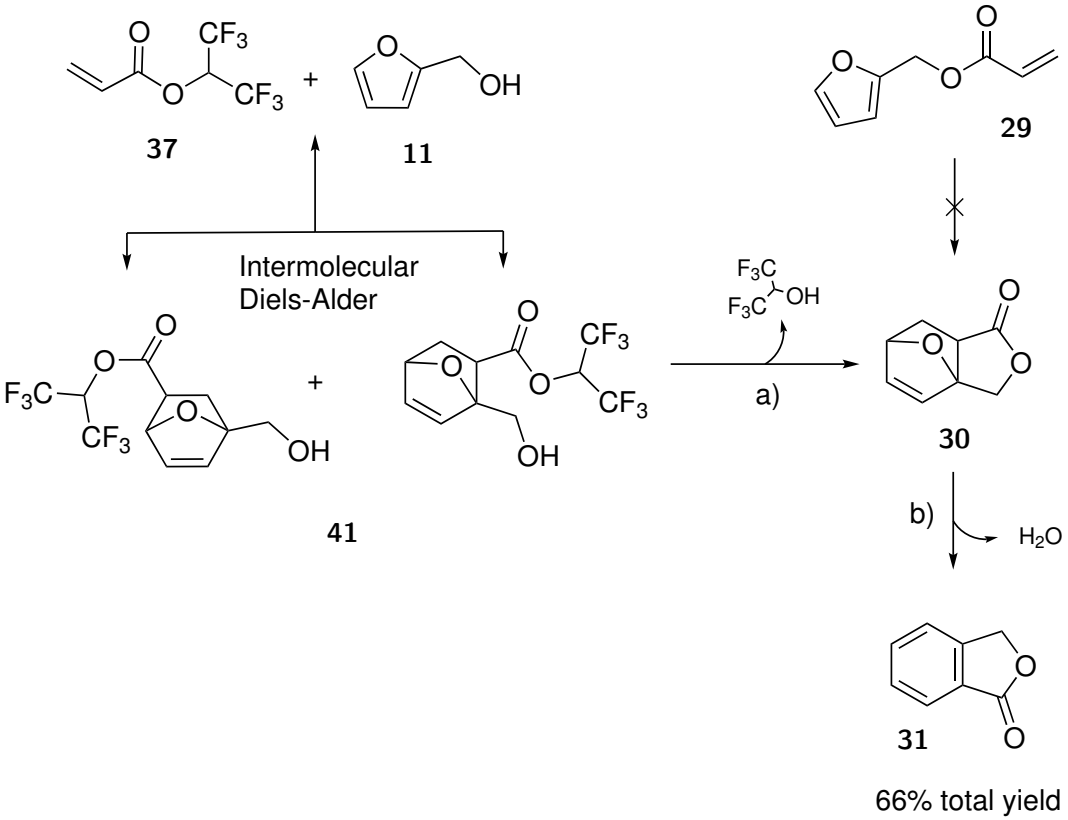

SCHEME 3.1: Main route for the production of phthalide (**31**), investigated in this thesis. a) Neat DA reaction at 80 °C of FuAl (**11**) and HFIPAcr with a 2:3 molar ratio in the presence of 1 mol % $NaHCO_3$. b) Aromatisation of lactone at 80 °C in the presence of 0.5 eq. MSA and 4 eq Ac_2O.

3.2 Outlook

Further studies into this route, should mainly focus on optimisation of the two different steps, with the view to creating a scalable process. In terms of yields and time requirements optimisation efforts should first focus on the DA-lactonisation step, since aromatisation is already very high yielding. In particular there is scope to improve the selectivity of the reaction by reducing FuAcr (**29**) formation, perhaps by further optimisation of the base loading, type and form (e.g. surface area). Furthermore, if HFIP (or any other activating group) is used it needs to be recovered in a high yield from the reaction for recycling. It was already observed by NMR that

free HFIP is generated during the reaction, however due to the small scale its recovery has not been attempted so far. It is also possible that other activated acrylates might prove to be better choices, for example nonafluorotertbutyl or petafluorophenol acrylates are interesting alternatives that could be investigated going forward. One significant problem observed during these studies was that the reaction stalls at around 65% of lactone, even though starting materials remain. The exact reason for this is not well understood at the moment, but understanding and solving this problem could provide significant improvement in overall yield. If this is not possible ways to recycle the starting materials need to be developed, for example by distillation or by direct crystallization of the lactone, allowing the remaining starting materials to be easily separated.

As far as the aromatisation conditions are concerned, the relatively high yields obtained for only acid catalysed aromatisation compared to other systems still show the potential of omitting the relatively expensive Ac_2O (**45**). Since we only scratched the surface, an intensive screening of different acids, solvents, and concentrations could potentially lead to a clearer understanding of this reaction and further improvements in yields by suppressing side reactions which currently produce black polymeric material.

Lastly, the oxidation of phthalide (**31**) to phthalic anhydride (**20**) remains to be investigated.

Chapter 4

Experimental section

4.1 Chemicals

All reagents were purchased from commercial sources and used as received unless stated otherwise. Acryloyl chloride was purchased from Merck; $Sc(OTf)_3$, $Y(OTf)_3$, $Ga(OTf)_3$, $Hf(OTf)_4$, $In(OTf)_3$ from Acros; Hexafluoroisopropanol and trifluoroethyl acrylate from Fluorochem; Hexafluoroisopropylacrylate from TCl; Furfurylalcohol, methyl acrylate, methanesulfonic acid, acetic anhydride, $NaHCO_3$, $NaCH_3COO$, $NaCHCl_2COO$, tetrahydrofuran (THF), Celite® Hyflo Supercel, $ZnCl_2$, allyl chloride, tetra-n-butylammonium bromide (TBAB), 4-dimethylaminopyridine (DMAP), triethylamine (Et_3N), methyl iodide, nitrobenzene and acetic acid from Sigma-Aldrich; dichloromethane (DCM), chloroform ($CHCl_3$), hexanes, ethyl acetate and toluene from InterCheM; $CDCl_3$, DMSO-d_6 from Euriso-top and toluene-d_8 from Cambridge Isotope Laboratories.

4.2 Analysis methods

^{1}H and ^{13}C NMR measurements were performed on a an Agilent MRF400 or a Varian AS400 spectrometer at RT running at 400 and 101 MHz respectively. Chemical shifts are reported in ppm relative to TMS by using the residual solvent resonance as the internal reference. For normal ^{1}H, ^{13}C, COSY, HSQC, HMBC the standard pulse sequences available in VNMRJ 4.2 were used. For quantitative ^{1}H NMR the relaxation delay was set to 25 seconds and the pulse angle to 90°.

GC-MS was performed on a Shimadzu GC-MS QP 2010 with a VF-5MS (30 mm x 0.25 mm 0.25 µm) column and a medium polarity guard column (5 m). Samples were injected at 265 °C. The initial column temperature was 40 °C which was held for 5 minutes, then increased to 280 °C with a heating rate of 10 °C/minute, and then held at that temperature for 5 minutes. All samples were dissolved in chloroform and the injected volume was 0.1 µL.

GPC analysis was performed using a Polymer labarotories PL-GPC-50 plus system, equipped with 3 PLGel mixed E (3 µm) columns. The solvent used was the same as the carrier liquid, (stabilised) THF with 1 v/v % acetic acid with a flow rate of 1 ml/min at 40 °C. Monitoring was by UV detection at 254 nm.

High resolution ESI TOF-MS + spectra were recorded on a Walters LCT Premier XE KE317 Micromass Technologies spectrometer in acetonitrile at 80 °C.

IR spectra were recorded on the Perkin Elmer FT-IR spectrometer equipped with the universal ATR sampling station.

For single X-ray crystallography of the lactone (**30**), a total of 13608 reflections were measured on a Bruker Proteum diffractometer with rotating anode and Helios optics (λ = 1.54184 Å) at a temperature of 150(2) K up to a resolution of $(\sin\theta/\lambda)_{max}$

= 0.59 $Å^{-1}$. The Eval15 software[61] was used for the intensity integration. A multi-scan absorption correction and scaling was performed with SADABS[62] (correction range 0.59-0.75). 1190 Reflections were unique (R_{int} = 0.044), of which 1137 were observed [I>2σ(I)]. The structure was solved with Patterson superposition methods using SHELXT.[63] Least-squares refinement was performed with SHELXL-2018[64] against F^2 of all reflections. Non-hydrogen atoms were refined freely with anisotropic displacement parameters. All hydrogen atoms were located in difference Fourier maps and refined with a riding model. 101 Parameters were refined with no restraints. R1/wR2 [I > 2σ(I)]: 0.0348 / 0.0879. R1/wR2 [all refl.]: 0.0356 / 0.0884. S = 1.074. Extinction parameter EXTI = 0.0037(4). Residual electron density between -0.14 and 0.21 e/$Å^3$. Geometry calculations and checking for higher symmetry was performed with the PLATON program.[65]

4.3 DFT calculations

The ADF modeling suite by SCM,[49–51] which uses density functional theory, was used for calculating the energies of the substrates, transition states and products. For all the calculations, the hybrid B3-LYP-D3 XC functional was used together with the TZ2P[66] basis set. This functional and basis set are commonly used for calculations on organic molecules.[52,53] All simulations were performed in the gas phase and thus no solvent effects were considered. All structures drawn in the graphical user interface were first pre-optimised using the Universal Force Fields (UFF) method, before performing the actual geometry optimisation with the above mentioned XC functional and basis set, yielding an electronic internal energy, U_{el}.

4.3.1 Internal energies of the intramolecular DA reaction

For calculating the electronic internal energy (U_{el}) of the intramolecular DA substrates (**29**, **29**, **29**), it was taken into account that different conformers with different local minima exist for these substrates. Therefore, after drawing the substrate of interest in the graphical user interface (GUI) of the ADFinput, all possible conformers of the substrate were generated using the build in conformer generator. The five conformers with the lowest energy were then geometry optimised, using the appropriate XC functional. The optimised conformer with the lowest U_{el} was then chosen as the ground state conformer for the specific substrate (U_{GS}, 1 in Figure 2.2 a).

The intramolecular DA products (U_{pr}, 4 in Figure 2.2 a) do not have this conformational freedom and thus were only pre-optimised using the Universal Force Fields (UFF) method, before the actual geometry optimisation with the appropriate XC functional.

The substrate conformer needed for DA reaction (U_{Conf}, 2 in Figure 2.2 a) was generated from the corresponding DA product by removing/adding the appropriate carbon bonds to remake the substrates. This geometry was than pre-optimised and subsequently geometry optimised to yield U_{Conf}.

In order to find the geometry and electronic internal energy of the transition state ($U^{\ddagger}$, 3 in Figure 2.2 a), first an approximate transition state was searched for, using the linear transit method. In this method, starting from the optimised geometry of the substrate conformer needed for DA reaction (U_{Conf}, 2 in Figure 2.2 a), C_1 and C_4 (See Scheme 4.1 for numbering) are fixed at their relative positions and are brought closer to one another in 10 equal steps to about 1.2 Å. For each of these steps, the geometry of the rest of the system is optimised while the two atoms stay

fixed at their relative position. Once optimised, the two atoms move a step closer to each other and stay fixed for the next optimisation. This process is continued for all the steps. At a certain distance, the optimised internal energy of the whole system should exhibit a maximum. The actual transition state geometry and energy ($U^{\ddagger}$) can then be calculated from the coordinates of this approximation by performing a transition state search[67,68] with distance C_1 to C_4 as the reaction coordinates and appropriate XC functional and basis set settings.

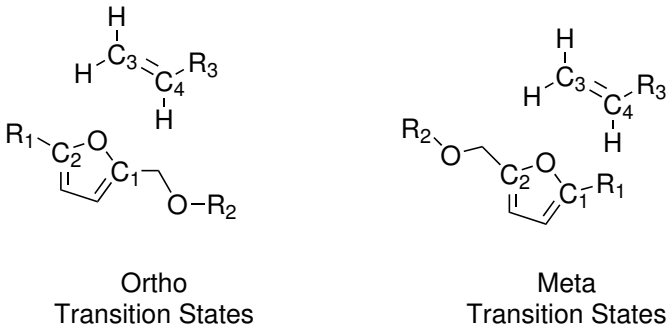

SCHEME 4.1: Numbering of atoms in transition state for linear transit. Note that R_2 and R_3 of the ortho transition states are connected to each other in the intramolecular DA reaction.

4.3.2 Internal energies of the intermolecular DA reaction

For calculations involving the intermolecular DA reactions, the optimised geometries and internal energies of the seperate diene and dienophile substrates were first calculated by simply drawing the molecules in the GUI and performing a pre-optimisation with a subsequent geometry optimisation. Note that these molecules do not have much conformational freedom and therefore, conformers were not taken into account.

The optimised geometries of both the diene and dienophile were then loaded into the GUI and placed in such a way that the distance of C_1 to C_4 (Scheme 4.1) was about 2.5-5 Å and the orientation of the substrates would yield the desired DA product (i.e. ortho/meta and endo/exo). The internal energy of the interacting substrate pairs was then calculated for every possible starting position of the DA reaction (i.e. ortho/meta and endo/exo) by optimising the geometry of the interacting complex. For each DA substrate pair, the lowest of the four energies was taken as the ground state energy (U_{GS}, 1 in Figure 2.2 b) and used to calculate all of the transition state and reaction energies for that specific substrate pair.

For calculating the transition state geometries and energies ($U^{\ddagger}$, 3 in Figure 2.2 b), the same starting point was taken as for calculating U_{GS}. However, instead of direct optimisation, a linear transit was now run, decreasing the distance between C_1 and C_4 (Scheme 4.1) in 10 steps to 1.2 Å. For some reactions it was however necessary to fix C_2 to C_3 or fix both C_1 to C_4 and C_2 to C_3 in order to obtain a good approximation for the transition state. Just as for the intramolecular reaction, the geometry with the highest energy was now taken as the starting point for the transition state search to yield the actual transtion state geometry and energy ($U^{\ddagger}$).

Finally the DA product internal energies (U_pr, 4 in Figure 2.2 b) were calculated by placing the optimised geometries of the diene and dienophile in the right isomeric orientation with C_1 and C_4 as well as C_2 and C_3 about 2.5 Å apart. Starting from this

complex, the appropriate carbon bonds were removed/added to give the desired DA product. This was then pre-optimised and geometry optimised to yield the final DA product internal energies (U_{Pr}) and geometries.

4.3.3 Calculating Gibbs free energies

By computing the harmonic frequencies for a given optimised system at a specific temperature, one can calculate the Gibbs free energy of: the ground state (G_{GS}), conformer needed for DA reaction (G_{Conf}), transition state ($G^{\ddagger}$) and product (G_{Pr}). Frequencies are calculated numerically with the integration set to Becke Good at 323 K. Using the thermodynamic properties U_{el}, U_{nuc} and S as calculated from the frequency calculations, the program then calculates the Gibbs free energy (assuming ideal gas) for the given geometry at a specific temperature in the following way

$$G = H - TS = U + pV/n - TS = Uel + Unuc + pV/n - TS \tag{4.1}$$

The Gibbs free energy change of reaction ($\Delta_r G$), Gibbs free energy of activation ($\Delta G^{\ddagger}$) and the Gibbs free energy required to get from the ground state to the conformer needed in the DA reaction (ΔG_{Conf}) could be calculated in the following way:

$$\Delta_r G = G_{Pr} - G_{GS} \tag{4.2}$$

$$\Delta G^{\ddagger} = G^{\ddagger} - G_{GS} \tag{4.3}$$

$$\Delta G_{Conf} = G_{Conf} - G_{GS} \tag{4.4}$$

Lastly, the Gibbs free energy of activation for the retro-DA reaction $\Delta G_r^{\ddagger}$ could be calculated with the following formula:

$$\Delta G_r^{\ddagger} = G^{\ddagger} - G_{Pr} \tag{4.5}$$

4.3.4 Calculating FMO gaps

The energies of the frontier molecular orbitals were calculated from the optimised geometries of the substrate(s). Entering ADFlevels, the orbital energies can easily be seen. Calculating the difference in orbital energy for the normal (δE_{nd}) and inverse electron demand (δE_{id}) were done using the following formulas:

$$\Delta E_{nd} = E_{LUMOdp} - E_{HOMOde} \tag{4.6}$$

$$\Delta E_{id} = E_{LUMOde} - E_{HOMOdp} \tag{4.7}$$

In this equation E_{LUMOdp}, E_{LUMOde}, E_{HOMOdp} and E_{HOMOde} are the energies of the LUMO or HOMO of the diene (de) or dienophile (dp).

4.4 Synthesis

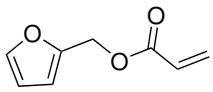

Furfuryl acrylate (29)[45]: A solution of FuAl (**11**, 10.00 g, 102 mmol, 1 eq.) and Et_3N (12.87 g, 127 mmol, 1.25 eq.) in DCM (175 mL) was cooled to 0 °C using an ice bath. Acryloyl chloride (10.14 g, 112 mmol, 1.10 eq.) was added dropwise to the solution over the course

of 10 minutes and then the mixture was stirred for 2 hours before being allowed to warm to RT. The reaction was then quenched by the addition of water (200 mL) and brought to pH < 7 using 1 M HCl. The organic layer was collected and washed with aqueous $NaHCO_3$ (pH $\sim$ 8), brine (x2, 200 mL), dried ($MgSO_4$) and concentrated under reduced pressure to yield the product as an amber liquid (14.65 g, 94 %). NMR results were consistent with literature.[39] ^{1}H NMR (400 MHz, $CDCl_3$) δ 7.43 (dd, J = 2.8, 1.9 Hz, 1H), 6.47 – 6.45 (m, 1H), 6.42 (dd, J = 6.0, 2.1 Hz, 1H), 6.38 – 6.34 (m, 1H), 6.19 – 6.09 (m, 1H), 5.84 (dt, J = 10.4, 2.1 Hz, 1H), 5.15 (s, 2H).

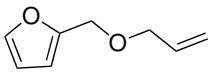

Furfuryl allyl ether (34)[39]: FuAl (**11**, 3.00 g, 31 mmol, 1 eq) and TBAB (1.97 g, 6 mmol, 0.20 eq.) were added to 50 w/w % NaOH in water (15 mL). Allyl chloride (4.68 g, 62 mmol, 2 eq.) was then added dropwise at RT over 10 minutes with vigorous stirring (> 300 RPM). After 1 hour another equivalent of allyl chloride was added and the mixture was warmed to 40 °C and stirred overnight. Water (100 mL) was then added followed by Et_2O (100 mL). The organic layer was separated, washed with brine (2x, 100 mL), dried ($MgSO_4$) and concentrated under reduced pressure. The crude product was re-suspended in cyclohexane (200 mL) and concentrated under reduced pressure again to help remove residual allyl alcohol by azeotropic distillation. This yielded the product as an amber liquid (4.3 g, 96 %). NMR results were consistent with literature.[39] ^{1}H NMR (400 MHz, $CDCl_3$) δ 7.43 – 7.37 (m, 1H), 6.32 (ddd, J = 9.3, 4.9, 2.4 Hz, 2H), 5.99 – 5.84 (m, 1H), 5.34 – 5.14 (m, 2H), 4.45 (s, 2H), 4.05 – 3.94 (m, 2H).

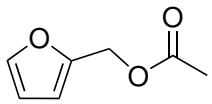

Furfuryl acetate (36): A solution of FuAl (**11**, 10.00 g, 102 mmol, 1 eq.) and Ac_2O (**45**, 12.49 g, 1.2 eq) was brought to 80 °C and DMAP (0.012 g, 0.1 mol %) was added. After stirring the mixture overnight at 80 °C, it was allowed to cool to RT and ethanol (10mL) was added to react with any Ac_2O that was left. Upon washing with aqueous $NaHCO_3$ (100 ml, pH $\sim$ 8), bubbels started to appear indicating that any acid was deprotonated and transferred to the water layer. The organic layer was collected and washed with brine (x2, 200 mL), dried ($MgSO_4$) and concentrated under reduced pressure to yield the product as an amber liquid (12.41 g, 94 %). NMR results were consistent with literature.[69] ^{1}H NMR (400 MHz, $CDCl_3$) δ 7.45 – 7.35 (m, 1H), 6.36 (ddd, J = 5.1, 1.9, 1.1 Hz, 2H), 5.03 (s, 2H), 2.05 (d, J = 0.6 Hz, 3H).

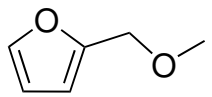

Methoxymethyl furan (39): FuAl (**11**, 10.00 g, 102 mmol, 1 eq) and TBAB (6.57 g, 20 mmol 0.20 eq.) were added to 50 w/w % NaOH in water (50 mL). Methyl iodide (28.9 g, 204 mmol, 2 eq.) was then added dropwise to the mixture at RT over 10 minutes with vigorous stirring (> 300 RPM). After stirring for 4 hours, water (100 mL) was added followed by Et_2O (100 mL). The organic layer was collected and $Na_2S_2O_3$ was added to reduce any I_2 to I^-. It was then washed with water, (2x, 100 mL), brine (2x, 100 mL), dried ($MgSO_4$) and concentrated under reduced pressure yielding the product as an amber liquid (4.02 g, 35 %). NMR results were consistent with literature.[70] ^{1}H NMR (400 MHz, $CDCl_3$) δ 7.43 – 7.35 (m, 1H), 6.36 – 6.27 (m, 2H), 4.38 (s, 2H), 3.35 (s, 3H).

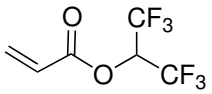

Hexafluoroisopropylacrylate (37): A suspension of 1,1,1,3,3,3-hexafluoroisopropanol (49.91 g, 297 mmol, 1.2 eq.) and $Sc(OTf)_3$ (0.10 g, 0.20 mmol, 0.08 mol %) were stirred at RT and acryloyl chloride (22.40 g, 248 mmol, 1 eq.) was added dropwise over the course of 5 minutes. Bubbels were formed from the $Sc(OTf)_3$ flocks and pH paper indicated that the

escaping gas was acidic, consistent with the production of HCl in this reaction. After stirring the mixture overnight at RT, $NaHCO_3$ was added to the stirred suspension until pH paper indicated a pH > 7. It was then filtered and the clear filtrate was distilled under N_2. Two clear and colourless liquid fractions were collected at ∼ 80 °C and at ∼ 105 °C. NMR analysis showed the clear and colourless distillate received at 105 °C to be product. NMR results were consistent with those reported by sigma aldrich. ^{1}H NMR (400 MHz, $CDCl_3$) δ 6.64 (dd, J = 17.2, 0.7 Hz, 1H), 6.29 – 6.17 (m, 1H), 6.15 – 6.06 (m, 1H), 5.88 – 5.75 (m, 1H).

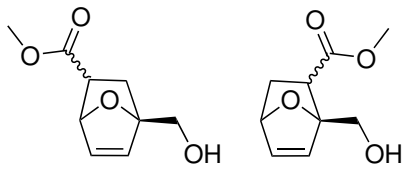

DA products FuAl and MeAc (38)[54]: A solution of FuAl (**11**, 50.00 g, 510 mmol, 1 eq.) and MeAc (**27**, 52.68 g, 612 mmol, 1.2 eq) was stirred neat overnight at 70 °C overnight. The amber mixture was put under reduced pressure and subsequently distilled under high vacuum at RT. The residue yielded the amber viscous liquid product (24.14 g, 26 %). Characteristic NMR peaks used for distinguishing the 4 different products: ^{1}H NMR (400 MHz, $CDCl_3$) δ 5.16 (d, J = 1.7 Hz, 1H), 5.14 (dd, J = 4.8, 1.5 Hz, 5H), 5.09 (dd, J = 4.6, 1.6 Hz, 1H), 4.97 (dd, J = 4.7, 1.7 Hz, 7H).

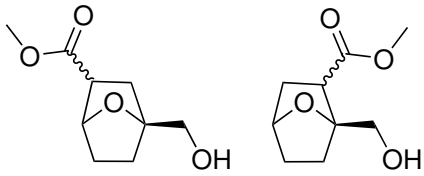

Hydrogenated DA products FuAl and MeAc (43): A suspension of crude FuAl and MeAc DA product (**38**, 10.00 g) and Pd/C (0.10 g, 5 wt % metal on carbon) was air sealed and flushed with N_2 for 2 minutes. THF (50 mL) was then added and the flask containing the mixture was degassed and subsequently regassed with H_2 using a balloon. The mixture was stirred overnight at RT and was brought to normal atmosphere before filtering and concentrating the mixture under reduced pressure. It was subsequently distilled at 50 °C under high vacuum to remove any starting DA substrates left. The viscous amber liquid residue contained the crude product (4.4 g). The products could not be characterised by NMR. GC-MS retention times: 17.29 (m/z=186), 17.59 (m/z=186), 17.80 (m/z=186) and 18.12 (m/z=186).

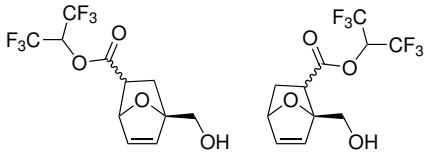

DA products of FuAl and HFIPAcr (41): A solution of FuAl (**11**, 4.42 g, 45 mmol, 1 eq.) and HFIPAcr (**37**, 10 g, 45 mmol, 1 eq.) was stirred overnight at RT. The mixture was concentrated under reduced pressure to yield the crude DA product (with FuAl) as an amber liquid (7.2 g). Characteristic NMR peaks used for distinguishing the 4 different products: ^{1}H NMR (400 MHz, $CDCl_3$) δ 3.43 (ddd, J = 8.8, 4.6, 3.9 Hz, 1H), 3.30 (dd, J = 9.2, 3.6 Hz, 1H), 2.76 (dd, J = 8.4, 3.8 Hz, 1H), 2.68 (dd, J = 8.1, 4.1 Hz, 1H).

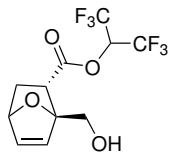

The endo/ortho DA product could be isolated using silica column chromatography with the eluent gradually increasing from 10 v/v % ethylacetate in hexanes to 30 v/v %. Fractions containing the pure product were pulled together and concentrated under reduced pressure to yield an amber liquid. ^{1}H NMR (400 MHz, $CDCl_3$) δ 6.50 (dd, J = 5.8, 1.5 Hz, 1H), 6.09 (d, J = 5.8 Hz, 1H), 5.69 (hept, J = 6.1 Hz, 1H), 5.04 (dd, J = 4.6, 1.6 Hz, 1H), 4.19 (dd, J = 33.0, 12.7 Hz, 2H), 3.28 (dd, J

= 9.2, 3.5 Hz, 1H), 2.34 (ddd, J = 11.8, 9.2, 4.7 Hz, 1H), 1.77 (dd, J = 11.7, 3.6 Hz, 1H). ^{13}C NMR (101 MHz, $CDCl_3$) δ 168.9, 138.6, 132.1, 91.4, 78.8, 66.5, 61.2, 42.0, 31.3.

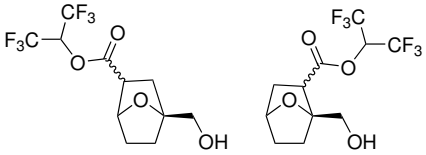

Hydrogenated DA products of FuAl and HFIPAcr (42): A suspension of crude FuAl and HFIPAcr DA product (**41**), 0.10 g) and Pd/C (0.0015 g, 5 wt % metal on carbon) was air sealed and flushed with N_2 for 2 minutes. THF (50 mL) was then added and the flask containing the mixture was degassed and subsequently regassed with H_2 using a balloon. The mixture was stirred overnight at RT and was brought to normal atmosphere before filtering and concentrating the mixture under reduced pressure. The viscous amber liquid residue contained the crude hydrogenated product. The products could not be characterised by NMR. GC-MS retention times: 14.87 (m/z = 322), 15.22 (m/z = 322), 15.65 (m/z = 322) and 17.72 (m/z = 154).

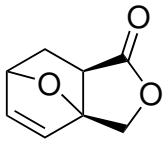

Lactone (30): A suspension of FuAl (**11**, 4.42 g, 45 mmol, 1 eq.), HFIPAcr (**37**, 11.00 g, 50 mmol, 1.1 eq.) and $NaHCO_3$ (0.04 g, 0.45 mmol, 1 mol %) was stirred at 80 °C overnight. Upon stirring for an hour, a colour change of light amber to black was observed. After 22 hours the mixture was brought to RT and the product was seperated using silica column chromatography with the eluent gradually increasing from 10 v/v % ethylacetate in hexanes to 30 v/v %. The fractions containing the pure product were pulled together and concentrated under reduced pressure yielding an amber liquid that crystallised to a clear light brown crystal over the course of 1 minute. Single crystal X-Ray details: C8H8O3, Fw = 152.14, colourless block, 0.36 x 0.23 x 0.10 mm^3, orthorhombic, Pbca (no. 61), a = 8.87439(11), b = 11.6699(3), c = 13.2000(2) Å, V = 1367.04(4) Å^3, Z = 8, Dx = 1.478 g/cm^{-}3, μ = 0.96 mm^{-}1. ^{1}H NMR (400 MHz, $CDCl_3$) 6.49 – 6.42 (m, 2H), 5.12 (d, J = 4.6 Hz, 1H), 4.77 (d, J = 11.0 Hz, 1H), 4.68 (d, J = 11.0 Hz, 1H), 2.54 (dd, J = 8.8, 3.4 Hz, 1H), 2.26 (ddd, J = 11.9, 4.4, 3.5 Hz, 1H), 1.69 (dd, J = 11.9, 8.8 Hz, 1H). ^{13}C NMR: (101 MHz, $CDCl_3$) δ 176.0, 137.6, 131.8, 92.2, 79.5, 69.1 , 45.0, 29.3. HR-MS (ESI) C8H8O3 $[2M+Na]^+$ m/z required 327.0796; found 327.0845.

Aromatisation intermediates (47, 48): A solution of Ac_2O (**45**, 300 mg, 2.94 mmol, 4 eq.) and MSA (35 mg, 0.37 mmol, 0.5 eq.) was stirred for 5 minutes at RT. Lactone (**30**, 112 mg, 0.74 mmol, 1 eq.) was added to the stirred solution on ice and stored in the fridge overnight after 1 hour of stirring on ice. $CHCl_3$ (20 ml) and $NaHCO_3$ (1 g) was added to neutralise the MSA and stop the reaction. The suspension was filtered, washed with water (2 x 20 ml), brine (2 x 20 ml), dried ($MgSO_4$) and concentrated under reduced pressure. The product was seperated using silica column chromatography with the eluent gradually increasing from 5 v/v % ethylacetate in hexanes to 30 v/v %. The fractions containing the mixed product were pulled together and concentrated under reduced pressure yielding a crude mixture of 2 aromatisation products as an amber liquid.

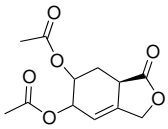

Diacetate (**47**): ^{1}H NMR (400 MHz, $CDCl_3$) δ 5.76 (tdd, J = 3.3, 2.0, 1.2 Hz, 1H), 5.51 (dddd, J = 6.3, 5.3, 3.7, 2.6 Hz, 1H), 5.14 (ddd, J = 12.0, 7.7, 4.1 Hz, 1H), 4.88 – 4.80 (m, 2H), 3.36 – 3.28 (m, 1H), 2.53 (ddd, J = 12.4, 5.2, 4.2 Hz, 1H), 1.78 – 1.65 (m, 1H). Note that the hydrogens belonging to the acetate groups could not be

distinguished in the mixture and are therefore not listed here. ^{13}C NMR (101 MHz, $CDCl_3$) δ 173.7, 170.6, 170.3, 137.6, 119.5, 71.7, 71.7, 69.8, 38.8, 28.3, 21.0, 21.0.

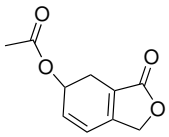

Monoacetate (**48**): ^{1}H NMR (400 MHz, $CDCl_3$) δ 6.41 – 6.35 (m, 2H), 5.60 (ddd, J = 7.8, 5.0, 4.2 Hz, 1H), 4.80 – 4.66 (m, 2H), 2.80 – 2.71 (m, 2H). Note that the hydrogens belonging to the acetate groups could not be distinguished in the mixture and are therefore not listed here. ^{13}C NMR (101 MHz, $CDCl_3$) δ 172.6, 170.0, 153.6, 132.4, 122.6, 121.7, 69.9, 65.1, 24.3, 21.0.

4.5 Quantitative experiments

DA time experiments: For all quantitative DA reaction experiments (including production of lactone, **30**), diene and dienophile were added in a 1:1 molar ratio (2 mmol, 1 eq), unless stated otherwise, to a starfish vile (8 mL) together with nitrobenzene (62 mg, 0.5 mmol, 0.25 eq) as an internal standard (IS). Mixing all of the components at RT, gave a homogeneous solution, and a sample (20 µL) was taken immediately for quantitative NMR analysis which served as the t=0 hours point. Depending on the specific conditions, base (for lactonisation) or/and solvent was added (if necessary) and the reaction mixture was stirred and heated to the desired temperature in the closed vial. NMR samples for analysis were then taken after 1, 2 and 22 hours and spectra were immediately recorded in $CDCl_3$ unless stated otherwise. Depending on the reaction, more time points were taken in a similar way.

Aromatisation time experiments: A solution of lactone (**30**, 33 mg, 0.22 mmol) and IS nitrobenzene (6.7 mg, 0.06 mmol, 0.25 eq.) in $CDCl_3$ (1 ml) was stirred for 1 minute. A sample for NMR analysis was taken to serve as the t=0 hours point. The sample was loaded back in the vial and the solvent was evaporated off under reduced pressure. A mixture with the appropriate amount of MSA and Ac_2O was stirred at RT for 5 minutes and added to the lactone mixture at RT (unless stated otherwise). A sample (20 µL) of the mixture was then taken for NMR analysis and depending on the conditions stirred at 80 °C or 20 °C. Samples for NMR analysis were taken after 1 and 2 hours. Depending on the conversion of lactone and aromatisation intermediate, the reaction was followed for longer times until no lactone and aromatisation intermediate was left. When the reaction was done in a solvent, the appropriate amount of solvent was added together with the MSA (and Ac_2O). In the case when an NMR solvent was used, the t=0 hours point was measured in the solvent and not evaporated afterwards.

Appendix A

DFT computational results

TABLE A.1: DFT Gibbs free energy changes for the intramolecular DA reaction calculated at 323 K. ΔG_{Conf} is the difference in energy between the substrate ground state and the conformer that is needed to proceed to DA reaction. $\Delta G^{\ddagger}$ is the activation energy for the forward DA reaction with respect to the substrate ground state. $\Delta G_r^{\ddagger}$ is the activation energy for the retro-DA reaction with respect to the product ground state. $\Delta_r G$ is the difference between substrate and product ground state energy.

	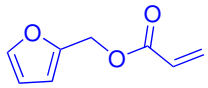 **29**				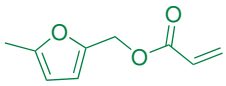 **35**			 **34**		
	ΔG_{Conf}	$\Delta G^{\ddagger}$	$\Delta G_r^{\ddagger}$	$\Delta_r G$	ΔG_{Conf}	$\Delta G^{\ddagger}$	$\Delta_r G$	ΔG_{Conf}	$\Delta G^{\ddagger}$	$\Delta_r G$
Endo	8,7	48,4	19.2	29,2	8,4	48,2	29,1	0,5	41,9	23,8
Exo	9,5	39,5	25.7	13,8	10,0	39,2	14,3	1,3	31.6	10.1

TABLE A.2: DFT Gibbs free energy changes for the intermolecular DA reaction calculated at 323 K. $\Delta G^{\ddagger}$ is the activation energy for the forward DA reaction with respect to the substrate ground state. $\Delta G_r^{\ddagger}$ is the activation energy for the forward DA reaction with respect to the product ground state. $\Delta_r G$ is the difference between substrate and product ground state energy.

	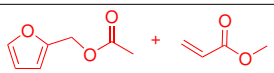 **36 & 27**			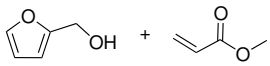 **11 & 27**			 **11 & 37**		
	$\Delta G^{\ddagger}$	$\Delta G_r^{\ddagger}$	$\Delta_r G$	$\Delta G^{\ddagger}$	$\Delta G_r^{\ddagger}$	$\Delta_r G$	$\Delta G^{\ddagger}$	$\Delta G_r^{\ddagger}$	$\Delta_r G$
Endo/Ortho	31,4	20,0	11,4	24,4	15.4	9,0	24,2	13.7	10,5
Exo/Ortho	31,8	20,1	11,7	25,4	13.7	11,7	24,0	13.0	11.0
Endo/Meta	32,6	22,3	10,3	28,9	20.4	8,6	25,2	16.8	8.4
Exo/Meta	33,2	22,0	11,3	29,7	21.1	8,6	26,7	18.5	8.2

Appendix B

NMR spectra

B.1 Furfuryl acrylate (29)

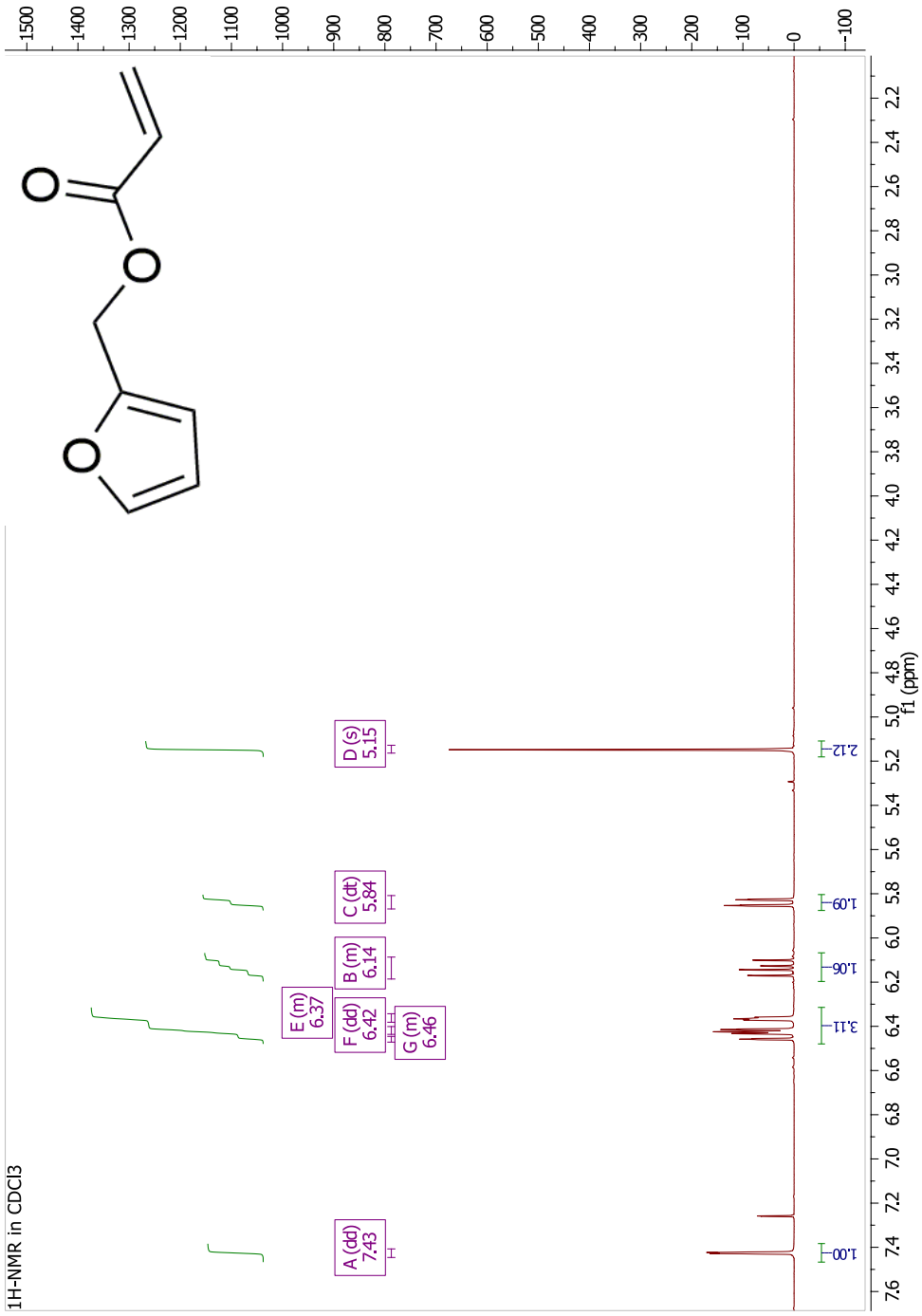

B.2 Furfuryl allyl ether (34)

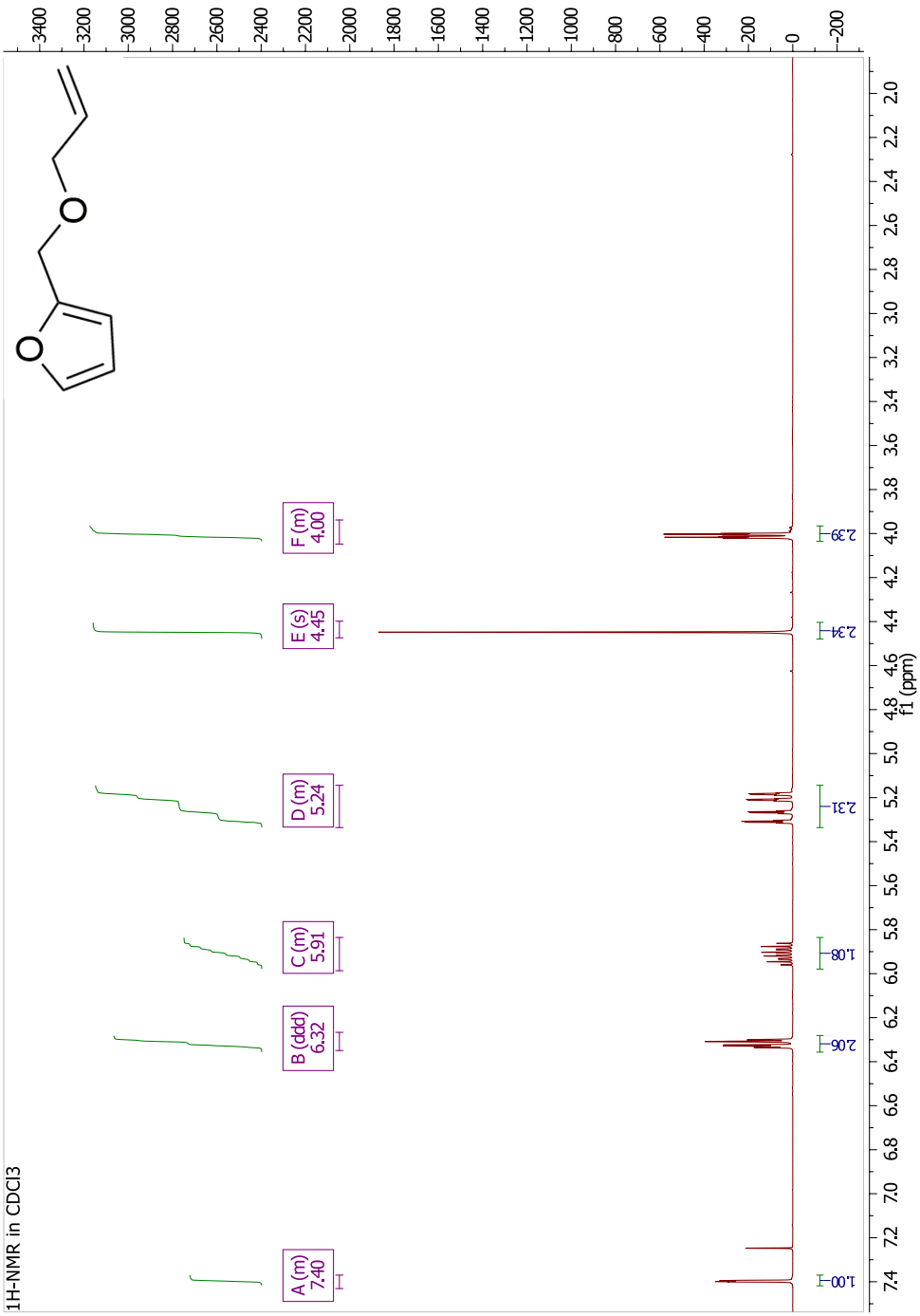

B.3 Furfuryl alcohol (11)

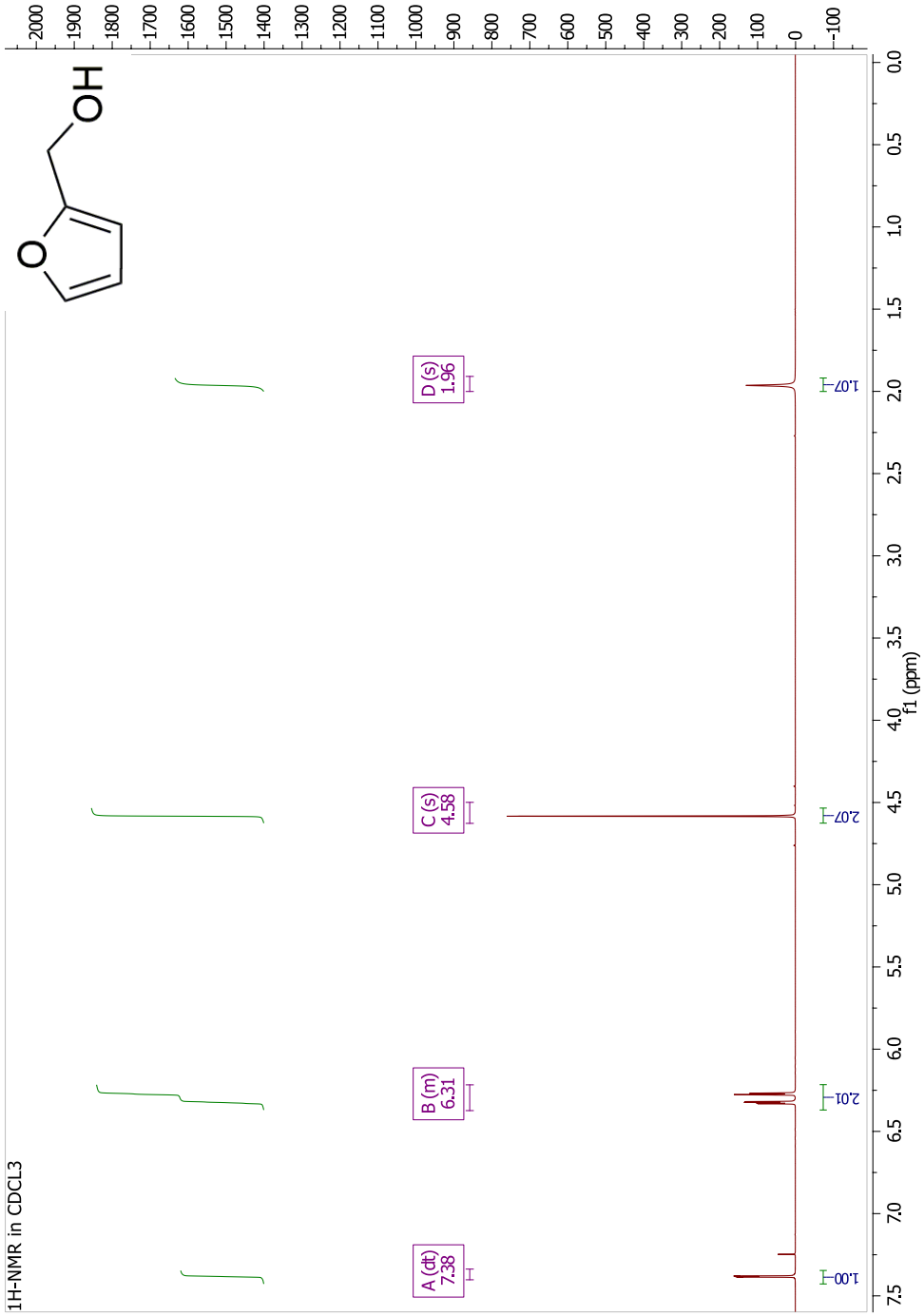

B.4 Furfuryl acetate (36)

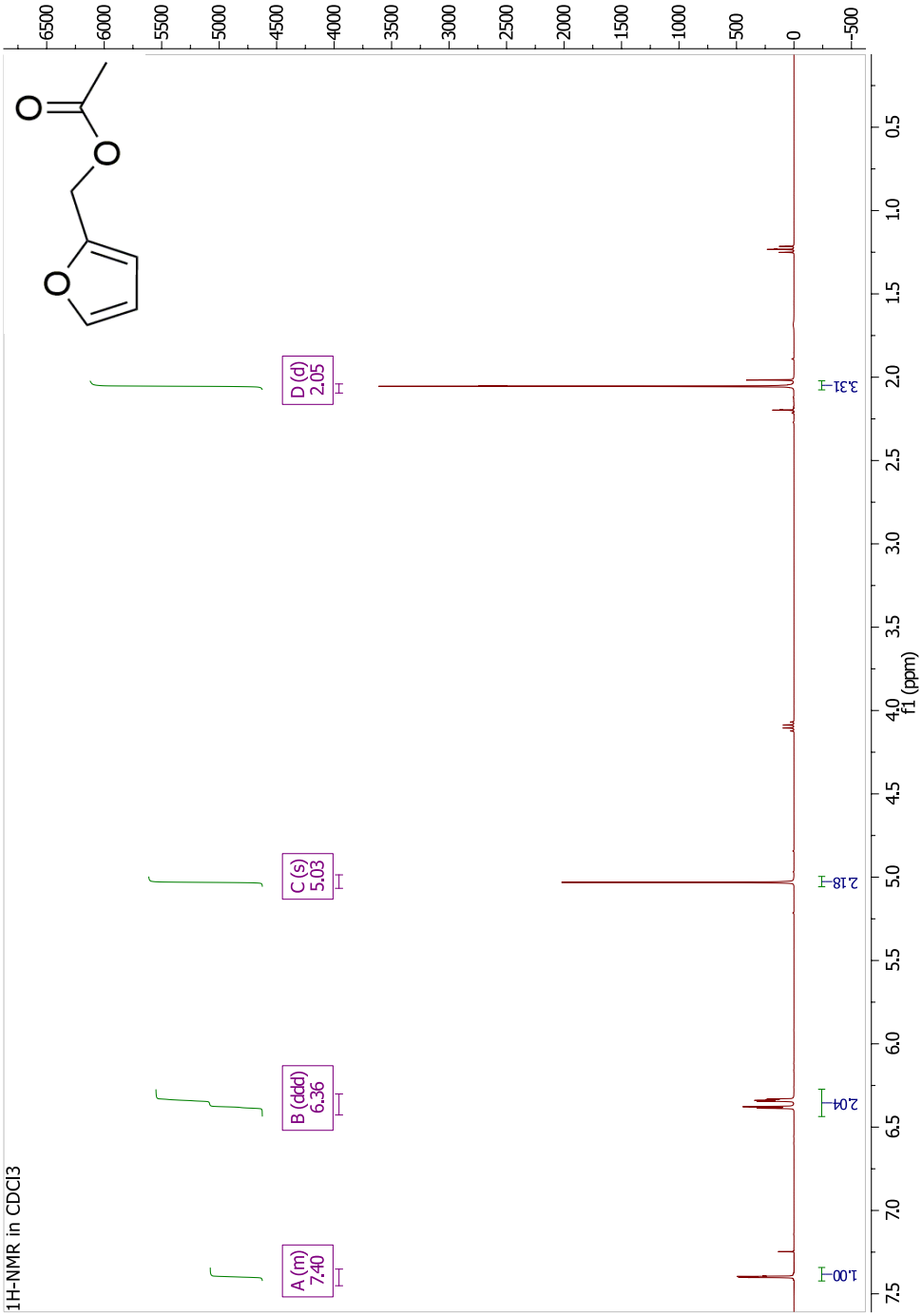

B.5 Methoxymethyl furan (39)

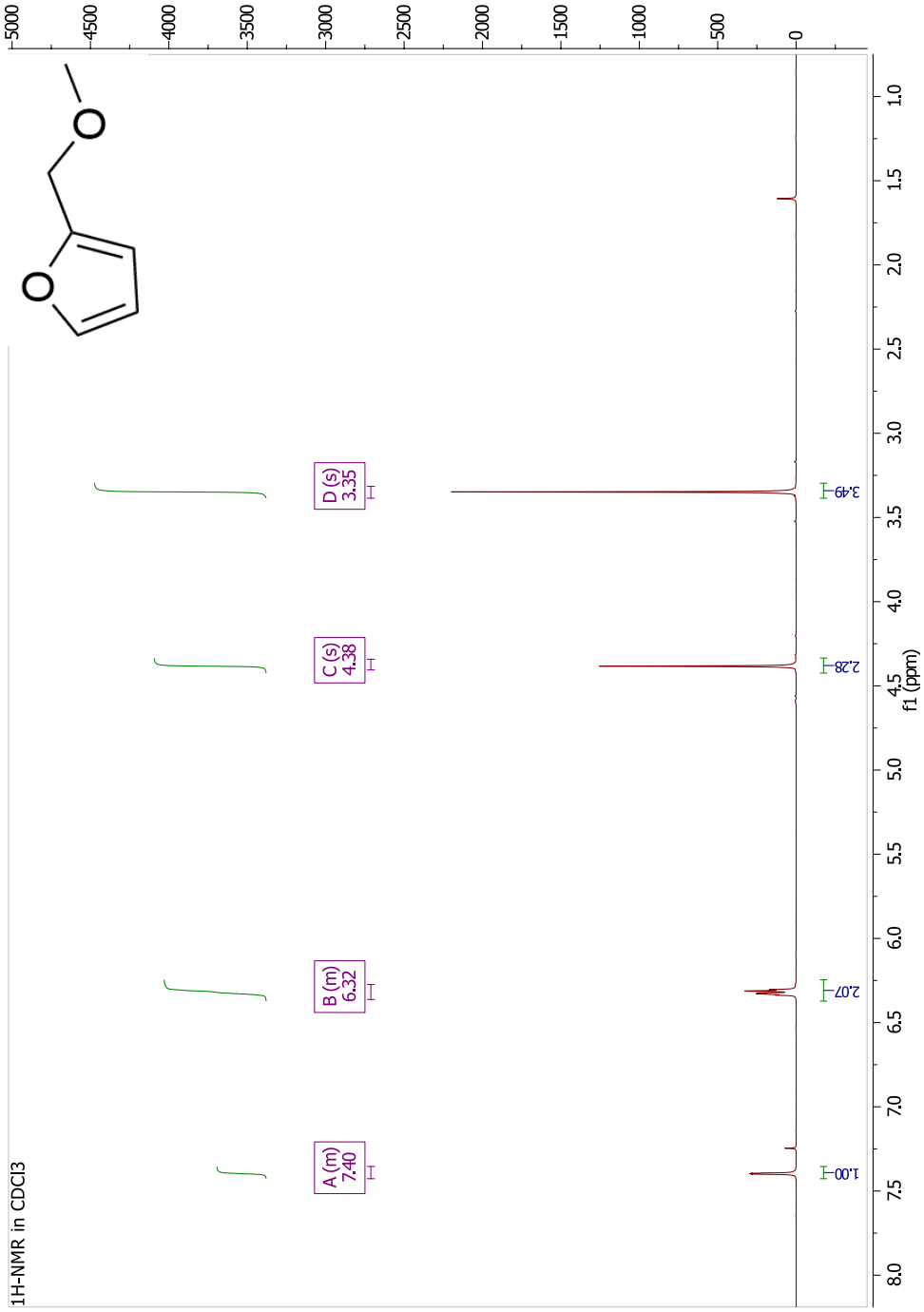

B.6 Methyl acrylate (27)

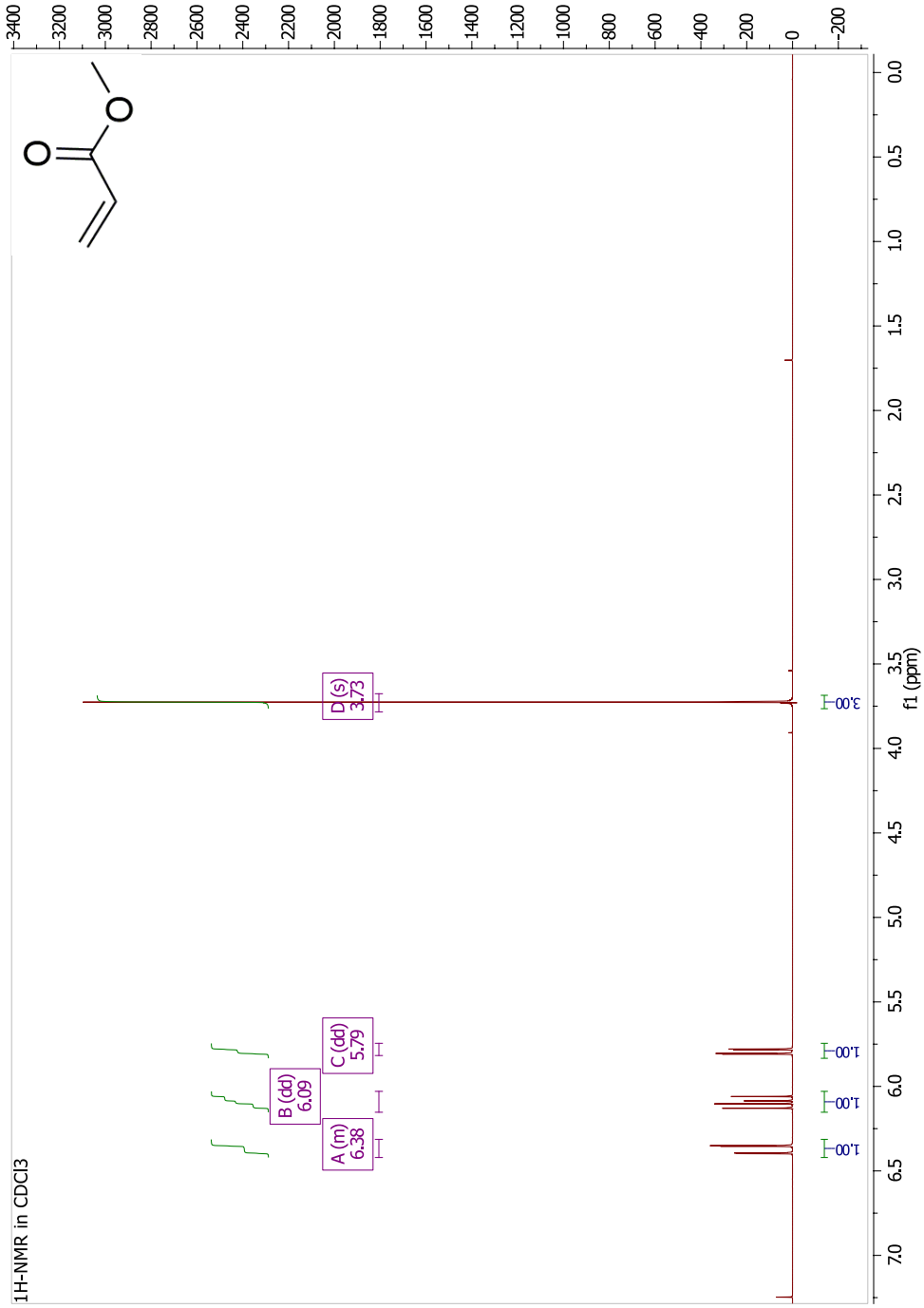

B.7 1,1,1,3,3,3-hexafluoroisopropyl acrylate (37)

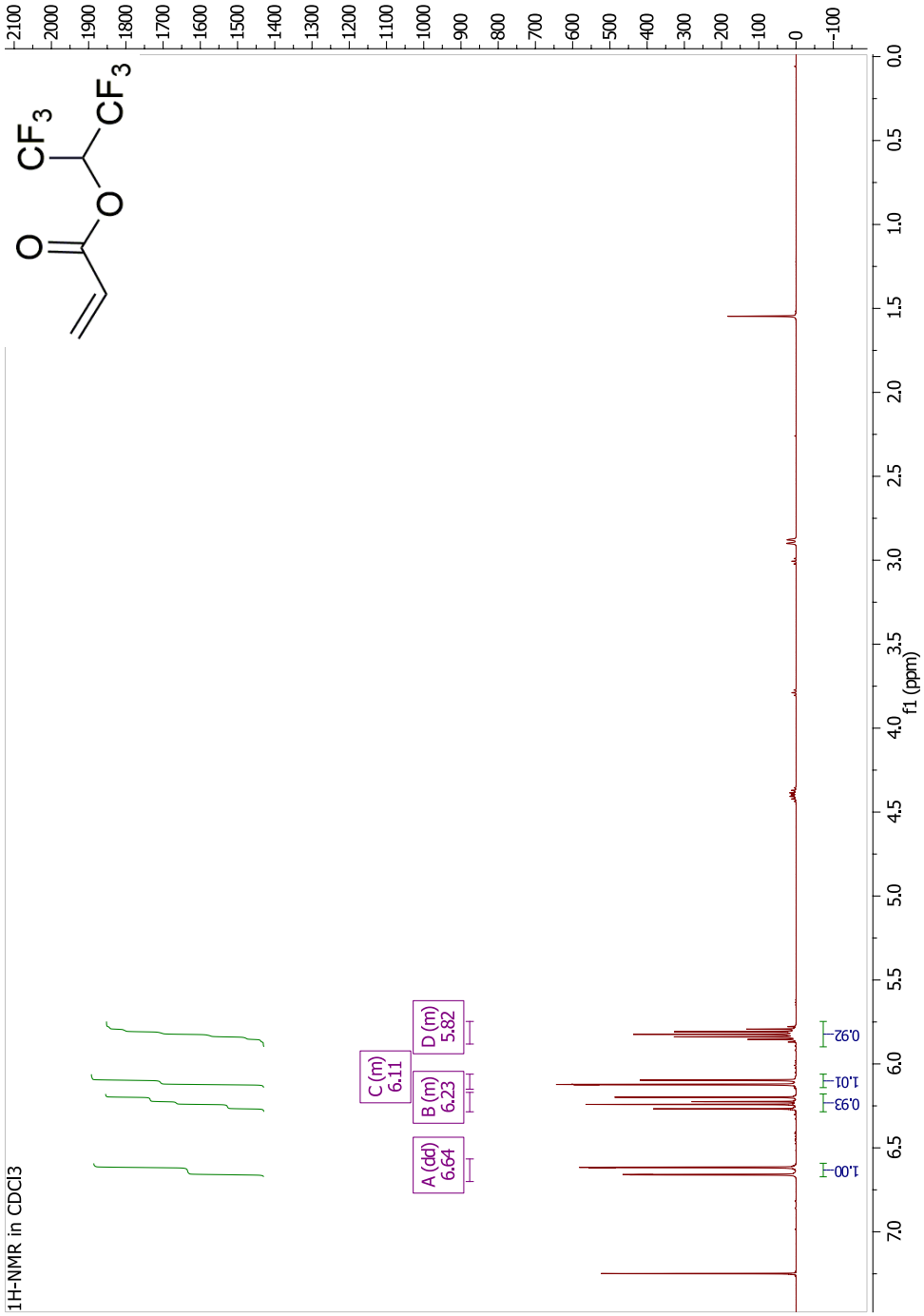

B.8 Lactone (30)

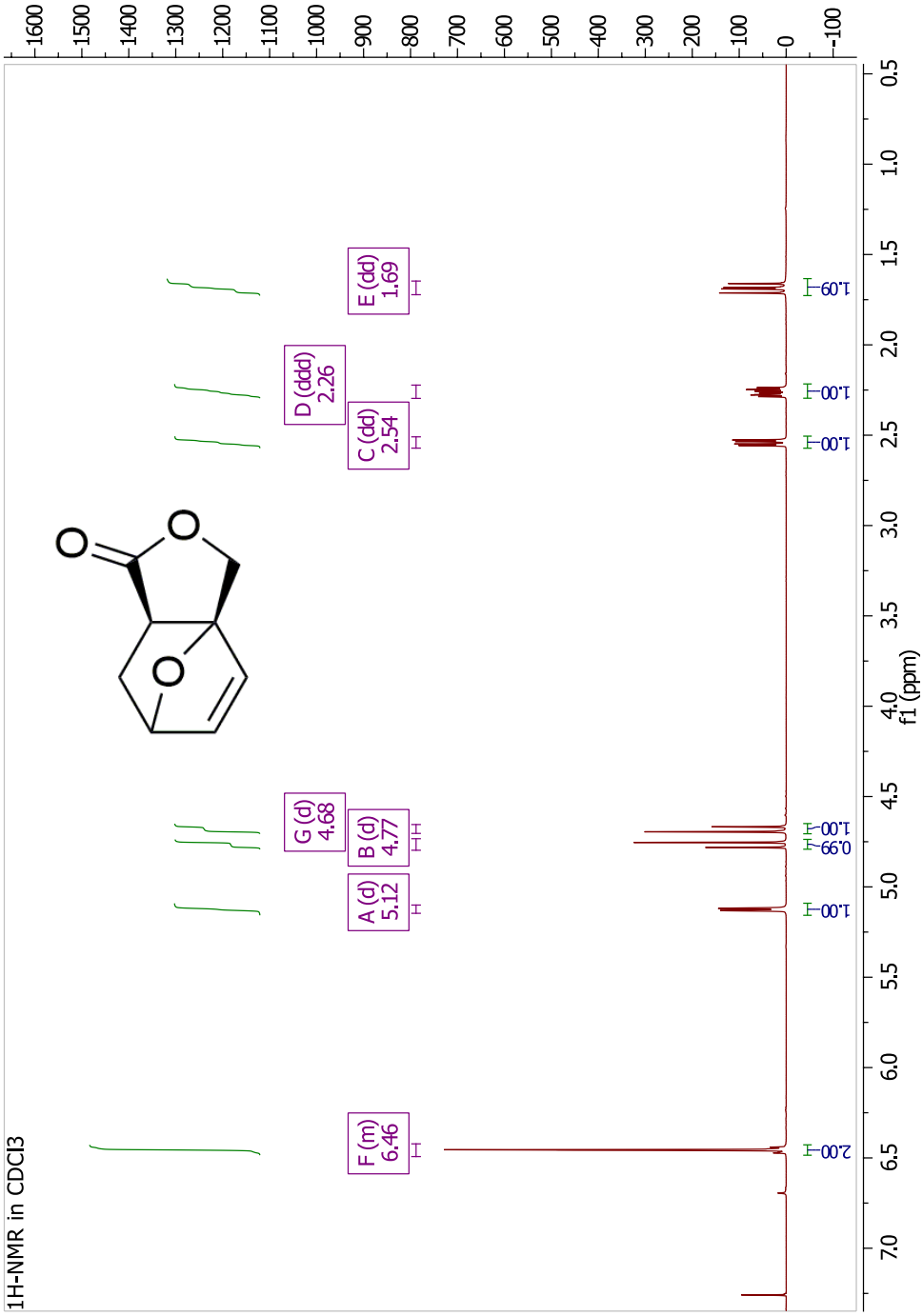

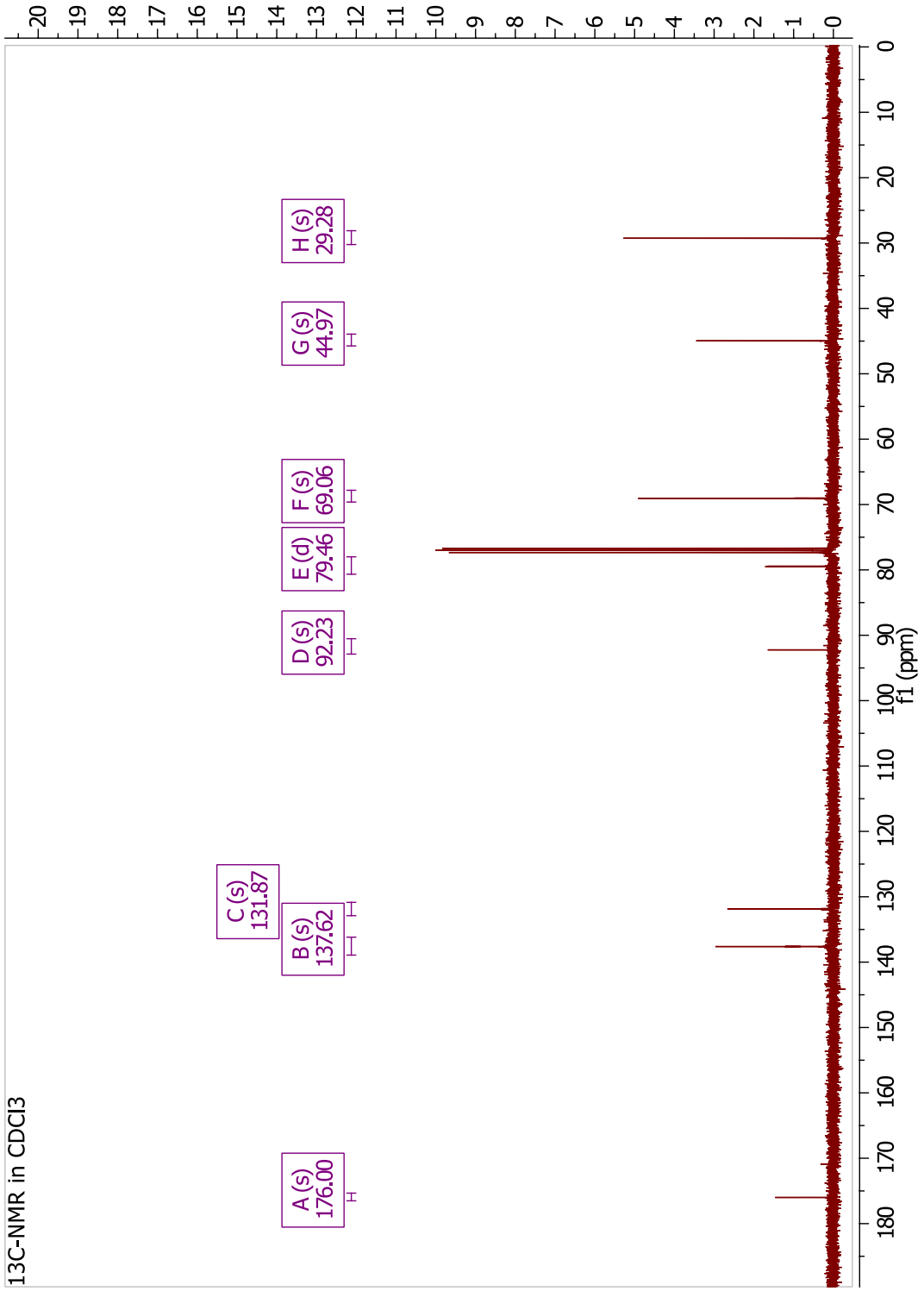
13C-NMR in CDCl3
A (s)
176.00
B (s)
137.62
C (s)
131.87
D (s)
92.23
E (d)
79.46
F (s)
69.06
G (s)
44.97
H (s)
29.28
f1 (ppm)

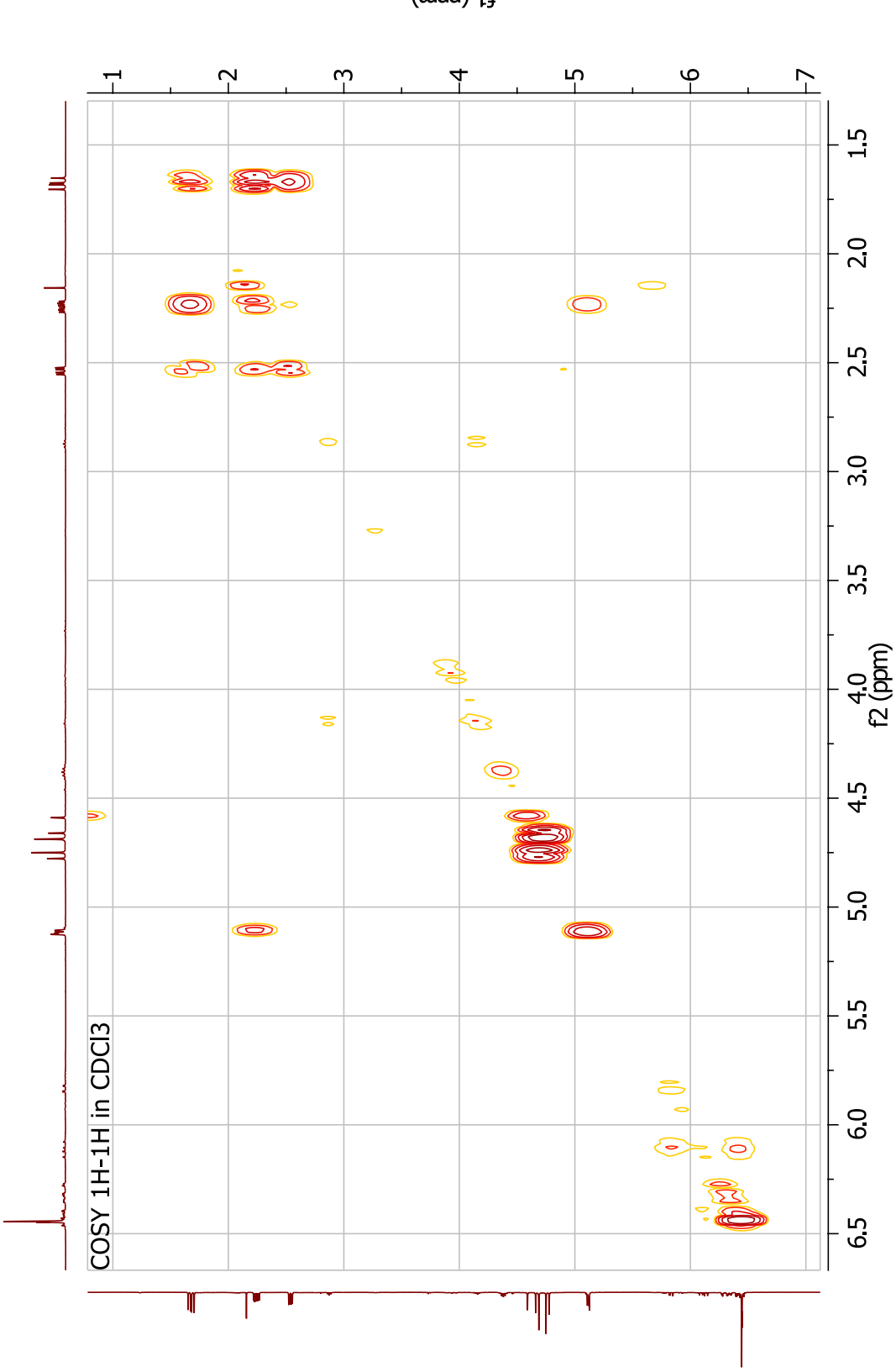
COSY 1H-1H in CDCl3
f2 (ppm)
f1 (ppm)
1.5
2.0
2.5
3.0
3.5
4.0
4.5
5.0
5.5
6.0
6.5
1
2
3
4
5
6
7

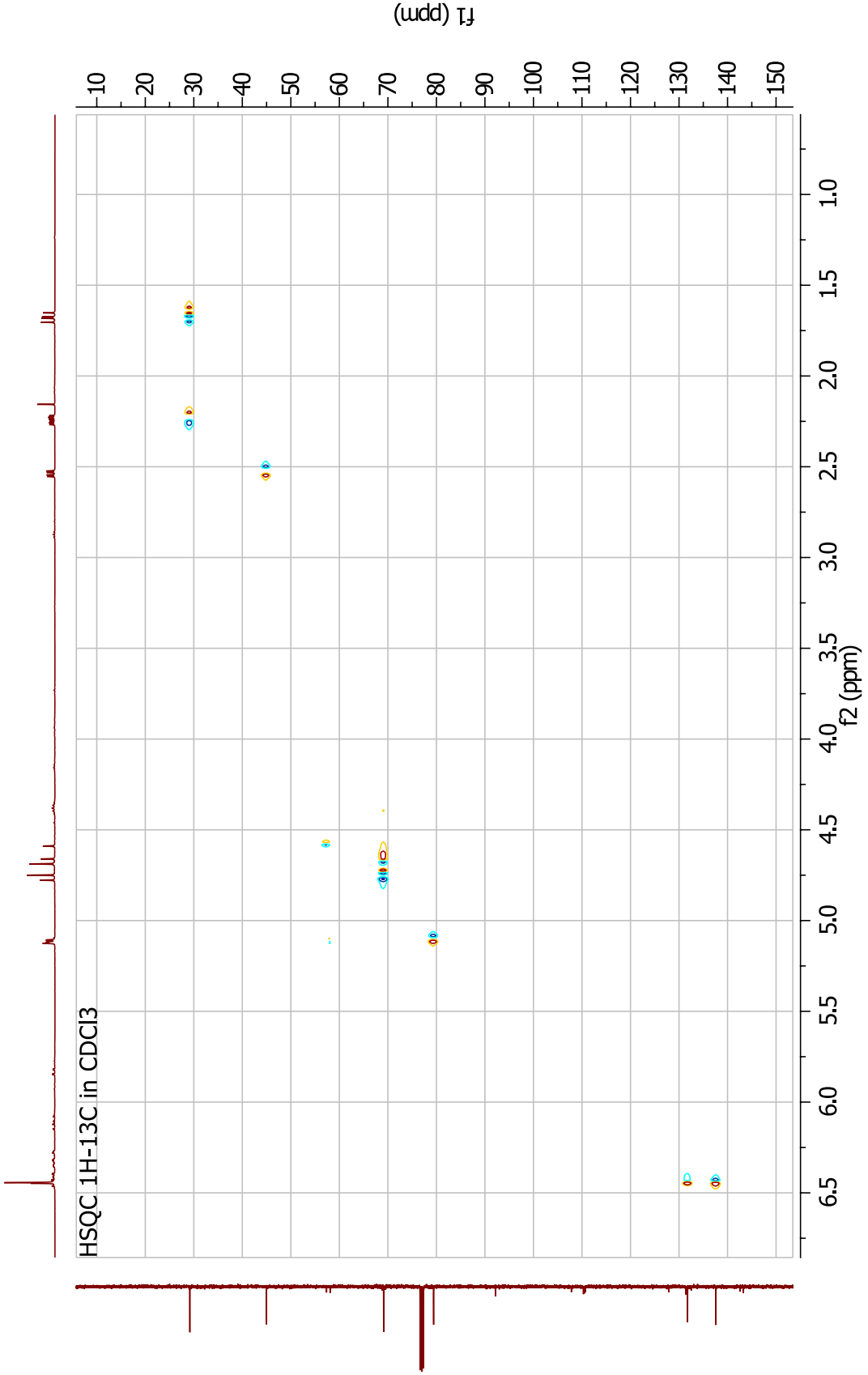
HSQC 1H-13C in CDCl3
f2 (ppm)
f1 (ppm)

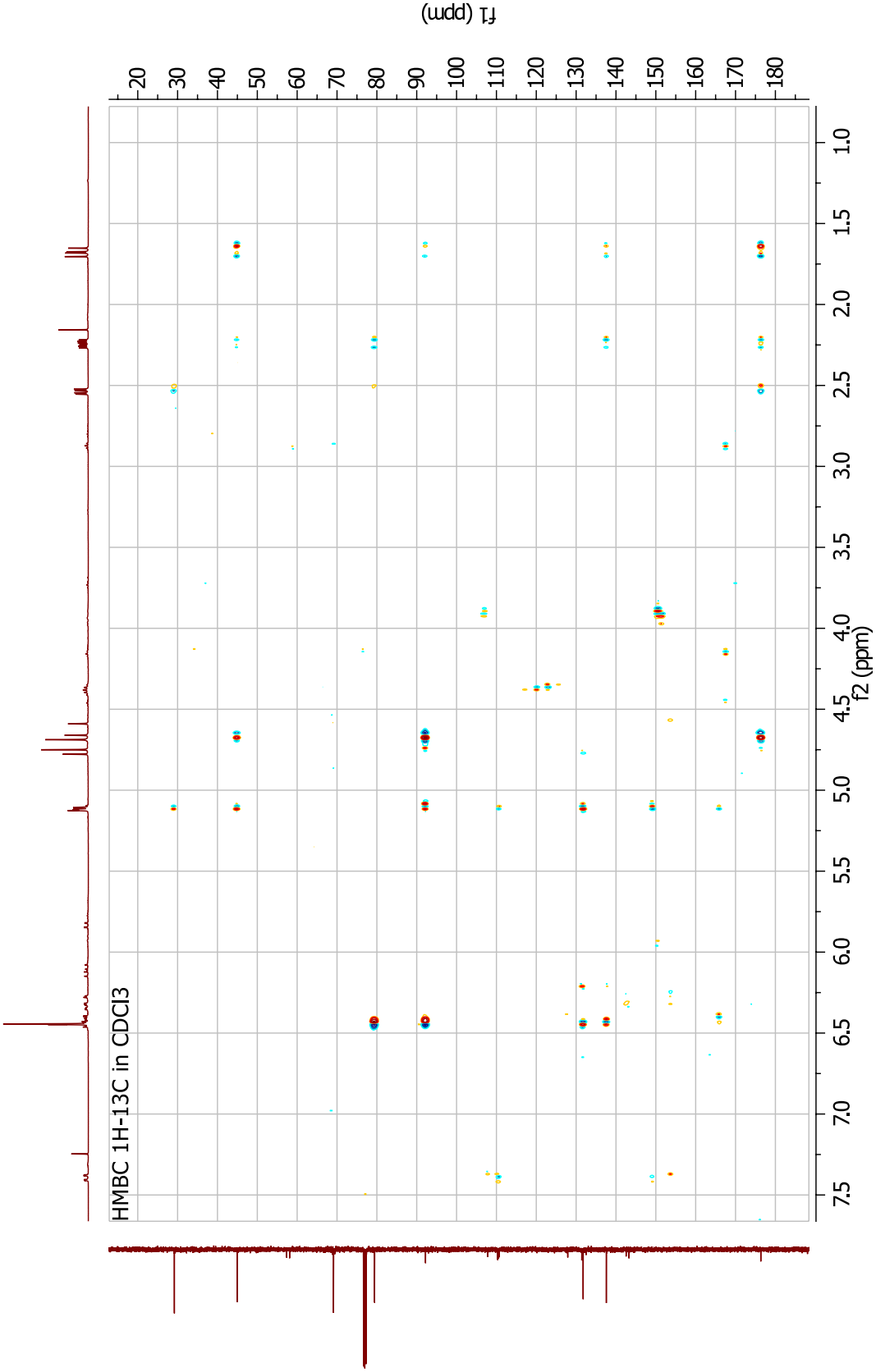
HMBC 1H-13C in CDCl3
f2 (ppm)
f1 (ppm)

B.9 Mixture of FuAl and MeAc DA products (38)

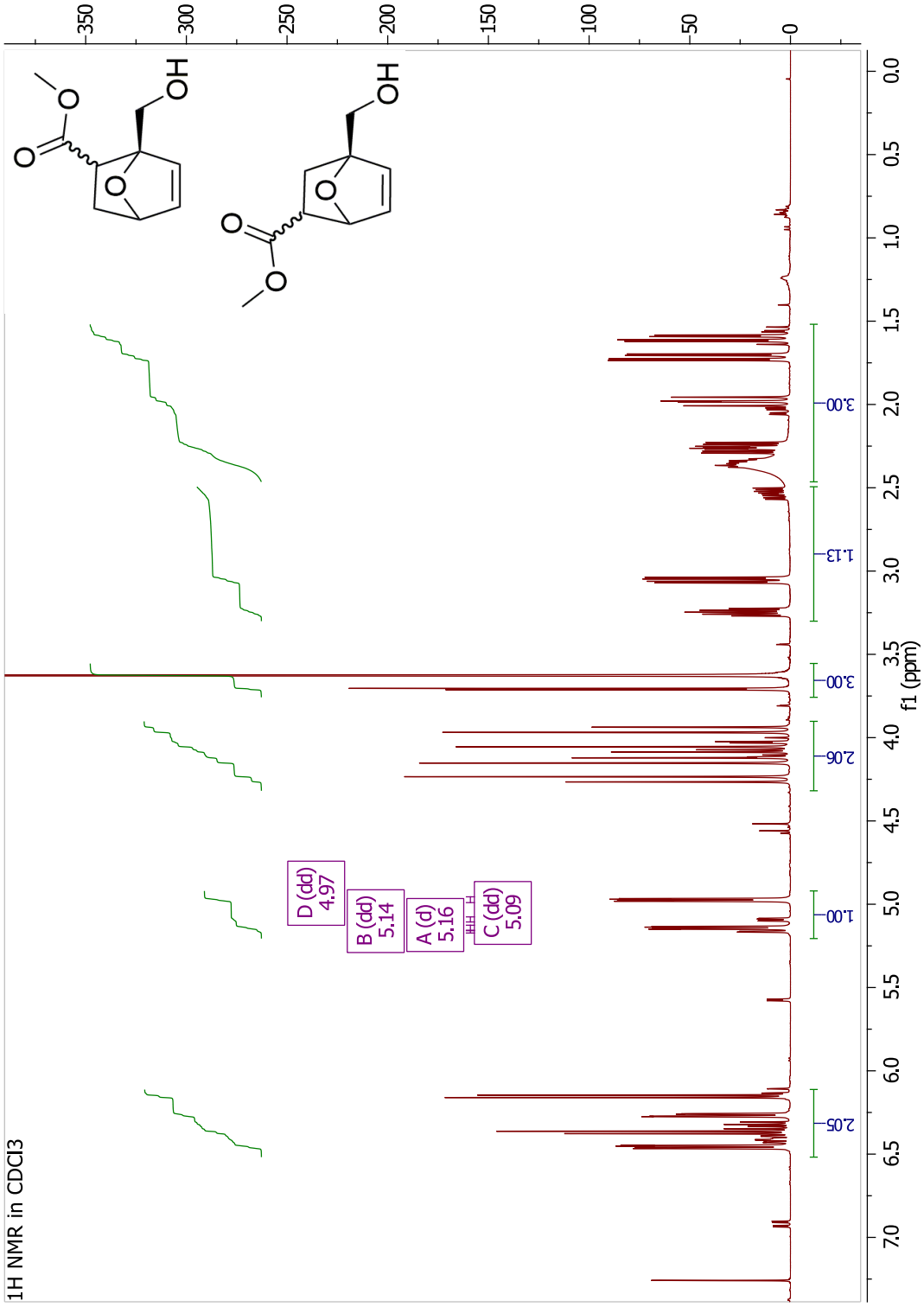

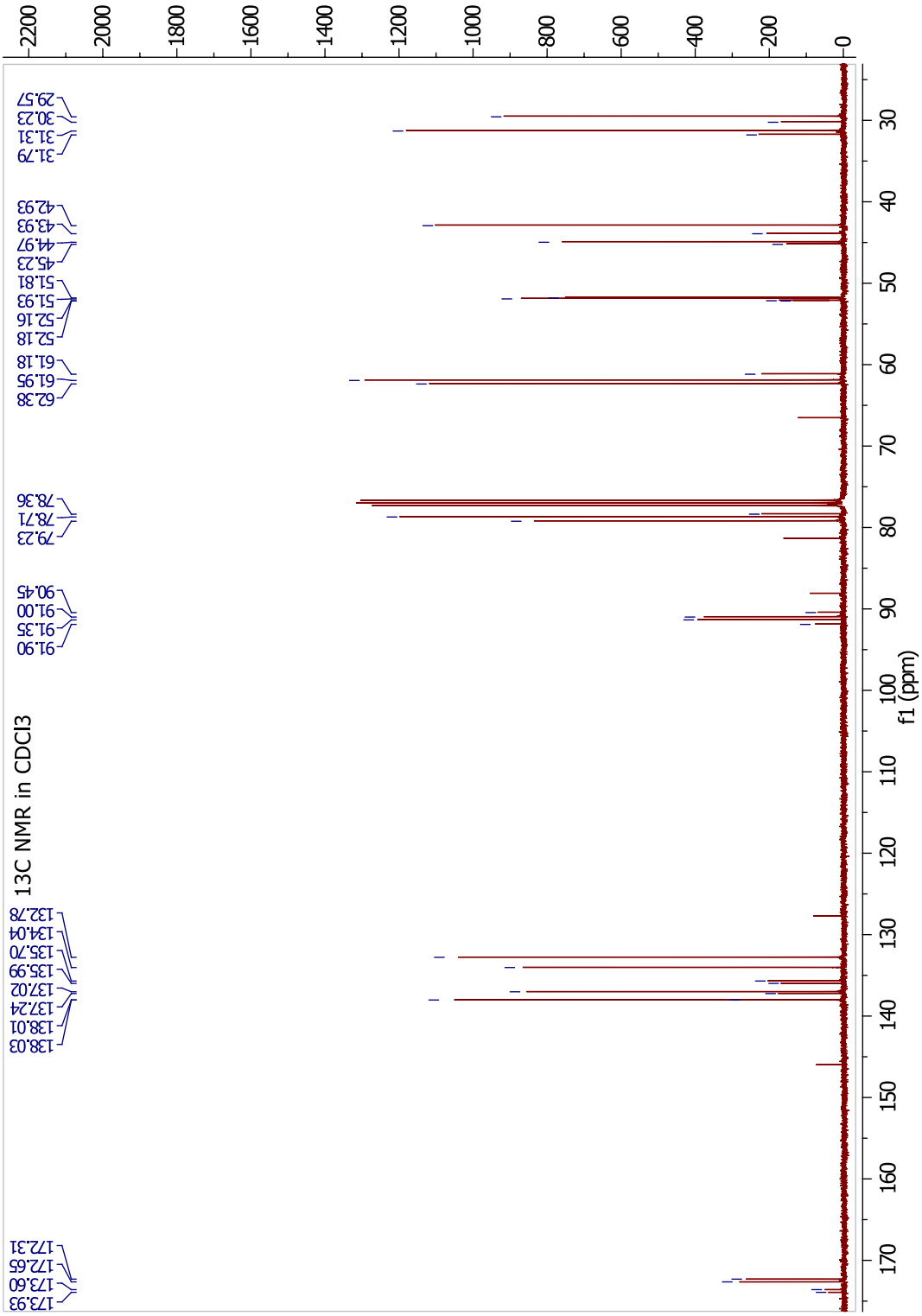
13C NMR in CDCl3
173.93
173.60
172.65
172.31
138.03
138.01
137.24
137.02
135.99
135.70
134.04
132.78
91.90
91.35
91.00
90.45
79.23
78.71
78.36
62.38
61.95
61.18
52.18
52.16
51.93
51.81
45.23
44.97
43.93
42.93
31.79
31.31
30.23
29.57
f1 (ppm)

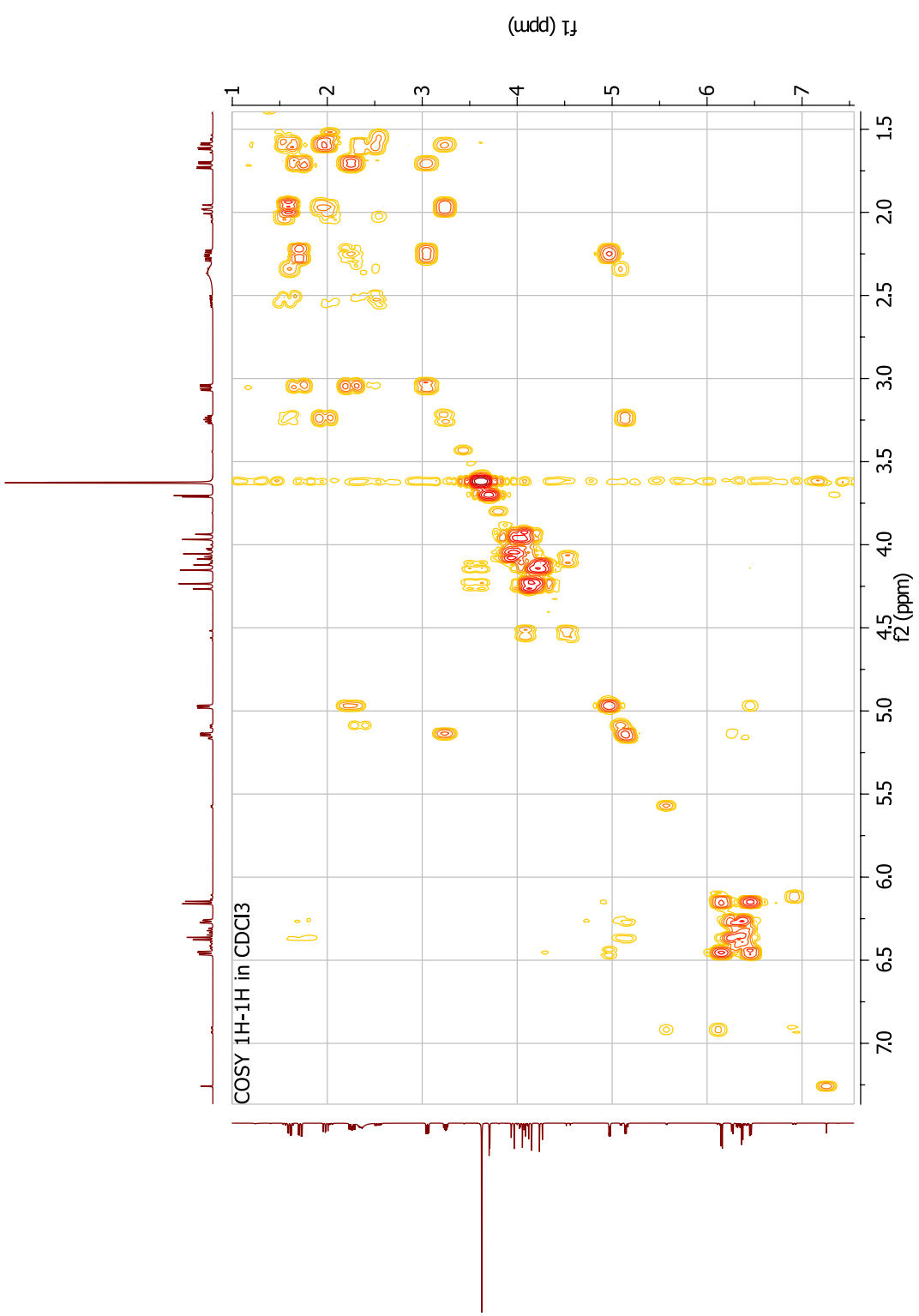
COSY 1H-1H in CDCl3
f2 (ppm)
f1 (ppm)
1.5
2.0
2.5
3.0
3.5
4.0
4.5
5.0
5.5
6.0
6.5
7.0
1
2
3
4
5
6
7

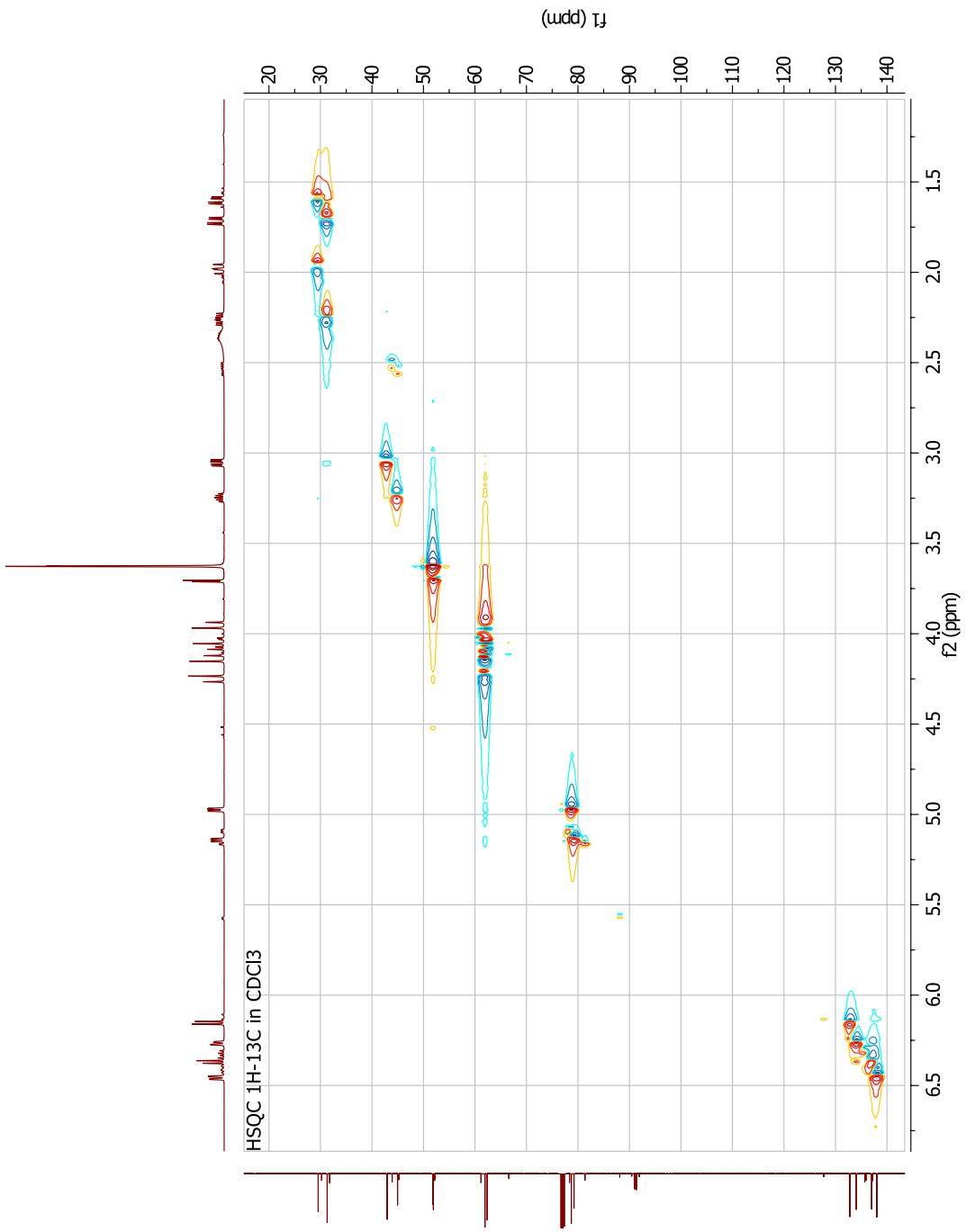
HSQC 1H-13C in CDCl3
f2 (ppm)
f1 (ppm)

B.10 FuAl and HFIPAcr Endo/Ortho DA product (41A)

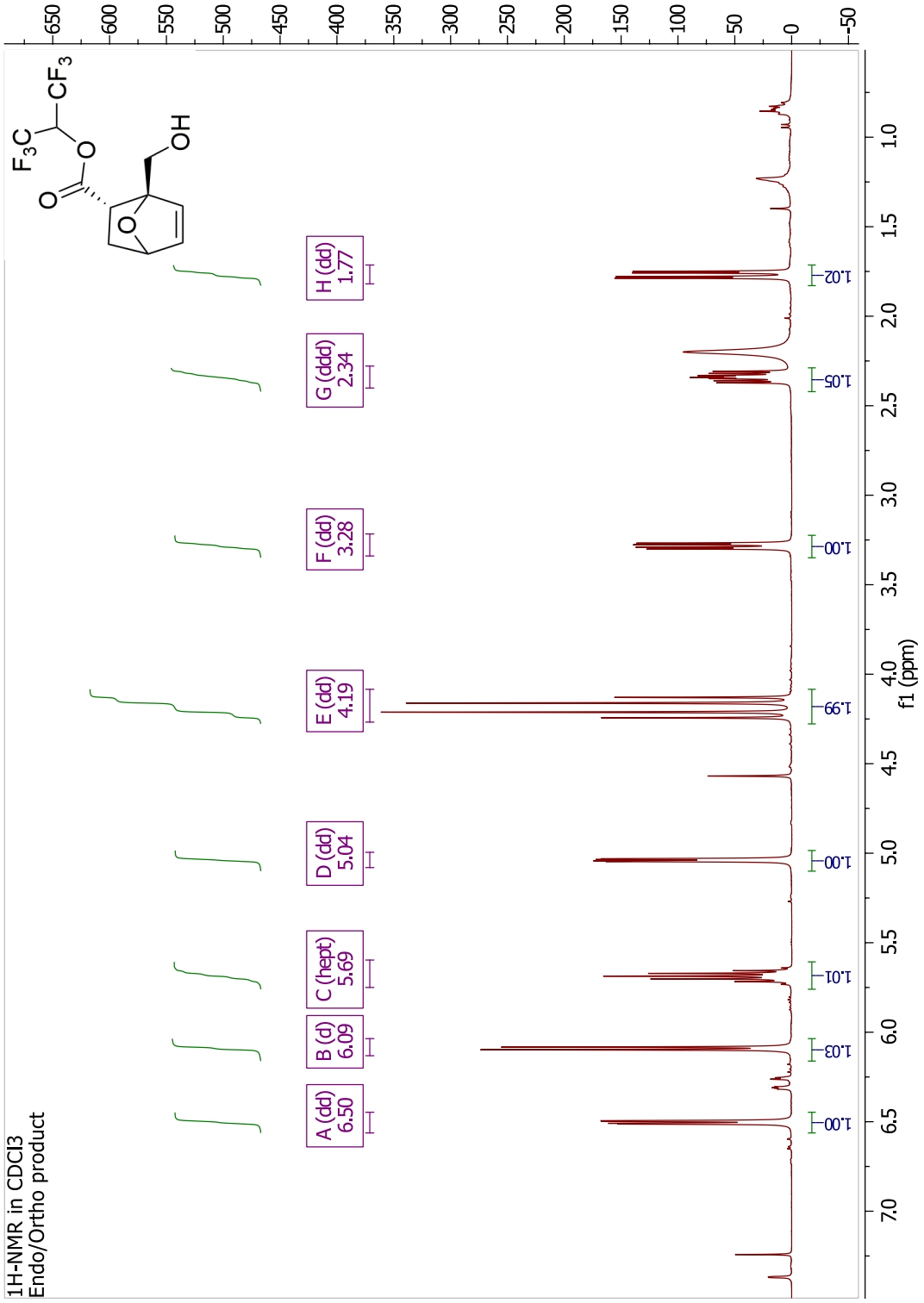

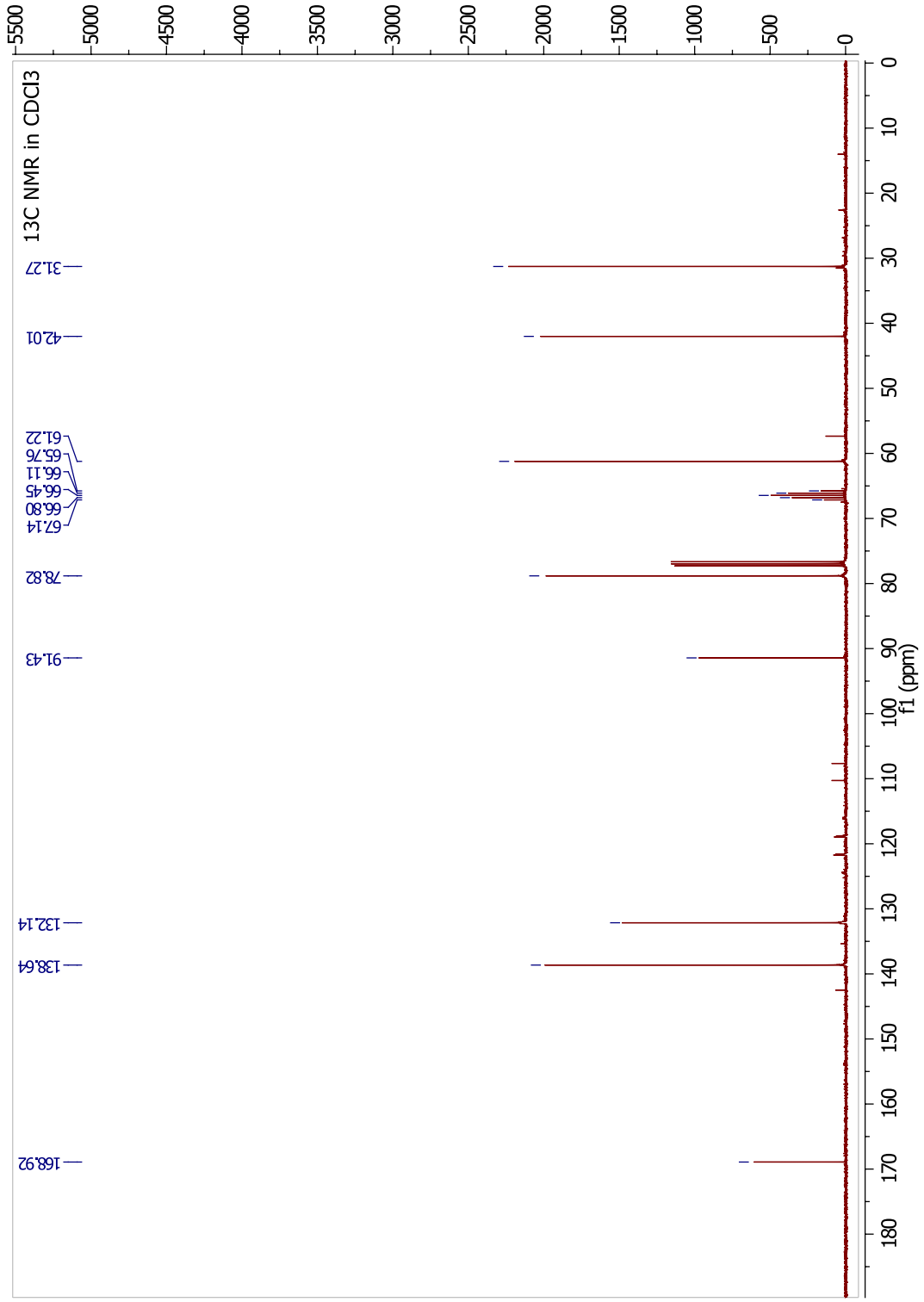
13C NMR in CDCl3
168.92
138.64
132.14
91.43
78.82
67.14
66.80
66.45
66.11
65.76
61.22
42.01
31.27
f1 (ppm)

B.11 FuAl and HFIPAcr crude DA products (41)

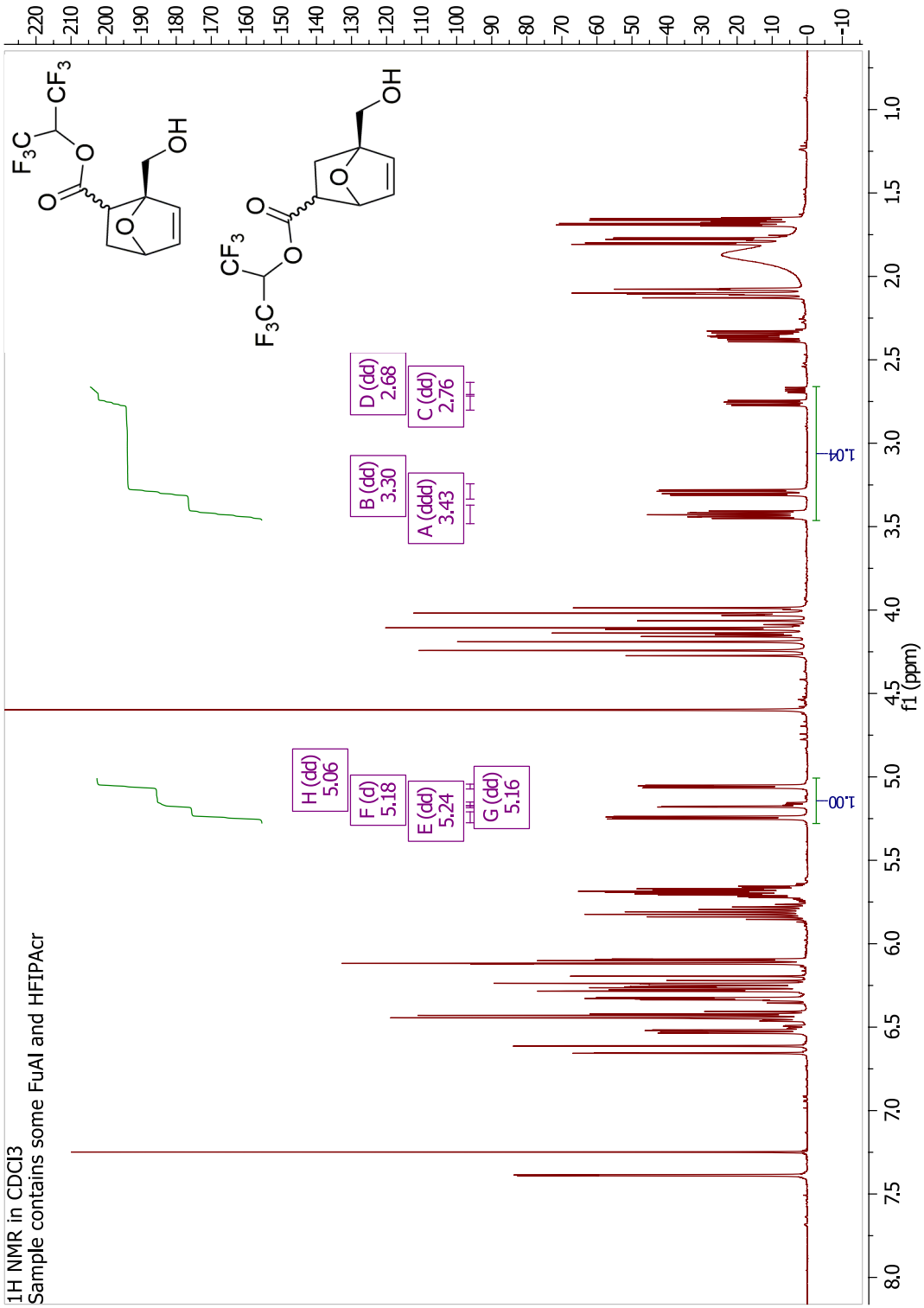

B.12 Crude NMR of 3-formyl benzoic acid in aromatisation product mixture(44)

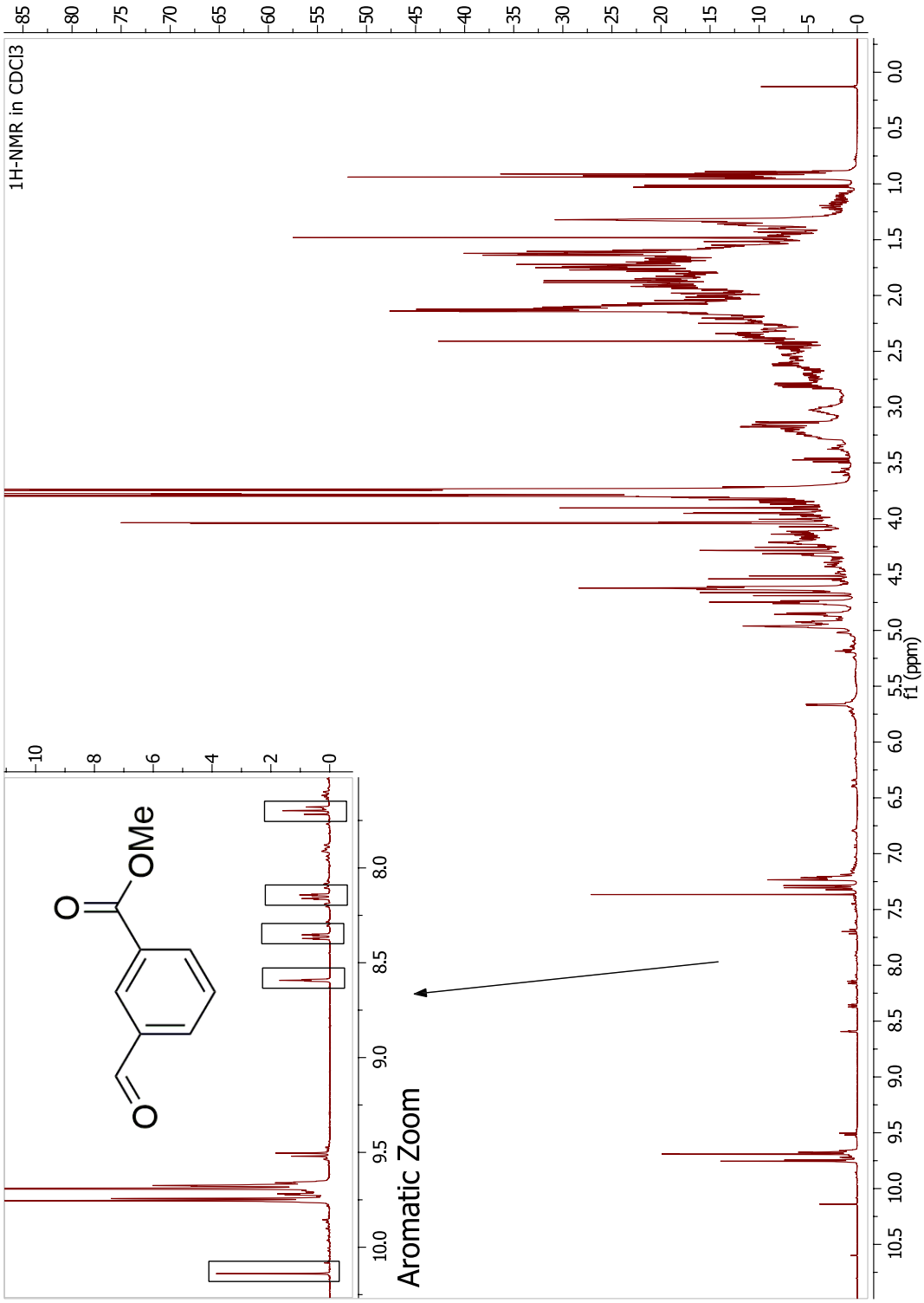

B.13 Diacetate aromatisation intermediate (47)

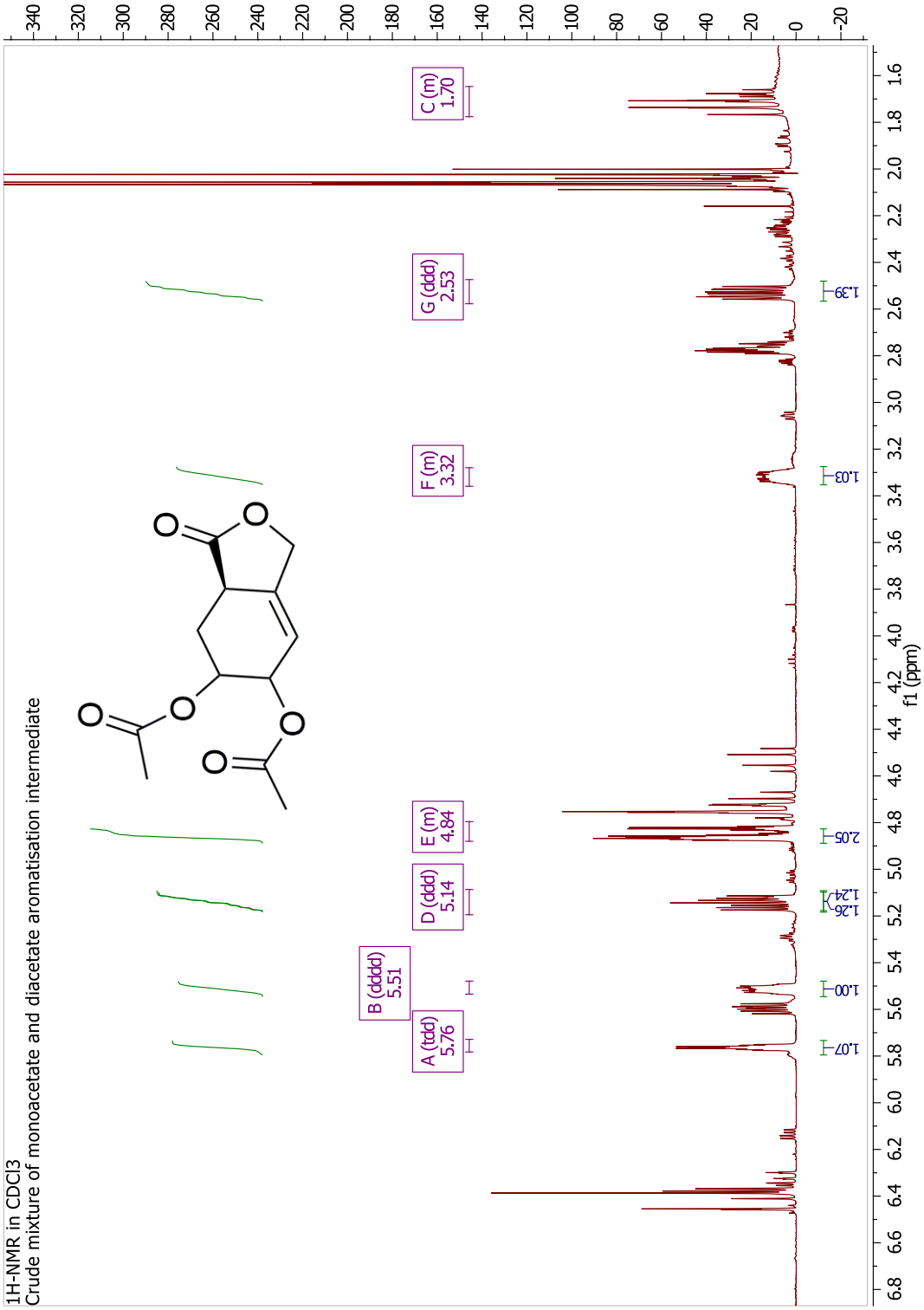

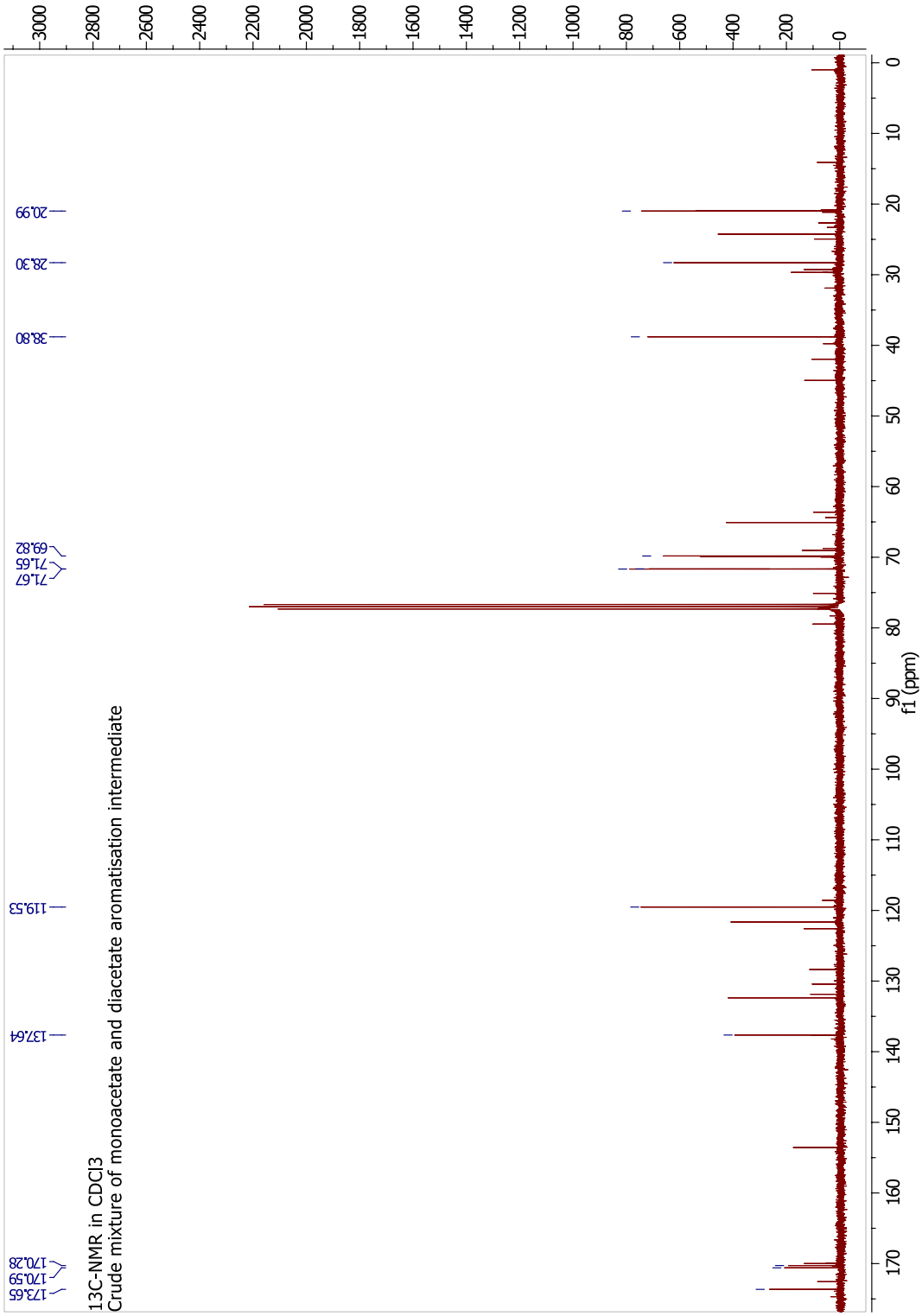
13C-NMR in CDCl3
Crude mixture of monoacetate and diacetate aromatisation intermediate
173.65
170.59
170.28
137.64
119.53
69.82
71.65
71.67
38.80
28.30
20.99
f1 (ppm)

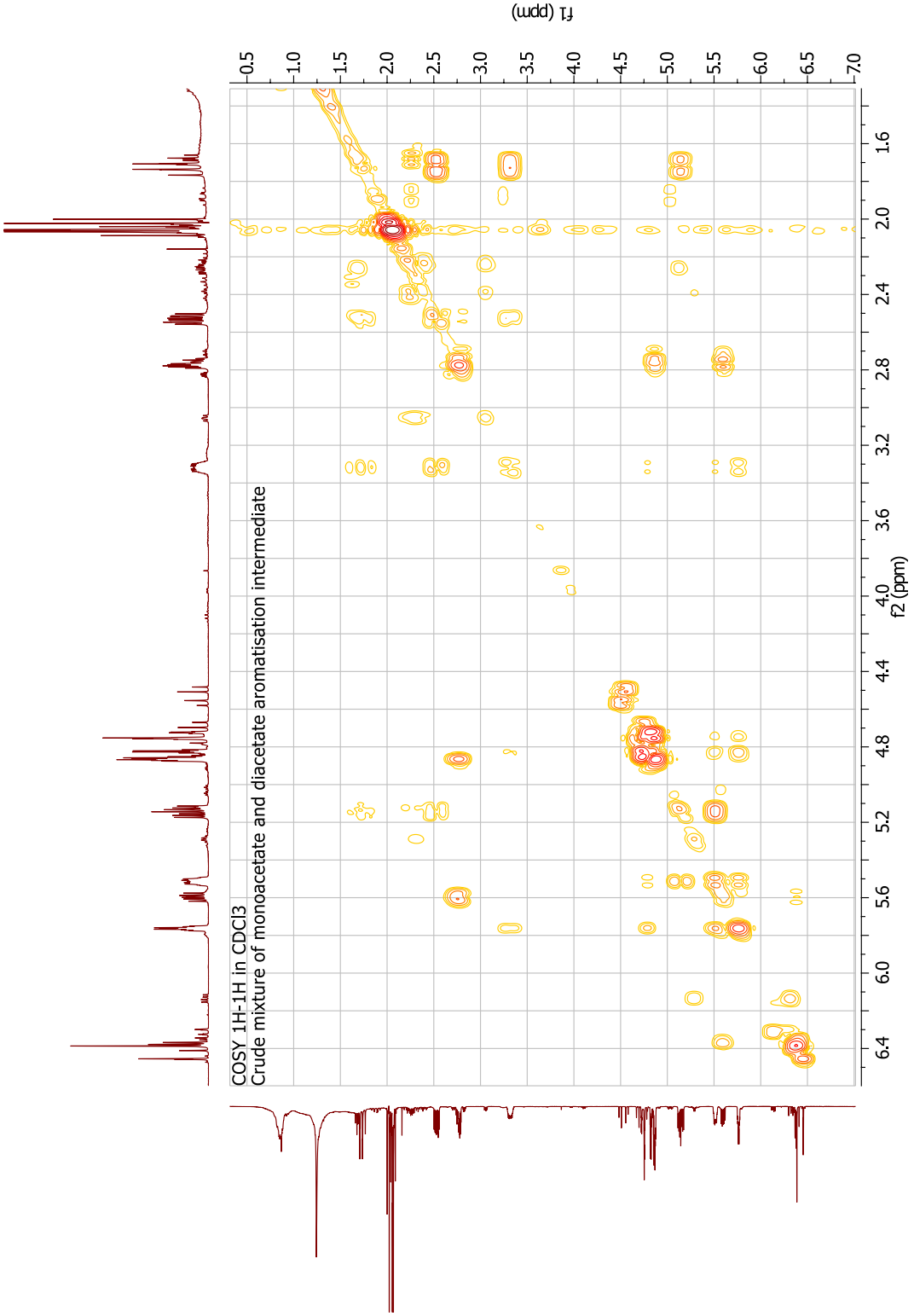
COSY 1H-1H in CDCl3
Crude mixture of monoacetate and diacetate aromatisation intermediate
f2 (ppm)
f1 (ppm)

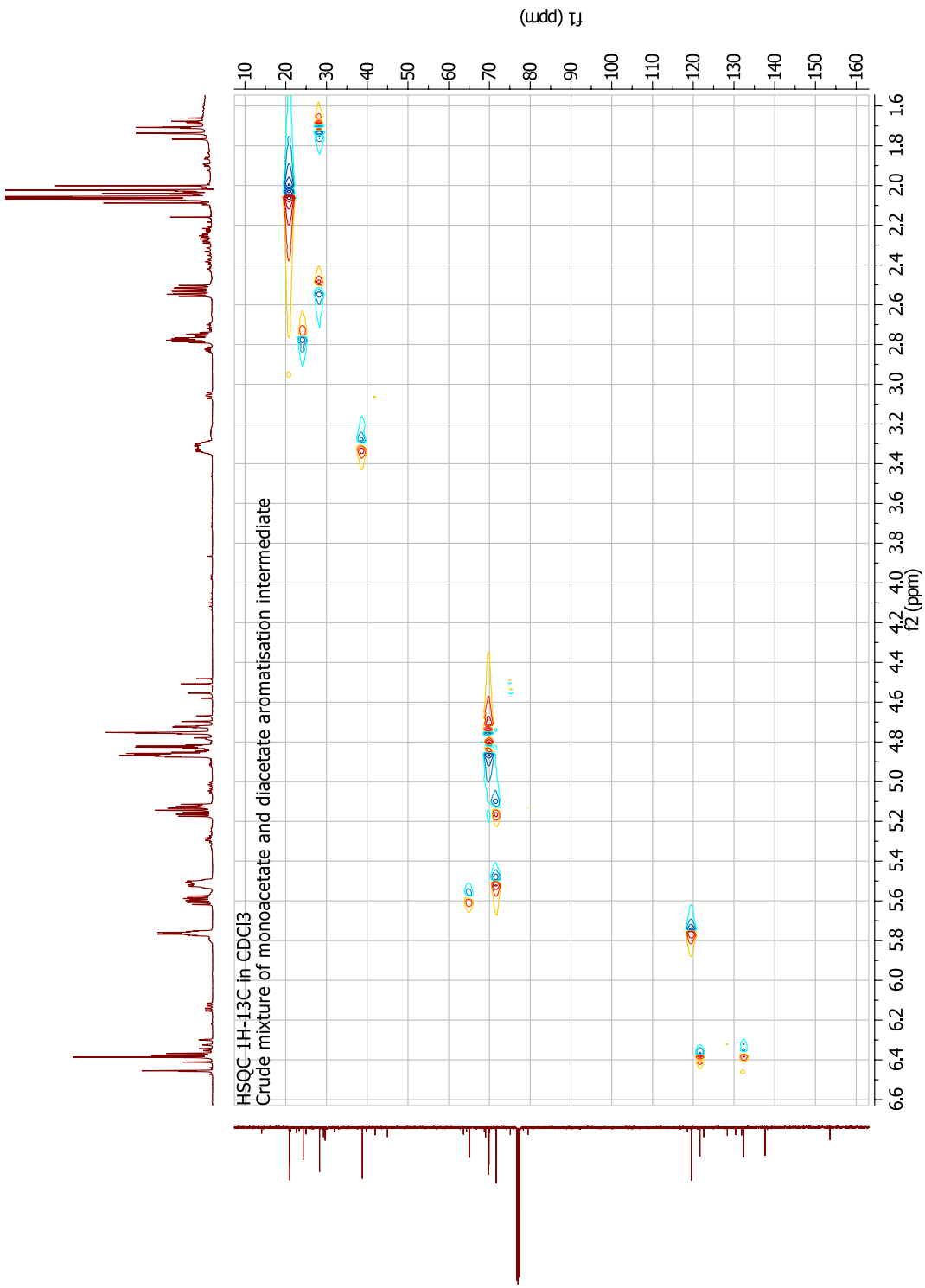
HSQC 1H-13C in CDCl3
Crude mixture of monoacetate and diacetate aromatisation intermediate
f1 (ppm)
f2 (ppm)

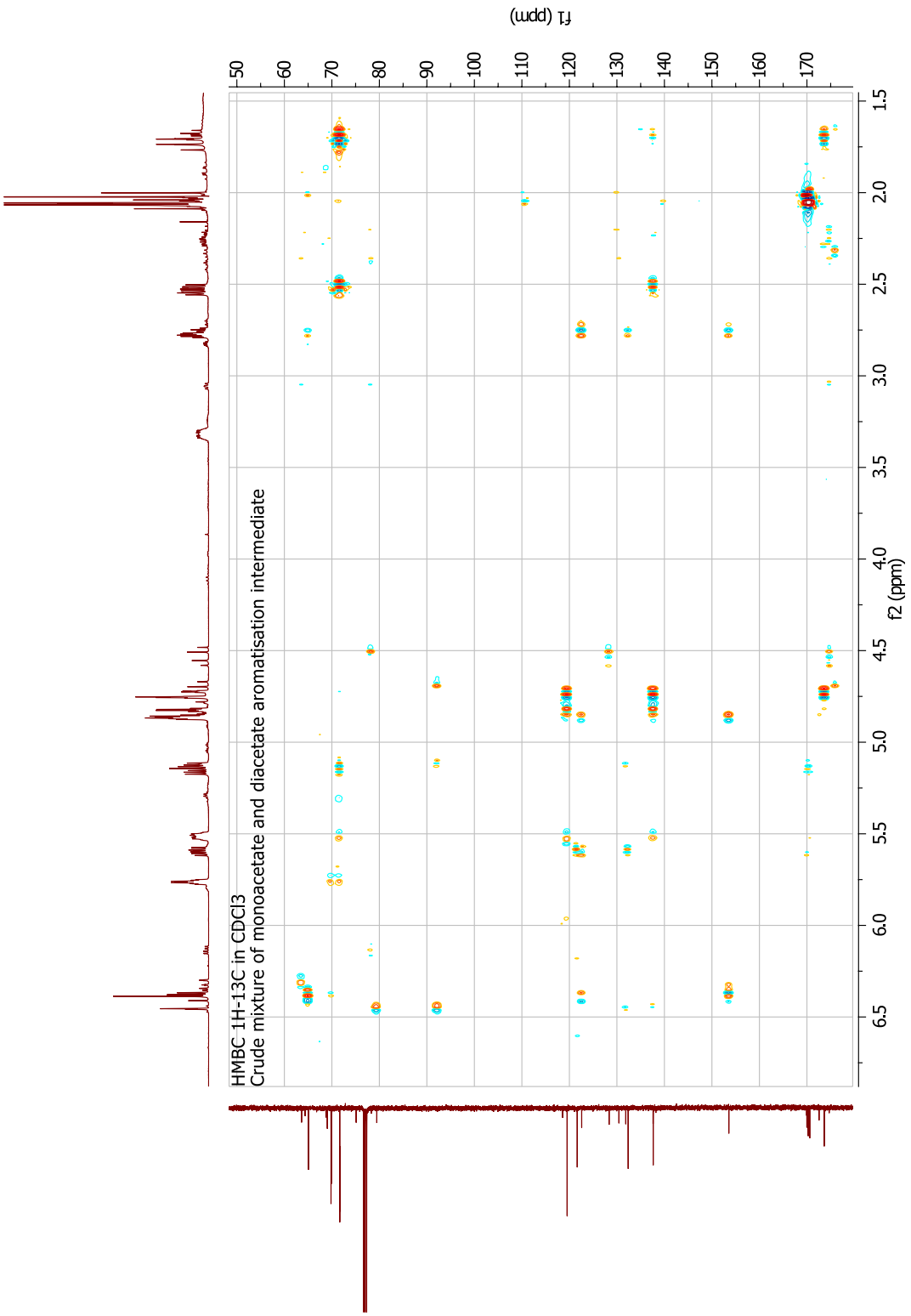
HMBC 1H-13C in CDCl3
Crude mixture of monoacetate and diacetate aromatisation intermediate
f2 (ppm)
f1 (ppm)

B.14 Monoacetate aromatisation intermediate (48)

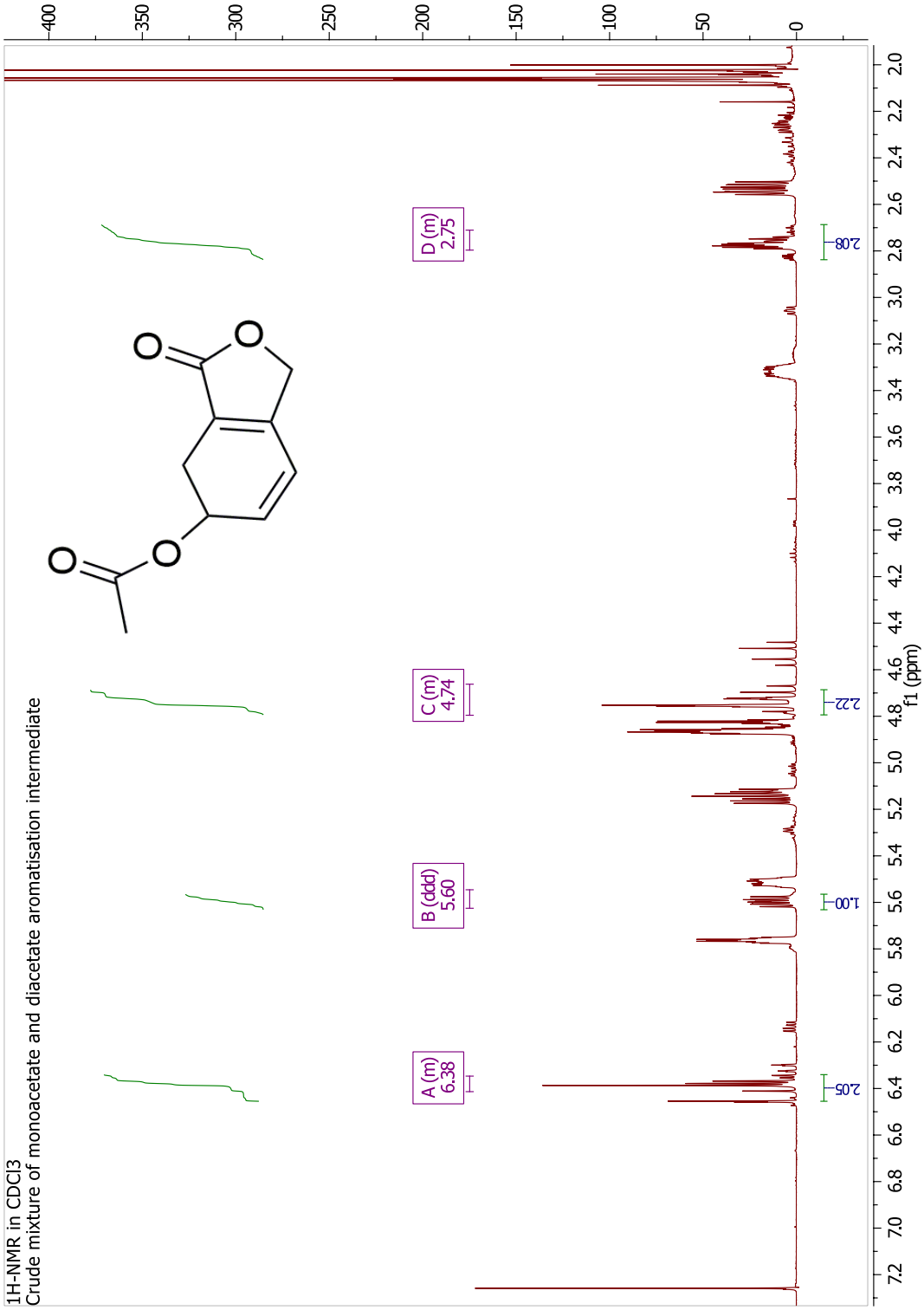

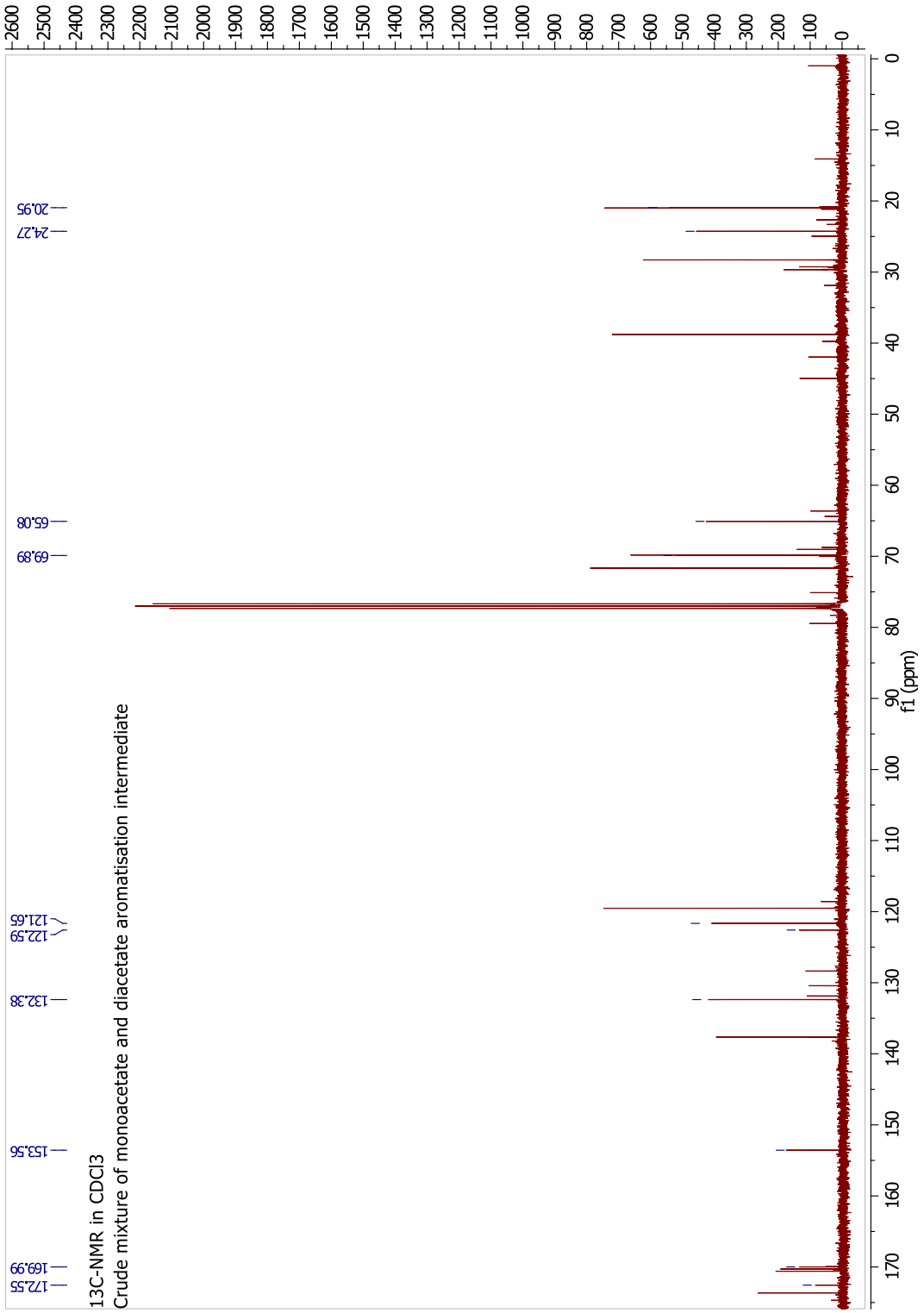
13C-NMR in CDCl3
Crude mixture of monoacetate and diacetate aromatisation intermediate
20.95
24.27
65.08
69.89
121.65
122.59
132.38
153.56
169.99
172.55
f1 (ppm)

B.15 Phthalide (31)

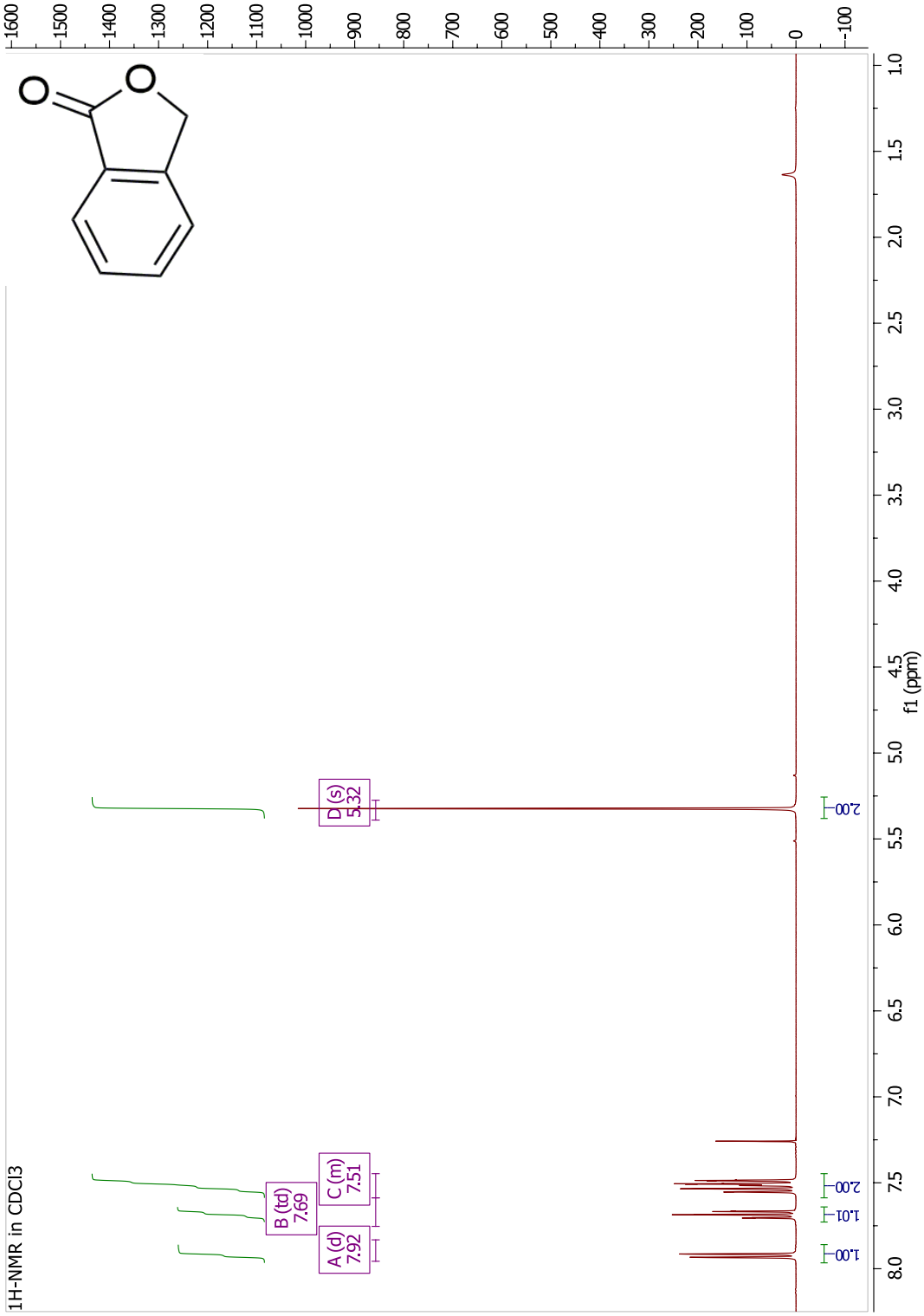

Bibliography

[1] Claus Hviid Christensen et al. "The Renewable Chemicals Industry". In: *ChemSusChem* 1.4 (Apr. 2008), pp. 283–289. ISSN: 18645631. DOI: 10.1002/cssc.200700168. URL: http://doi.wiley.com/10.1002/cssc.200700168.

[2] Pieter C A Bruijnincx and Bert M. Weckhuysen. "Shale Gas Revolution: An Opportunity for the Production of Biobased Chemicals?" In: *Angewandte Chemie International Edition* 52.46 (Nov. 2013), pp. 11980–11987. ISSN: 14337851. DOI: 10.1002/anie.201305058. URL: http://doi.wiley.com/10.1002/anie.201305058.

[3] Amy E. Settle et al. "Heterogeneous Diels–Alder catalysis for biomass-derived aromatic compounds". In: *Green Chemistry* 19.15 (2017), pp. 3468–3492. ISSN: 1463-9262. DOI: 10.1039/C7GC00992E. URL: http://xlink.rsc.org/?DOI=C7GC00992E.

[4] Fabian Lenk et al. "On the usage of agricultural raw materials – energy or food? An assessment from an economics perspective". In: *Biotechnology Journal* 2.12 (Dec. 2007), pp. 1497–1504. ISSN: 18606768. DOI: 10.1002/biot.200700153. URL: http://doi.wiley.com/10.1002/biot.200700153.

[5] Chun-Hui Zhou et al. "Catalytic conversion of lignocellulosic biomass to fine chemicals and fuels". In: *Chemical Society Reviews* 40.11 (2011), p. 5588. ISSN: 0306-0012. DOI: 10.1039/c1cs15124j. URL: http://xlink.rsc.org/?DOI=c1cs15124j.

[6] Gregg T. Beckham et al. "Opportunities and challenges in biological lignin valorization". In: *Current Opinion in Biotechnology* 42.March (Dec. 2016), pp. 40–53. ISSN: 09581669. DOI: 10.1016/j.copbio.2016.02.030. URL: http://linkinghub.elsevier.com/retrieve/pii/S0958166916300520.

[7] Roger A Sheldon. "Green and sustainable manufacture of chemicals from biomass: state of the art". In: *Green Chem.* 16.3 (2014), pp. 950–963. ISSN: 1463-9262. DOI: 10.1039/C3GC41935E. URL: http://xlink.rsc.org/?DOI=C3GC41935E.

[8] Avelino Corma, Sara Iborra, and Alexandra Velty. "Chemical Routes for the Transformation of Biomass into Chemicals". In: *Chemical Reviews* 107.6 (June 2007), pp. 2411–2502. ISSN: 0009-2665. DOI: 10.1021/cr050989d. URL: http://pubs.acs.org/doi/abs/10.1021/cr050989d.

[9] R. Kolodziej and J. Scheib. "Bio-isobutanol: The next-generation biofuel". In: *Hydrocarbon Processing* 91.9 (2012). ISSN: 00188190.

[10] Thomas J Farmer and Mark Mascal. "Platform Molecules". In: *Introduction to Chemicals from Biomass*. Ed. by Fabien Deswarte and James Clark. Second Edi. John Wiley & Sons, Ltd, 2015. Chap. 4, pp. 89–155.

[11] Fabrizio Cavani, Stefania Albonetti, and Francesco Basile. "Aromatics from Biomasses: Technological Options for Chemocatalytic Transformations". In: *Chemicals and Fuels from Bio-Based Building Blocks*. Ed. by Fabrizio Cavani et al. Wiley-VCH Verlag GmbH & Co. KGaA, 2016. Chap. 2, pp. 33–48.

[12] Furkan H. Isikgor and C. Remzi Becer. "Lignocellulosic biomass: a sustainable platform for the production of bio-based chemicals and polymers". In: *Polymer Chemistry* 6.25 (2015), pp. 4497–4559. ISSN: 1759-9954. DOI: 10.1039/C5PY00263J. URL: http://xlink.rsc.org/?DOI=C5PY00263J.

[13] Chun-Chih Chang et al. "Ultra-selective cycloaddition of dimethylfuran for renewable p-xylene with H-BEA". In: *Green Chem.* 16.2 (2014), pp. 585–588. ISSN: 1463-9262. DOI: 10.1039/C3GC40740C. URL: http://xlink.rsc.org/?DOI=C3GC40740C.

[14] Andy Maneffa, Peter Priecel, and Jose A. Lopez-Sanchez. "Biomass-Derived Renewable Aromatics: Selective Routes and Outlook for p -Xylene Commercialisation". In: *ChemSusChem* 9.19 (Oct. 2016), pp. 2736–2748. ISSN: 18645631. DOI: 10.1002/cssc.201600605. URL: http://doi.wiley.com/10.1002/cssc.201600605.

[15] Mika Shiramizu and F. Dean Toste. "On the Diels-Alder Approach to Solely Biomass-Derived Polyethylene Terephthalate (PET): Conversion of 2,5-Dimethylfuran and Acrolein into p-Xylene". In: *Chemistry - A European Journal* 17.44 (Oct. 2011), pp. 12452–12457. ISSN: 09476539. DOI: 10.1002/chem.201101580. URL: http://doi.wiley.com/10.1002/chem.201101580.

[16] Hong Je Cho et al. "Renewable p -Xylene from 2,5-Dimethylfuran and Ethylene Using Phosphorus-Containing Zeolite Catalysts". In: *ChemCatChem* 9.3 (Feb. 2017), pp. 398–402. ISSN: 18673880. DOI: 10.1002/cctc.201601294. URL: http://doi.wiley.com/10.1002/cctc.201601294.

[17] Eyas Mahmoud et al. "Diels–Alder and Dehydration Reactions of Biomass-Derived Furan and Acrylic Acid for the Synthesis of Benzoic Acid". In: *ACS Catalysis* 5.11 (Nov. 2015), pp. 6946–6955. ISSN: 2155-5435. DOI: 10.1021/acscatal.5b01892. URL: http://dx.doi.org/10.1021/acscatal.5b01892http://pubs.acs.org/doi/10.1021/acscatal.5b01892.

[18] Sara K. Green et al. "Diels–Alder cycloaddition of 2-methylfuran and ethylene for renewable toluene". In: *Applied Catalysis B: Environmental* 180 (Jan. 2016), pp. 487–496. ISSN: 09263373. DOI: 10.1016/j.apcatb.2015.06.044. URL: http://dx.doi.org/10.1016/j.apcatb.2015.06.044http://linkinghub.elsevier.com/retrieve/pii/S0926337315300035.

[19] Eyas Mahmoud, Donald A. Watson, and Raul F. Lobo. "Renewable production of phthalic anhydride from biomass-derived furan and maleic anhydride". In: *Green Chem.* 16.1 (2014), pp. 167–175. ISSN: 1463-9262. DOI: 10.1039/C3GC41655K. URL: http://xlink.rsc.org/?DOI=c3gc41655khttp://xlink.rsc.org/?DOI=C3GC41655K.

[20] Shanmugam Thiyagarajan et al. "Substituted Phthalic Anhydrides from Biobased Furanics: A New Approach to Renewable Aromatics". In: *ChemSusChem* 8.18 (Sept. 2015), pp. 3052–3056. ISSN: 18645631. DOI: 10.1002/cssc.201500511. URL: http://doi.wiley.com/10.1002/cssc.201500511.

[21] Kendall N. Houk. "Frontier molecular orbital theory of cycloaddition reactions". In: *Accounts of Chemical Research* 8.11 (Nov. 1975), pp. 361–369. ISSN: 0001-4842. DOI: 10.1021/ar50095a001. URL: http://pubs.acs.org/doi/abs/10.1021/ar50095a001.

[22] Roald Hoffmann and R. B. Woodward. "Orbital Symmetries and endo-exo Relationships in Concerted Cycloaddition Reactions". In: *Journal of the American Chemical Society* 87.19 (Oct. 1965), pp. 4388–4389. ISSN: 0002-7863. DOI: 10.1021/ja00947a033. URL: http://pubs.acs.org/doi/abs/10.1021/ja00947a033.

[23] Yongge Qiu. "Substituent effects in the Diels-Alder reactions of butadienes, cyclopentadienes, furans and pyroles with maleic anhydride". In: *Journal of Physical Organic Chemistry* 28.5 (May 2015), pp. 370–376. ISSN: 08943230. DOI: 10.1002/poc.3421. URL: http://doi.wiley.com/10.1002/poc.3421.

[24] Raphaël Robiette, Jaqueline Marchand-Brynaert, and Daniel Peeters. "Influence of Diene Substitution on Transition State Stabilization in DielsAlder Reaction". In: *The Journal of Organic Chemistry* 67.19 (Sept. 2002), pp. 6823–6826. ISSN: 0022-3263. DOI: 10.1021/jo025796u. URL: http://pubs.acs.org/doi/abs/10.1021/jo025796u.

[25] Taha Salavati-fard et al. "Catalysis of the Diels–Alder Reaction of Furan and Methyl Acrylate in Lewis Acidic Zeolites". In: *ACS Catalysis* 7.3 (Mar. 2017), pp. 2240–2246. ISSN: 2155-5435. DOI: 10.1021/acscatal.6b02682. URL: http://pubs.acs.org/doi/10.1021/acscatal.6b02682.

[26] Matheus Adrianus; (NL). Dam et al. *PROCESS FOR THE PREPARATION OF A BENZENE DERIVATIVE. U.S. Patent No. WO/2013/048248. Washington, DC: U.S. Patent and Trademark Office.* 2013. URL: https://patentscope.wipo.int/search/en/detail.jsf?docId=WO2013048248.

[27] C. Luke Williams et al. "Cycloaddition of Biomass-Derived Furans for Catalytic Production of Renewable p -Xylene". In: *ACS Catalysis* 2.6 (June 2012), pp. 935–939. ISSN: 2155-5435. DOI: 10.1021/cs300011a. URL: http://pubs.acs.org/doi/10.1021/cs300011a.

[28] Shanmugam Thiyagarajan et al. "A Facile Solid-Phase Route to Renewable Aromatic Chemicals from Biobased Furanics". In: *Angewandte Chemie International Edition* 55.4 (Jan. 2016), pp. 1368–1371. ISSN: 14337851. DOI: 10.1002/anie.201509346. URL: http://doi.wiley.com/10.1002/anie.201509346.

[29] Homer C. Genuino et al. "Selectivity Control in the Tandem Aromatization of Bio-Based Furanics Catalyzed by Solid Acids and Palladium". In: *ChemSusChem* 10.1 (Jan. 2017), pp. 277–286. ISSN: 18645631. DOI: 10.1002/cssc.201600776. URL: http://doi.wiley.com/10.1002/cssc.201600776.

[30] Kelly K Miller et al. "Synthesis of Biobased Terephthalic Acid from Cycloaddition of Isoprene with Acrylic Acid". In: *ACS Sustainable Chemistry & Engineering* 2.8 (Aug. 2014), pp. 2053–2056. ISSN: 2168-0485. DOI: 10.1021/sc5003038. URL: http://pubs.acs.org/doi/10.1021/sc5003038.

[31] Jennifer J. Lee and George A. Kraus. "One-pot formal synthesis of biorenewable terephthalic acid from methyl coumalate and methyl pyruvate". In: *Green Chem.* 16.4 (2014), pp. 2111–2116. ISSN: 1463-9262. DOI: 10.1039/C3GC42487A. URL: http://xlink.rsc.org/?DOI=C3GC42487A.

[32] Yuya Tachibana, Saori Kimura, and Ken-ichi Kasuya. "Synthesis and Verification of Biobased Terephthalic Acid from Furfural". In: *Scientific Reports* 5.1 (July 2015), p. 8249. ISSN: 2045-2322. DOI: 10.1038/srep08249. URL: http://www.nature.com/srep/2015/150204/srep08249/full/srep08249.htmlhttp://www.nature.com/articles/srep08249.

[33] Noelia Alonso-Fagúndez et al. "Selective Conversion of Furfural to Maleic Anhydride and Furan with VO x / Al 2 O 3 Catalysts". In: *ChemSusChem* 5.10 (Oct. 2012), pp. 1984–1990. ISSN: 18645631. DOI: 10.1002/cssc.201200167. URL: http://doi.wiley.com/10.1002/cssc.201200167.

[34] Wei Zhang et al. "A study of furfural decarbonylation on K-doped Pd/Al2O3 catalysts". In: *Journal of Molecular Catalysis A: Chemical* 335.1-2 (Feb. 2011), pp. 71–81. ISSN: 13811169. DOI: 10.1016/j.molcata.2010.11.016. URL: http://dx.doi.org/10.1016/j.molcata.2010.11.016http://linkinghub.elsevier.com/retrieve/pii/S1381116910004693.

[35] Transparency Market Research. *Phthalic Anhydride Market for Phthalate Plasticizers, Unsaturated Polyester Resins (UPRs), Alkyd Resins and Other Applications - Global Industry Analysis, Size, Share, Growth, Trends and Forecast 2013 - 2019*. Tech. rep. 2013, p. 74. URL: https://www.transparencymarketresearch.com/phthalic-anhydride.html.

[36] Stephanie G. Wettstein et al. "A roadmap for conversion of lignocellulosic biomass to chemicals and fuels". In: *Current Opinion in Chemical Engineering* 1.3 (Aug. 2012), pp. 218–224. ISSN: 22113398. DOI: 10.1016/j.coche.2012.04.002. URL: http://linkinghub.elsevier.com/retrieve/pii/S2211339812000342.

[37] Rathin Datta and Michael Henry. "Lactic acid: recent advances in products, processes and technologies — a review". In: *Journal of Chemical Technology & Biotechnology* 81.7 (July 2006), pp. 1119–1129. ISSN: 0268-2575. DOI: 10.1002/jctb.1486. URL: http://doi.wiley.com/10.1002/jctb.1486.

[38] Minsu Kim and Hyunjoo Lee. "Highly Selective Production of Acrylic Acid from Glycerol via Two Steps Using Au/CeO 2 Catalysts". In: *ACS Sustainable Chemistry & Engineering* 5.12 (Dec. 2017), pp. 11371–11376. ISSN: 2168-0485. DOI: 10.1021/acssuschemeng.7b02457. URL: http://pubs.acs.org/doi/10.1021/acssuschemeng.7b02457.

[39] G. O. Torosyan et al. "Ammonium salts in alkylation reactions. 34. Synthesis and intramolecular cyclization of unsaturated esters with a furfuryl group". In: *Chemistry of Heterocyclic Compounds* 26.4 (Apr. 1990), pp. 390–392. ISSN: 0009-3122. DOI: 10.1007/BF00497206. URL: http://dx.doi.org/10.1007/BF00497206http://link.springer.com/10.1007/BF00497206.

[40] Axel G Griesbeck, Banu Öngel, and Murat Atar. "New phthalimide-methionine dyad-based fluorescence probes for reactive oxygen species: Singlet oxygen, hydrogen peroxide, and hypochlorite". In: *Journal of Physical Organic Chemistry* 30.9 (Sept. 2017), e3741. ISSN: 08943230. DOI: 10.1002/poc.3741. URL: http://doi.wiley.com/10.1002/poc.3741.

[41] Duc-hiep Bach et al. "Synthesis and biological activity of new phthalimides as potential anti-inflammatory agents". In: *Bioorganic & Medicinal Chemistry* 25.13 (July 2017), pp. 3396–3405. ISSN: 09680896. DOI: 10.1016/j.bmc.2017.04.027. URL: http://dx.doi.org/10.1016/j.bmc.2017.04.027http://linkinghub.elsevier.com/retrieve/pii/S0968089617303681.

[42] Xin Chen, Zheng Xu, and Toshio Okuhara. "Liquid phase esterification of acrylic acid with 1-butanol catalyzed by solid acid catalysts". In: *Applied Catalysis A: General* 180.1-2 (Apr. 1999), pp. 261–269. ISSN: 0926860X. DOI: 10.1016/S0926-860X(98)00337-8. URL: http://www.sciencedirect.com/science/article/pii/S0926860X98003378http://linkinghub.elsevier.com/retrieve/pii/S0926860X98003378.

[43] Junzo Otera. "Transesterification". In: *Chemical Reviews* 93.4 (June 1993), pp. 1449–1470. ISSN: 0009-2665. DOI: 10.1021/cr00020a004. URL: http://pubs.acs.org/doi/abs/10.1021/cr00020a004.

[44] Mekki Choura, Naceur M. Belgacem, and Alessandro Gandini. "Acid-Catalyzed Polycondensation of Furfuryl Alcohol: Mechanisms of Chromophore Formation and Cross-Linking". In: *Macromolecules* 29.11 (Jan. 1996), pp. 3839–3850. ISSN: 0024-9297. DOI: 10.1021/ma951522f. URL: http://pubs.acs.org/doi/abs/10.1021/ma951522f.

[45] Kay Louise Robinson et al. *REVERSIBLE POLYMERIC GELATION FOR OILFIELD APPLICATIONS. U.S. Patent No. US2009126932 (A1). Washington, DC: U.S. Patent and Trademark Office.* 2009. URL: https://worldwide.espacenet.com/publicationDetails/biblio?CC=US&NR=2009126932&KC=&FT=E&locale=en_EP.

[46] Jrgen Sauer and Reiner Sustmann. "Mechanistic Aspects of Diels-Alder Reactions: A Critical Survey". In: *Angewandte Chemie International Edition in English* 19.10 (Oct. 1980), pp. 779–807. ISSN: 0570-0833. DOI: 10.1002/anie.198007791. URL: http://dx.doi.org/10.1002/anie.198007791http://doi.wiley.com/10.1002/anie.198007791.

[47] Michael E. Jung and Jacquelyn Gervay. "Solvent effects in intramolecular Diels-Alder reactions of 2-furfuryl methyl fumarates: evidence for a polar transition state". In: *Journal of the American Chemical Society* 111.14 (July 1989), pp. 5469–5470. ISSN: 0002-7863. DOI: 10.1021/ja00196a065. URL: http://pubs.acs.org/doi/abs/10.1021/ja00196a065.

[48] Michael E. Jung and Jacquelyn Gervay. "gem-Dialkyl effect in the intramolecular Diels-Alder reaction of 2-furfuryl methyl fumarates: the reactive rotamer effect, the enthalpic basis for acceleration, and evidence for a polar transition state". In: *Journal of the American Chemical Society* 113.1 (Jan. 1991), pp. 224–232. ISSN: 0002-7863. DOI: 10.1021/ja00001a032. URL: http://pubs.acs.org/doi/abs/10.1021/ja00001a032.

[49] G te Velde et al. "Chemistry with ADF". In: *Journal of Computational Chemistry* 22.9 (July 2001), pp. 931–967. ISSN: 0192-8651. DOI: 10.1002/jcc.1056. URL: http://dx.doi.org/10.1002/jcc.1056http://doi.wiley.com/10.1002/jcc.1056.

[50] C Fonseca Guerra et al. "Towards an order- N DFT method". In: *Theoretical Chemistry Accounts: Theory, Computation, and Modeling (Theoretica Chimica Acta)* 99.6 (Nov. 1998), pp. 391–403. ISSN: 1432-881X. DOI: 10.1007/s002140050353. URL: https://doi.org/10.1007/s002140050353http://link.springer.com/10.1007/s002140050353.

[51] Evert Jan Baerends et al. *ADF2017, SCM, Theoretical Chemistry, Vrije Universiteit, Amsterdam, The Netherlands, https://www.scm.com.*

[52] Sérgio Filipe Sousa, Pedro Alexandrino Fernandes, and Maria João Ramos. "General Performance of Density Functionals". In: *The Journal of Physical Chemistry A* 111.42 (Oct. 2007), pp. 10439–10452. ISSN: 1089-5639. DOI: 10.1021/jp0734474. URL: https://doi.org/10.1021/jp0734474http://pubs.acs.org/doi/abs/10.1021/jp0734474.

[53] Julian Tirado-Rives and William L Jorgensen. "Performance of B3LYP Density Functional Methods for a Large Set of Organic Molecules". In: *Journal of Chemical Theory and Computation* 4.2 (Feb. 2008), pp. 297–306. ISSN: 1549-9618. DOI: 10.1021/ct700248k. URL: http://pubs.acs.org/doi/abs/10.1021/ct700248k.

[54] Jinggang Wang et al. *A method of preparing the 4 - hydroxy methyl -7 - oxa-bicyclo [2.2.1] heptyl -5 - ene monomer. Patent No. CN104193759*. 2016. URL: https://encrypted.google.com/patents/CN104193759B?cl=no.

[55] Chemical Economics Handbook. *Isophthalic Acid*. Tech. rep. 2016. URL: https://ihsmarkit.com/products/isophthalic-acid-chemical-economics-handbook.html.

[56] Michael J. Minch. "Orientational dependence of vicinal proton-proton NMR coupling constants: The Karplus relationship". In: *Concepts in Magnetic Resonance* 6.1 (Jan. 1994), pp. 41–56. ISSN: 10437347. DOI: 10.1002/cmr.1820060104. URL: https://onlinelibrary.wiley.com/doi/abs/10.1002/cmr.1820060104http://doi.wiley.com/10.1002/cmr.1820060104.

[57] Do Hyun Ryu et al. "Catalytic enantioselective Diels–Alder reactions of furans and 1,1,1-trifluoroethyl acrylate". In: *Tetrahedron Letters* 48.33 (Aug. 2007), pp. 5735–5737. ISSN: 00404039. DOI: 10.1016/j.tetlet.2007.06.097. URL: http://dx.doi.org/10.1016/j.tetlet.2007.06.097http://linkinghub.elsevier.com/retrieve/pii/S0040403907012142.

[58] Jae Yi Sim et al. "Asymmetric synthesis of (+)-cis-nemorensic acid from a chiral Diels–Alder adduct of 2,5-dimethylfuran". In: *Chemical Communications* 47 (2007), p. 5064. ISSN: 1359-7345. DOI: 10.1039/b710537a. URL: http://xlink.rsc.org/?DOI=b710537a.

[59] Clara L Kelly and Nicholas E Leadbeater. "The Reaction of Hexafluoroisopropyl Esters with Amines: A Fast, Easy, Solvent-Free Approach to the Synthesis of Amides". In: *International Journal of Advanced Research in Chemical Science* 3.7 (2016), pp. 27–34. ISSN: 23490403. DOI: 10.20431/2349-0403.0307005. URL: https://www.arcjournals.org/pdfs/ijarcs/v3-i7/5.pdf.

[60] Pei Nian Liu et al. "Triflic acid adsorbed on silica gel as an efficient and recyclable catalyst for the addition of β-dicarbonyl compounds to alcohols and alkenes". In: *Green Chemistry* 12.6 (2010), p. 1049. ISSN: 1463-9262. DOI: 10.1039/b926142g. URL: http://xlink.rsc.org/?DOI=b926142g.

[61] Antoine M M Schreurs, Xinyi Xian, and Loes M. J. Kroon-Batenburg. "EVAL15 : a diffraction data integration method based on ab initio predicted profiles". In: *Journal of Applied Crystallography* 43.1 (Feb. 2010), pp. 70–82. ISSN: 0021-8898. DOI: 10.1107/S0021889809043234. URL: http://scripts.iucr.org/cgi-bin/paper?S0021889809043234.

[62] George M Sheldrick. *SADABS, Universität Göttingen, Germany*. 2014.

[63] George M Sheldrick. "SHELXT – Integrated space-group and crystal-structure determination". In: *Acta Crystallographica Section A Foundations and Advances* 71.1 (Jan. 2015), pp. 3–8. ISSN: 2053-2733. DOI: 10.1107/S2053273314026370. URL: https://doi.org/10.1107/S2053273314026370.

[64] George M. Sheldrick. "Crystal structure refinement with SHELXL". In: *Acta Crystallographica Section C Structural Chemistry* 71.1 (Jan. 2015), pp. 3–8. ISSN: 2053-2296. DOI: 10.1107/S2053229614024218. URL: http://scripts.iucr.org/cgi-bin/paper?S2053229614024218.

[65] Anthony L Spek. "Structure validation in chemical crystallography". In: *Acta Crystallographica Section D Biological Crystallography* 65.2 (Feb. 2009), pp. 148–155. ISSN: 0907-4449. DOI: 10.1107/S090744490804362X. URL: https://doi.org/10.1107/S090744490804362Xhttp://scripts.iucr.org/cgi-bin/paper?S090744490804362X.

[66] E. Van Lenthe and E. J. Baerends. "Optimized Slater-type basis sets for the elements 1-118". In: *Journal of Computational Chemistry* 24.9 (July 2003), pp. 1142–1156. ISSN: 0192-8651. DOI: 10.1002/jcc.10255. URL: http://doi.wiley.com/10.1002/jcc.10255.

[67] Louis Versluis and Tom Ziegler. "The determination of molecular structures by density functional theory. The evaluation of analytical energy gradients by numerical integration". In: *The Journal of Chemical Physics* 88.1 (Jan. 1988), pp. 322–328. ISSN: 0021-9606. DOI: 10.1063/1.454603. URL: https://doi.org/10.1063/1.454603http://aip.scitation.org/doi/10.1063/1.454603.

[68] Liangyou Fan and Tom Ziegler. "Nonlocal density functional theory as a practical tool in calculations on transition states and activation energies. Applications to elementary reaction steps in organic chemistry". In: *Journal of the American Chemical Society* 114.27 (Dec. 1992), pp. 10890–10897. ISSN: 0002-7863. DOI: 10.1021/ja00053a027. URL: https://doi.org/10.1021/ja00053a027http://pubs.acs.org/doi/abs/10.1021/ja00053a027.

[69] Yoshiyasu Baba et al. "Structure-Based Design of a Highly Selective Catalytic Site-Directed Inhibitor of Ser/Thr Protein Phosphatase 2B (Calcineurin)". In: *Journal of the American Chemical Society* 125.32 (Aug. 2003), pp. 9740–9749. ISSN: 0002-7863. DOI: 10.1021/ja034694y. URL: https://doi.org/10.1021/ja034694yhttp://pubs.acs.org/doi/abs/10.1021/ja034694y.

[70] Na-Na Li et al. "Palladium-Catalyzed C–H Homocoupling of Furans and Thiophenes Using Oxygen as the Oxidant". In: *Organic Letters* 16.10 (May 2014), pp. 2732–2735. ISSN: 1523-7060. DOI: 10.1021/ol501019y. URL: https://doi.org/10.1021/ol501019yhttp://pubs.acs.org/doi/10.1021/ol501019y.